



UNIVERSITAT
POLITÈCNICA
DE VALÈNCIA



UNIVERSITAT POLITÈCNICA DE VALÈNCIA

School of Aerospace Engineering and Industrial
Design

Development of an academic flight simulator for the study
of the flight dynamics of conventional configuration aircraft

End of Degree Project

Bachelor's Degree in Aerospace Engineering

AUTHOR: Villanueva Chulvi, Lucía

Tutor: Martí Gómez-Aldaraví, Pedro

Cotutor: Carreres Talens, Marcos

ACADEMIC YEAR: 2022/2023

Acknowledgments

First of all, I would like to thank my tutor, Pedro Martí, for guiding me through the process and helping me with every problem that has arisen. I would also like to thank Marcos Carreres, co-tutor of the project, for having both of them given me the opportunity to do this final degree project.

I would like to thank my parents and my sister for being patient with me and supporting me these four years. For believing in me.

Finally, I would like to thank my friends for always having my back.

Thanks to everyone who has helped me get this far.

Abstract

The aim of this project is to programme an academic flight simulator that will allow the study of the performance of conventional configuration aircraft. To achieve this purpose, the methodology and literature of the Flight Mechanics course has been followed. Using MATLAB numerical solver *ode45*, it has been possible to integrate the differential equations that describe the movement of a rigid body, known as *Bryan Equations*. Subsequently, a study of the flight dynamics of the McDonnell Douglas F-18 Hornet was carried out during the execution of a series of manoeuvres using the simulator in question. The vertical equilibrium has also been studied in cruise conditions with the aim of verifying the proper functioning of the simulator. Finally, an exhaustive analysis is made of the results obtained in each case study. Once completed, the simulator may be used by the students to carry out their own analyses and to check the results obtained.

Keywords: flight simulator, flight mechanics, Bryan Equations, numerical solver.

Resumen

El objetivo de este proyecto es programar un simulador de vuelo académico que permita el estudio de las actuaciones de aeronaves de configuración convencional. Para lograr este propósito se ha seguido la metodología docente de la asignatura Mecánica del Vuelo. Haciendo uso del solver numérico *ode45* de MATLAB, se ha podido integrar las ecuaciones diferenciales que describen el movimiento de un cuerpo rígido, conocidas como *Ecuaciones de Bryan*. Posteriormente, se ha realizado un estudio de la dinámica de vuelo del McDonnell Douglas F-18 Hornet en la ejecución de una serie de maniobras empleando el simulador programado. Se ha estudiado además el equilibrado en condiciones de crucero con el objetivo de comprobar el correcto funcionamiento. Finalmente se hará un análisis exhaustivo de los resultados obtenidos en cada caso de estudio. Una vez finalizado, el simulador en cuestión podrá ser utilizado por los estudiantes en la realización de sus propios análisis y para comprobar los resultados obtenidos.

Palabras clave: simulador de vuelo, mecánica del vuelo, Ecuaciones de Bryan, solver numérico.

Resum

L'objectiu d'aquest projecte és programar un simulador de vol acadèmic que permeti l'estudi de les actuacions d'aeronaus de configuració convencional. Per aconseguir aquest propòsit s'ha seguit la metodologia docent de l'assignatura Mecànica del Vol. Fent ús del solver numèric *ode45* de MATLAB, s'ha pogut integrar les equacions diferencials que descriuen el moviment d'un cos rígid, conegudes com a *Equacions de Bryan*. Posteriorment, s'ha realitzat un estudi de la dinàmica de vol del McDonnell Douglas F-18 Hornet en l'execució d'una sèrie de maniobres emprant el simulador programat. S'ha estudiat a més l'equilibrat en condicions de creuer amb l'objectiu de comprovar el correcte funcionament. Finalment es farà una anàlisi *exhaustiva dels resultats obtinguts en cada cas d'estudi. Una vegada finalitzat, el simulador en qüestió podrà ser utilitzat pels estudiants en la realització de les seues pròpies anàlisis i per a comprovar els resultats obtinguts.

Paraules clau: simulador de vol, mecànica del vol, Equacions de Bryan, solver numèric.

Contents

1	Introduction	1
1.1	Objectives	2
2	Theoretical background	3
2.1	Aviation and simulators origin	3
2.2	Coordinate system	4
2.3	Bryan equations	7
2.4	Euler-Rodrigues Quaternions	9
2.5	Aerodynamic model	10
2.6	Propulsion models	12
3	Methodology	14
3.1	Aircraft of study	14
3.2	Development of the flight simulator	17
4	Presentation of results	20
4.1	Vertical plane equilibrium	20
4.2	Vertical turn	24
4.3	Gliding flight	28
4.4	Dive recovery	31
4.5	Horizontal turn	35
4.6	Helical turn	40
4.7	Verification with the Airbus A320-200	44
4.7.1	Equilibrium in the vertical plane	44
4.7.2	Gliding flight	47
5	Conclusions	50
5.1	Future work	50
6	Relation of the project to the Sustainable Development Goals of the Agenda 2030	52
7	Scope Statement	54
7.1	Standard regulations	54
7.2	Specific regulations	59
7.2.1	Resource specifications	59
7.2.2	Quality requirements	60
7.2.3	Warranty and maintenance requirements	60
7.2.4	Legal and contractual requirements	60

7.2.5	Revision of costs	60
7.2.6	Deposit	60
8	Budget of the project	61
8.1	Cost calculation	62
8.2	Overall budget	63
	Bibliography	66
A	Orientation methods	68
A.1	Euler Axis	68
A.2	Quaternions Formulation	69
B	Three-view of the aircraft	71
C	MATLAB code	72
C.1	Aircraft Parameters	72
C.2	Function for the thrust model	74
C.3	Function for the aerodynamic model	75
C.4	Function for the <i>Bryan Equations</i> in body-fixed axes	76
C.5	Function for the <i>Bryan Equations</i> in wind axes	79
C.6	Function for the <i>Bryan Equations</i> with quaternions	86
C.7	Flight simulator	90

List of Figures

2.1.1 <i>Le Tonneau Antoinette</i> [13]	4
2.1.2 <i>Link Trainer</i> [4]	4
2.2.1 Body-fixed reference frame [18]	5
2.2.2 Wind reference frame [18]	5
2.2.3 Aerodynamic Angles [17]	6
3.1.1 McDonnell Douglas F/A-18 [5]	14
3.2.1 Flight simulator development	17
4.1.1 Plot of the time evolution of the linear velocities for vertical equilibrium	21
4.1.2 Plot of the time evolution of the angular velocities for vertical equilibrium	22
4.1.3 Plot of the time evolution of the aerodynamic angles for vertical equilibrium	22
4.1.4 Plot of the time evolution of the Euler angles for vertical equilibrium	23
4.1.5 Plot of the two-dimensional trajectory of the vertical equilibrium	24
4.2.1 Plot of the time evolution of the airspeed for the loop	25
4.2.2 Plot of the time evolution of the angular velocities for the loop	26
4.2.3 Plot of the time evolution of the Euler angles for the loop	26
4.2.4 Plot of the time evolution of the altitude for the loop	27
4.2.5 Plot of the three-dimensional trajectory of the loop	28
4.3.1 Plot of the time evolution of the airspeed for the gliding flight	29
4.3.2 Plot of the time evolution of the angle of attack for the gliding flight	29
4.3.3 Plot of the time evolution of the Euler angles for the gliding flight	30
4.3.4 Plot of the time evolution of the altitude for the gliding flight	30
4.3.5 Plot of the three-dimensional trajectory of the gliding flight	31
4.4.1 Plot of the time evolution of the airspeed for the dive recovery manoeuvre	32
4.4.2 Plot of the time evolution of the angular velocity q for the dive recovery manoeuvre	33
4.4.3 Plot of the aerodynamic angles for the dive recovery manoeuvre	33
4.4.4 Plot of the time evolution of the climb angle for the dive recovery manoeuvre	34
4.4.5 Plot of the time evolution of the altitude for the dive recovery manoeuvre	34
4.4.6 Plot of the three-dimensional trajectory of the dive recovery manoeuvre	35
4.5.1 Plot of the time evolution of the airspeed for the horizontal turn	36
4.5.2 Plot of the time evolution of the angular velocities for the horizontal turn	37
4.5.3 Plot of the time evolution of the aerodynamic angles for the horizontal turn	37

4.5.4 Plot of the time evolution of the bank angle and the climb angle for the horizontal turn	38
4.5.5 Plot of the time evolution of the heading angle for the horizontal turn	38
4.5.6 Plot of the three-dimensional trajectory of the horizontal turn	39
4.6.1 Plot of the time evolution of the airspeed for the helical turn	40
4.6.2 Plot of the time evolution of the angular velocities for the helical turn	41
4.6.3 Plot of the time evolution of the bank angle and the elevation angle for the helical turn	41
4.6.4 Plot of the time evolution of the turn rate for the helical turn	42
4.6.5 Plot of the three-dimensional trajectory of the helical turn	43
4.7.1 Plot of the time evolution of the linear velocities for the vertical equilibrium of the A320	45
4.7.2 Plot of the time evolution of the angular velocities for the vertical equilibrium of the A320	45
4.7.3 Plot of the time evolution of the aerodynamic angles for the vertical equilibrium of the A320	46
4.7.4 Plot of the time evolution of the Euler angles for the vertical equilibrium of the A320	46
4.7.5 Plot of the two-dimensional trajectory of the aerodynamic angles for the vertical equilibrium of the A320	47
4.7.6 Plot of the time evolution of the airspeed for the gliding flight for the A320	48
4.7.7 Plot of the time evolution of the aerodynamic angles for the gliding flight for the A320	48
4.7.8 Plot of the time evolution of the Euler angles for the gliding flight for the A320	49
4.7.9 Plot of the three-dimensional trajectory of the gliding flight for the A320	49
6.0.1 SDGs with higher degree of relationship	53
B.0.1 Three-view of the McDonnell Douglas F-18 Hornet[1]	71

List of Tables

2.6.1 Value of a according to altitude and type of engine	13
3.1.1 Geometrical data of the F-18	15
3.1.2 Data for the thrust model of the F-18	15
3.1.3 Value of the longitudinal stability derivatives of the F-18	16
3.1.4 Value of the aerodynamic derivatives of the F-18	16
3.1.5 Value of the control derivatives of the F-18	16
4.1.1 Value of the initial conditions for the vertical equilibrium	21
4.1.2 Value of the controls and the aerodynamic angles for the vertical equilibrium	21
4.2.1 Value of the controls for the vertical loop manoeuvre	24
4.2.2 Initial value of the quaternions for the loop manoeuvre	25
4.3.1 Value of the initial conditions for the gliding flight manoeuvre	28
4.3.2 Value of the controls for the gliding flight	28
4.4.1 Value of the initial conditions for the dive recovery manoeuvre	32
4.4.2 Value of the controls for the dive recovery manoeuvre	32
4.5.1 Value of the initial conditions for the horizontal turn	36
4.5.2 Value of the controls for the horizontal turn	36
4.6.1 Value of the initial conditions for the helical turn	40
4.6.2 Value of the controls for the helical turn	40
4.7.1 Value of the initial conditions for the vertical equilibrium of the A320	44
4.7.2 Value of the controls and the aerodynamic angles for the vertical equilibrium of the A320	44
4.7.3 Value of the initial conditions for the gliding flight manoeuvre for the A320	47
4.7.4 Value of the controls for the gliding flight for the A320	47
6.0.1 Degree of relationship with the Sustainable Development Goals	52
8.2.1 Budget breakdown	64
8.2.2 Overall budget	65

List of Symbols

Angles

α	Angle of attack
α_0	Initial value of the angle of attack
$\dot{\alpha}$	Rate of change of the angle of attack
β	Slip angle
β_0	Initial value of the slip angle
$\dot{\beta}$	Rate of change of the slip angle
ϕ	Euler bank angle or Roll angle
θ	Euler elevation angle or Pitch angle
ψ	Euler azimuth angle or Yaw angle
ϕ_0, θ_0, ψ_0	Initial values of Bank, Elevation and Azimuth angles respectively
$\dot{\phi}, \dot{\theta}, \dot{\psi}$	Rates of change of Bank, Elevation and Azimuth angles respectively
μ, γ, χ	Bank angle, Climb angle and Heading respectively in wind axes
μ_0, γ_0, χ_0	Initial values of Bank angle, Climb angle and Heading respectively
$\dot{\mu}, \dot{\gamma}, \dot{\chi}$	Rates of change of Bank angle, Climb angle and Heading respectively

Bryan Equations

V	Airspeed
V_0	Initial value of the airspeed
\dot{V}	Rate of change of airspeed
u, v, w	Linear velocities
u_0, v_0, w_0	Initial value of the linear velocities
$\dot{u}, \dot{v}, \dot{w}$	Linear accelerations
p, q, r	Angular velocities in body-fixed axes

p_0, q_0, r_0 Initial values of the angular velocities in body-fixed axes

$\dot{p}, \dot{q}, \dot{r}$ Angular accelerations in body-fixed axes

p_w, q_w, r_w Angular velocities in wind axes

x, y, z Aircraft coordinates

x_0, y_0, z_0 Initial values of the aircraft coordinates

$\dot{x}, \dot{y}, \dot{z}$ Rate of change of aircraft coordinates

Controls

δ_A Ailerons deflection angle

δ_E Elevator deflection angle

δ_P Throttle lever

δ_R Rudder deflection angle

Forces and Moments

g Acceleration due to gravity

D Drag Force

Y Lateral Force

L Lift Force

L Roll Moment

M Pitch Moment

N Yaw Moment

$X_{a,b}$ Axial component of aerodynamic force in body-fixed axes

$Y_{a,b}$ Lateral component of aerodynamic force in body-fixed axes

$Z_{a,b}$ Vertical component of aerodynamic force in body-fixed axes

$X_{a,w}$ Axial component of aerodynamic force in wind axes

$Y_{a,w}$ Lateral component of aerodynamic force in wind axes

$Z_{a,w}$ Vertical component of aerodynamic force in wind axes

Geometry

b_w Wingspan

c_w Mean aerodynamic chord

I_{xx}, I_{yy}, I_{zz} Moments of inertia

I_{xz}, I_{yx}, I_{yz} Products of inertia

m Aircraft mass

S_w Wing area

L Aircraft length

Aerodynamic Derivatives

C_D Drag coefficient

C_{D0} Drag coefficient at zero lift

K Induced drag constant

C_L Lift coefficient

C_{L0} Lift coefficient at zero angle of attack and zero elevator deflection

$C_{L\alpha}$ Lift slope

$C_{L\delta E}$ Change in lift coefficient with elevator deflection

C_{Lq} Change in lift coefficient with q

$C_{L\dot{\alpha}}$ Change in lift coefficient with $\dot{\alpha}$

C_M Pitching Moment Coefficient

C_{M0} Pitching moment coefficient at zero angle of attack and zero elevator deflection

$C_{M\alpha}$ Change in pitching moment coefficient with angle of attack

$C_{M\delta E}$ Change in pitching moment coefficient with elevator deflection

C_{Mq} Change in pitching moment coefficient with q

$C_{M\dot{\alpha}}$ Change in pitching moment coefficient with $\dot{\alpha}$

C_Y Lateral Force Coefficient

$C_{Y\beta}$ Change in lateral force coefficient with slip angle

$C_{Y\delta A}$ Change in lateral force coefficient with aileron deflection

$C_{Y\delta R}$ Change in lateral force coefficient with rudder deflection

C_{Yp} Change in lateral force coefficient with p

C_{Yr} Change in lateral force coefficient with r

$C_{Y\dot{\beta}}$ Change in lateral force coefficient with $\dot{\beta}$

C_l Roll Moment Coefficient

$C_{l\beta}$ Change in roll moment coefficient with slip angle

$C_{l\delta A}$ Change in roll moment coefficient with aileron deflection
 $C_{l\delta R}$ Change in roll moment coefficient with rudder deflection
 C_{lp} Change in roll moment coefficient with p
 C_{lr} Change in roll moment coefficient with r
 $C_{l\dot{\beta}}$ Change in roll moment coefficient with $\dot{\beta}$
 C_N Yaw Moment Coefficient
 $C_{N\beta}$ Change in yaw moment coefficient with slip angle
 $C_{N\delta A}$ Change in yaw moment coefficient with aileron deflection
 $C_{N\delta R}$ Change in yaw moment coefficient with rudder deflection
 C_{Np} Change in yaw moment coefficient with p
 C_{Nr} Change in yaw moment coefficient with r
 $C_{N\dot{\beta}}$ Change in yaw moment coefficient with $\dot{\beta}$
 $C_{x,b}, C_{y,b}, C_{z,b}$ Aerodynamic force coefficients in body-fixed axes
 $C_{x,w}, C_{y,w}, C_{z,w}$ Aerodynamic force coefficients in wind axes

Quaternions

q_0, q_1, q_2, q_3 Euler-Rodrigues quaternions
 $q_{0,0}, q_{1,0}, q_{2,0}, q_{3,0}$ Initial values of the Euler-Rodrigues quaternions
 $\dot{q}_0, \dot{q}_1, \dot{q}_2, \dot{q}_3$ Rate of change of the Euler-Rodrigues quaternions
 η, ξ, ζ, χ Euler axis parameters
 $\dot{\eta}, \dot{\xi}, \dot{\zeta}, \dot{\chi}$ Rate of change of the Euler axis parameters

Atmosphere Model

$T(z)$ Temperature
 $a(z)$ Speed of sound
 $P(z)$ Pressure
 $\rho(z)$ Density
 $\sigma(z)$ Relative density
 T_0 Temperature at sea level
 P_0 Pressure at sea level
 ρ_0 Density at sea level

Thrust Model

T Thrust

T_x, T_y, T_z Axial, Lateral and Vertical components of thrust in body-fixed axes

$T_{x,w}, T_{y,w}, T_{z,w}$ Axial, Lateral and Vertical components of thrust in wind axes

T_0 Maximum thrust at $z=0, M=0$

ε Thrust angle

BPR Bypass ratio

M Mach number

C_e Specific fuel consumption

\dot{m}_0 Initial value of the fuel mass flow rate

\dot{m}_f Fuel mass flow rate

m_f Fuel mass

Matrices

R_α Rotation matrix about Y-axis of angle α

R_β Rotation matrix about Z-axis of angle β

$R_{\alpha\beta}$ Transformation matrix from wind to body-fixed axes

$R_{\beta\alpha}$ Transformation matrix from body-fixed to wind axes

R_ϕ Rotation matrix about X-axis of angle ϕ

R_θ Rotation matrix about X-axis of angle θ

R_ϕ Rotation matrix about X-axis of angle ϕ

R_η Euler axis transformation matrix

R_q Quaternion transformation matrix

Chapter 1

Introduction

With the passing of time and the development of technology, flight simulators have experienced a significant increase in popularity. They were first created to meet the need to train pilots in a safe environment, and nowadays their use has spread to a variety of fields. They can be found in a wide range of applications, from video games to even pilot qualifications.

Flight simulators have the capability to represent flight situations by means of computer software. They sometimes are additionally equipped with mechanical resources to reproduce the instruments and cockpit of the aircraft. Some simulators can also recreate a variety of weather conditions and even the movement of the aircraft to make the experience as realistic as possible.

They have also proved to be very useful in the field of engineering. They can be used in system testing by means of real-time simulations, or to carry out different analyses in aircraft design or accident investigation.

Despite the great diversity of existing simulators, however, none of them is intended for the academic environment, even though they are a common tool in the study of aircraft performance. This is why the need arises to develop a flight simulator based on the methodology used in the courses of *Mecánica del Vuelo* and *Ampliación de Mecánica del Vuelo*.

The aim is to create a flight simulator by implementing the equations that govern the dynamics, the *Bryan Equations*. In order to maximise its completeness, they will be presented in the two reference systems most commonly used in the course, body-fixed axes and wind axes, so that the user can choose as appropriate. The aerodynamic model of the aircraft will also have to be introduced, as well as the different propulsive models available, the choice of which will be left to the user. It will serve as a tool from which students will be able to analyse the performance of the aircraft and deepen their understanding of the concepts taught. It will also be designed to be intuitive and easy to use, so that the user can understand its operation.

Once completed, it will be used to analyse the performance of an aircraft, this being the McDonnell Douglas F-18 Hornet. Firstly, the aircraft will be equilibrated in cruise conditions and, afterwards, a succession of manoeuvres will be carried out during which the behaviour of the aircraft will be studied. Finally, data of the Airbus A320-200 will be used in order to verify the correct functioning of the simulator regardless the aircraft under study.

1.1 Objectives

The primary objectives pursued during the development of the project are as follows:

- To develop an academic flight simulator following the teaching methodology of the course *Mecánica del Vuelo*.
- To apply this simulator in the analysis of the flight dynamics of a conventional configuration aircraft during a variety of manoeuvres.
- To provide students with a tool to analyse aircraft performance and to verify the results of their analysis.

Additionally, a succession of secondary objectives are also envisaged:

- To implement the *Bryan Equations* in the different coordinate systems studied, as well as the aerodynamic and propulsive model.
- To create a user-friendly and intuitive tool where the user can follow and understand the process.
- To verify the correct operation of the simulator based on the equilibrium of the aircraft under cruise conditions.
- To ensure the proper performance of the simulator independently of the aircraft.
- To deepen and broaden the knowledge acquired in the courses *Mecánica del Vuelo* and *Ampliación de Mecánica del Vuelo*.

Chapter 2

Theoretical background

2.1 Aviation and simulators origin

To reach the skies has always been one of the most longed for accomplishments for mankind. Throughout history many people have tried to develop a machine that would allow them to fly, but most of them failed to.

The origins of aviation date back to China with the creation of the first kite around 2000 years ago, but it was not until centuries later, with the arrival of Marco Polo, that this idea spread along Europe. Years before, many tried to imitate the flight of birds by attaching wings to their arms and flapping them rapidly, but all these attempts failed miserably.

In XV century Leonardo da Vinci looked at the flight of birds, considering that flying machines should have flapping wings in order to fly. However, his studies remained as designs, such as the famous *Ornithopter*, but none were ever built.

All of these attempts were mainly based on empirical methods. It was not until the XIX century with George Cayley and his design of a glider that stability and aerodynamic forces were considered. He thus laid the foundations of aerodynamics and proved the importance of stability in an aircraft. Another notable figure was Otto Lilienthal, who made more than two thousand gliding flights until his death. Based on Lilienthal's work, the Wright brothers performed the first controlled powered flight in 1903, on board the *Flyer*. It is considered one of the most important breakthroughs that revolutionised the world of aviation.

Over time, aviation continued to evolve. However, pilots lacked experience, so the need arose to train them without facing the dangers of real flight. The first flight simulators were developed to meet these demands, giving the sensation of flying without the risks involved.

One of the first simulators, known as *Le tonneau Antoinette* consisted of stacked barrels mounted on a frame (Figure 2.1.1). Another example of a simulator is the *Sander Teacher*, which was a replica of an aeroplane mounted on an articulated joint, allowing roll, pitch and yaw movements.



Figure 2.1.1: *Le Tonneau Antoinette* [13]

In 1929 Ed Link built the *Link Trainer* (Figure 2.1.2), which simulated mechanical movements from the pedals and levers provided. Later, control instruments were added and it was further refined.



Figure 2.1.2: *Link Trainer* [4]

The arrival of analogue computers (1940s), used to solve the equations of motion, allowed the development of electronic simulators. In 1948 Curtis-Wright developed a simulator for the airline Pan American. He replicated the cockpit of the *Stratocruiser*, without any motion, but with fully operative instruments. It was at this point that motion was introduced into flight simulators, reaching 6 degrees of movement.

With the advances in technology, the mechanisms used could be refined, and even visual effects were added to achieve the greatest possible realism. Nowadays it is a field that is still in constant development, seeking to keep up with the latest technologies.

2.2 Coordinate system

In order to study the motion of an aircraft, the first step is to determine a coordinate system from which the position as well as the velocity and acceleration will be defined. Although there are several reference frames, only three will be relevant to the matter of study: body-fixed axes, wind axes and Earth-fixed axes.

Body-fixed axes are characterized for being fixed to the body, meaning that they move with the aircraft. The origin is located at the centre of mass, with the longitudinal axis pointing forward, that is, the nose of the aircraft, and the Y-axis perpendicular

to the symmetry plane towards the right wing. It should be taken into account that even though not every aircraft has a symmetry plane, it will be assumed in order to simplify the calculations. The Z-axis will be perpendicular to the XY plane, pointing downwards, as shown in Figure 2.2.1.

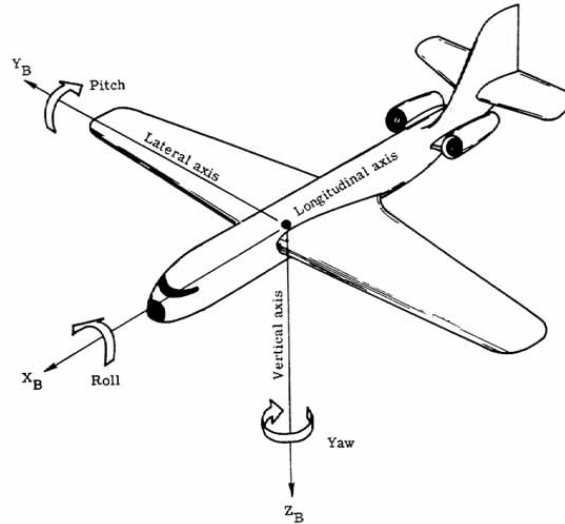


Figure 2.2.1: Body-fixed reference frame [18]

There exist different body-fixed systems, such as stability axes or principal axes of inertia, but with the purpose of simplification, principal axes of inertia will be considered.

Regarding wind axes, they are related to the aerodynamic velocity, with the origin located at the centre of mass of the aircraft. The X-axis will be pointing forward, aligned with the aerodynamic velocity vector, as seen in Figure 2.2.2. The Z-axis will be located at the vertical symmetry plane, pointing downwards, with the Y-axis forming a trihedron, heading towards the right side of the aircraft.

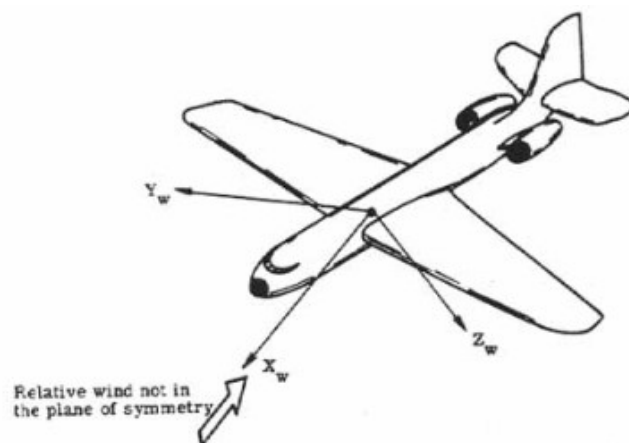


Figure 2.2.2: Wind reference frame [18]

It is possible to change from one system to another by applying a series of rotations as a function of the aerodynamic angles, as shown in Figure 2.2.3.

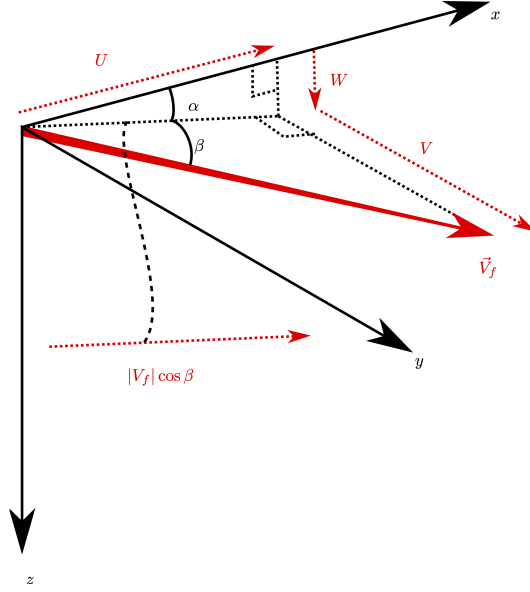


Figure 2.2.3: Aerodynamic Angles [17]

Thus, if a transformation from wind axes to body axes is to be performed, the procedure consists of a rotation of angle β about the Z-axis followed by a rotation of angle α around the Y-axis, as shown in Equation 2.1.

$$\begin{aligned}
 R_{\alpha\beta} = R_{\alpha}R_{\beta} &= \begin{bmatrix} \cos \alpha & 0 & -\sin \alpha \\ 0 & 1 & 0 \\ \sin \alpha & 0 & \cos \alpha \end{bmatrix} \begin{bmatrix} \cos \beta & -\sin \beta & 0 \\ \sin \beta & \cos \beta & 0 \\ 0 & 0 & 1 \end{bmatrix} \\
 &= \begin{bmatrix} \cos \alpha \cos \beta & -\cos \alpha \sin \beta & -\sin \alpha \\ \sin \beta & \cos \beta & 0 \\ \cos \beta \sin \alpha & -\sin \alpha \sin \beta & \cos \alpha \end{bmatrix} \tag{2.1}
 \end{aligned}$$

Conversely, if the opposite transformation is desired, the procedure is to use the inverse of the previous transformation matrix. Given the matrix is orthogonal, said inverse will be the transpose. The resulting matrix can be seen in the Equation 2.2:

$$R_{\beta\alpha} = R_{\alpha\beta}^{\top} = \begin{bmatrix} \cos \alpha \cos \beta & \sin \beta & \cos \beta \sin \alpha \\ -\cos \alpha \sin \beta & \cos \beta & -\sin \alpha \sin \beta \\ -\sin \alpha & 0 & \cos \alpha \end{bmatrix} \tag{2.2}$$

Finally, the Earth-fixed system will be considered, which will be necessary for various developments. It is characterised by being fixed on the surface of the earth, with the X-axis pointing north, the Y-axis pointing east and the Z-axis pointing towards the centre of the Earth.

On the other hand, similarly to the relation between wind and body systems, the same can be done with the body and Earth-fixed systems [14]. For this purpose, three consecutive rotations will be performed, first around Z-axis of angle ψ , then around Y-axis with angle θ , and finally, a rotation of angle ϕ about X-axis, as shown in Equation 2.3.

$$\begin{aligned}
R_\phi R_\theta R_\psi &= \begin{bmatrix} 1 & 0 & 0 \\ 0 & \cos \phi & \sin \phi \\ 0 & -\sin \phi & \cos \phi \end{bmatrix} \begin{bmatrix} \cos \theta & 0 & -\sin \theta \\ 0 & 1 & 0 \\ \sin \theta & 0 & \cos \theta \end{bmatrix} \begin{bmatrix} \cos \psi & \sin \psi & 0 \\ -\sin \psi & \cos \psi & 0 \\ 0 & 0 & 1 \end{bmatrix} \\
&= \begin{bmatrix} \cos \psi \cos \theta & \cos \theta \sin \psi & -\sin \theta \\ -\sin \psi \cos \phi + \cos \psi \sin \theta \sin \psi & \cos \psi \cos \psi + \sin \psi \sin \theta \sin \phi & \sin \phi \cos \theta \\ \sin \psi \sin \phi + \cos \psi \sin \theta \cos \phi & -\cos \psi \sin \phi + \sin \psi \sin \theta \cos \phi & \cos \phi \cos \theta \end{bmatrix} \quad (2.3)
\end{aligned}$$

2.3 Bryan equations

The first study of flight dynamics was in 1891 by Zhukowsky, with an analysis of the aerodynamic forces, and the variation in position of the centre of gravity. Later studies -Bryan (1904), Lanchester (1908), Painlevé (1909), Bozethat (1911) - contributed to reach a proper definition of aircraft stability, but still not rigorous enough. Finally in 1911 the complete equations as they are known nowadays were published by G. H. Bryan with the book *Stability in Aviation* [7].

The *Bryan Equations* allow describing the dynamics of a rigid body of 6 degrees of freedom: 3 corresponding to linear motion (Equation 2.4, Equation 2.9) and 3 corresponding to angular motion (Equation 2.5). There are two additional systems taken into account: *relations between angular velocity and Euler angles* (Equation 2.6, Equation 2.10) and the *kinematic equations* (Equation 2.7, Equation 2.11).

The equations are obtained by applying Newton's second Law. A number of assumptions have been accepted in order to simplify the calculations:

1. The aircraft is considered as a rigid-body.
2. The origin of the equations is the center of mass and therefore, the gravitational forces do not generate moments.
3. The influence of the Earth's rotation is neglected.
4. The movement of the atmosphere relative to the Earth is not considered.
5. The atmosphere is considered to be free of turbulence.
6. Plane of symmetry is assumed, implying $I_{yx} = I_{yz} = 0$.
7. Rotating inertia effects of engines or propellers are not taken into account.
8. The mass is constant.

Taking into account these hypothesis, the *Bryan Equations* in Cartesian coordinates are [10]:

$$\begin{aligned}
m(\dot{u} + qw - rv) &= T_x + X_{A,b} - mg \sin \theta \\
m(\dot{v} + ru - pw) &= T_y + Y_{A,b} + mg \cos \theta \sin \phi \\
m(\dot{w} + pv - qu) &= T_z + Z_{A,b} + mg \cos \theta \cos \phi
\end{aligned} \quad (2.4)$$

$$\begin{aligned}
(I_{xx}I_{zz} - I_{xz}^2)\dot{p} &= I_{zz}L + I_{xz}N + (I_{xz}(I_{xx} - I_{yy} + I_{zz}))pq + (I_{zz}(I_{yy} - I_{zz}) - I_{xz}^2)rq \\
I_{yy}\dot{q} &= M + (I_{zz} - I_{xx})pr + I_{xz}(r^2 - p^2) \\
(I_{xx}I_{zz} - I_{xz}^2)\dot{r} &= I_{xx}N + I_{xz}L + (I_{xx}(I_{xx} - I_{yy}) + I_{xz}^2)pq + (I_{xz}(I_{yy} - I_{xx} - I_{zz}))rq
\end{aligned} \tag{2.5}$$

$$\begin{aligned}
p &= \dot{\phi} - \dot{\psi} \sin \theta \\
q &= \dot{\theta} \cos \phi + \dot{\psi} \cos \theta \sin \phi \\
r &= \dot{\psi} \cos \theta \cos \phi - \dot{\theta} \sin \phi
\end{aligned} \tag{2.6}$$

$$\begin{aligned}
\dot{x} &= u \cos \psi \cos \theta + v(\cos \psi \sin \theta \sin \phi - \cos \phi \sin \psi) + w(\sin \theta \cos \phi \cos \psi + \sin \phi \sin \psi) \\
\dot{y} &= u \cos \theta \sin \psi + v(\cos \phi \cos \psi + \sin \theta \sin \phi \sin \psi) + w(-\cos \psi \sin \phi + \cos \phi \sin \theta \sin \psi) \\
\dot{z} &= -u \sin \theta + v \cos \theta \sin \phi + w \cos \theta \cos \phi
\end{aligned} \tag{2.7}$$

An additional set of equations is to be taken into account in order to be able to define the aerodynamic angles in Cartesian coordinates:

$$\begin{aligned}
\alpha &= \arctan \frac{w}{u} \\
\beta &= \arcsin \frac{v}{\sqrt{u^2 + v^2 + w^2}}
\end{aligned} \tag{2.8}$$

Whereas in wind axes, by performing the necessary transformations, the system of equations is as follows [11]. It is worth highlighting that index w implies that the variable is expressed in wind axes.

$$\begin{aligned}
m\dot{V} &= T_{x,w} + X_{A,w} - mg \sin \gamma \\
mVr_w &= T_{y,w} + Y_{A,w} + mg \cos \gamma \sin \mu \\
-mVq_w &= T_{z,w} + Z_{A,w} + mg \cos \gamma \cos \mu
\end{aligned} \tag{2.9}$$

$$\begin{aligned}
p_w &= \dot{\mu} - \dot{\chi} \sin \gamma \\
q_w &= \dot{\gamma} \cos \mu + \dot{\chi} \cos \gamma \sin \mu \\
r_w &= \dot{\chi} \cos \gamma \cos \mu - \dot{\gamma} \sin \mu
\end{aligned} \tag{2.10}$$

$$\begin{aligned}
\dot{x} &= V \cos \gamma \cos \chi \\
\dot{y} &= V \cos \gamma \sin \chi \\
\dot{z} &= -V \sin \gamma
\end{aligned} \tag{2.11}$$

It should be noted that due to the complexity that the system corresponding to the rotation acquires when transforming to wind axes, this transformation will not be taken into account, so the Equation 2.5 will be used for both reference systems.

It can be seen that there are twelve equations and fifteen unknowns, since the angular velocities in both reference frames are considered. It is then easy to deduce

that an additional set of equations is needed. Thus, a relation between the angular velocities in body axes and in wind axes is introduced by means of Equation 2.12.

$$\begin{aligned} p_w &= \cos \beta(p \cos \alpha + r \sin \alpha) + \sin \beta(q - \dot{\alpha}) \\ q_w &= -\sin \beta(p \cos \alpha + r \sin \alpha) + \cos \beta(q - \dot{\alpha}) \\ r_w &= r \cos \alpha - p \sin \alpha + \dot{\beta} \end{aligned} \quad (2.12)$$

With the *Bryan Equations* already described, one has the basis for describing any motion of a rigid body.

2.4 Euler-Rodrigues Quaternions

Together with the coordinate system, it is important to determine an orientation method, existing four different possibilities: Euler angles, direction-cosine formulation, Euler parameters and Euler axis. While Euler angles will be the chosen method, it can lead to a singularity known as *gimbal lock*, so it will be necessary to propose a solution free of singularities.

From Equation 2.6 the inverse relation (Equation 2.13) is obtained. It can be easily deduced that if the aircraft is positioned completely vertical ($\theta = \pm\pi/2$), both $\dot{\psi}$ and $\dot{\phi}$ become indeterminate, since $\cos(\pi/2) = 0$ and therefore $\dot{\psi} \rightarrow \infty$, $\dot{\phi} \rightarrow \infty$.

$$\begin{aligned} \dot{\phi} &= p + q \frac{\sin \phi \sin \theta}{\cos \theta} + r \frac{\cos \phi \sin \theta}{\cos \theta} \\ \dot{\theta} &= q \cos \phi - r \sin \phi \\ \dot{\psi} &= \frac{q \sin \phi + r \cos \phi}{\cos \theta} \end{aligned} \quad (2.13)$$

In order to avoid the aforementioned singularity, Euler parameters will be used, also known as Euler-Rodrigues parameters or quaternions. It is worth mentioning that there is not conformity with the notation for the quaternions. Given that the purpose of the flight simulator at issue is to be used by students, the notation will be in accordance to the course *Ampliación de Mecánica del Vuelo*. That way, index 0 corresponds to the scalar component and indices 1 to 3 correspond to the vector components.

Euler (1758) stated that differential movement could be described based on a translation and a rotation around an axis, the Euler Axis. These four parameters -vector $\{\xi, \zeta, \chi\}$ and rotation angle η - are related to the quaternions through Equation 2.14 [11], in such a way that rigid-body orientation is described by these new parameters. The scalar component, q_0 , represents the angle of rotation, while vector components, q_1, q_2, q_3 , define the axis of rotation.

$$\begin{pmatrix} q_0 \\ q_1 \\ q_2 \\ q_3 \end{pmatrix} = \begin{pmatrix} \cos \frac{\eta}{2} \\ \xi \sin \frac{\eta}{2} \\ \zeta \sin \frac{\eta}{2} \\ \chi \sin \frac{\eta}{2} \end{pmatrix} \quad (2.14)$$

The necessary equations for the correct development of the study will be shown below. The calculation process can be consulted in Appendix A.

In the first place, the relation between quaternions and Euler angles is computed:

$$\begin{aligned}
q_0 &= \cos \frac{\psi}{2} \cos \frac{\theta}{2} \cos \frac{\phi}{2} + \sin \frac{\psi}{2} \sin \frac{\theta}{2} \sin \frac{\phi}{2} \\
q_1 &= \cos \frac{\psi}{2} \cos \frac{\theta}{2} \sin \frac{\phi}{2} - \sin \frac{\psi}{2} \sin \frac{\theta}{2} \cos \frac{\phi}{2} \\
q_2 &= \cos \frac{\psi}{2} \sin \frac{\theta}{2} \cos \frac{\phi}{2} + \sin \frac{\psi}{2} \cos \frac{\theta}{2} \sin \frac{\phi}{2} \\
q_3 &= \sin \frac{\psi}{2} \cos \frac{\theta}{2} \cos \frac{\phi}{2} - \cos \frac{\psi}{2} \sin \frac{\theta}{2} \sin \frac{\phi}{2}
\end{aligned} \tag{2.15}$$

The inverse of Equation 2.15 is simply:

$$\begin{Bmatrix} \phi \\ \theta \\ \psi \end{Bmatrix} = \begin{Bmatrix} \arctan\left(\frac{2(q_0q_1+q_2q_3)}{1-2q_1^2-2q_2^2}\right) \\ \arcsin(2(q_0q_2 - q_1q_3)) \\ \arctan\left(\frac{2(q_0q_3+q_1q_2)}{1-2q_2^2-2q_3^2}\right) \end{Bmatrix}. \tag{2.16}$$

Furthermore, it is possible to obtain the temporal evolution of the quaternions as a function of the angular rates:

$$\begin{Bmatrix} \dot{q}_0 \\ \dot{q}_1 \\ \dot{q}_2 \\ \dot{q}_3 \end{Bmatrix} = \frac{1}{2} \begin{bmatrix} -q_1 & -q_2 & -q_3 \\ q_0 & -q_3 & q_2 \\ q_3 & q_0 & -q_1 \\ -q_2 & q_1 & q_0 \end{bmatrix} \begin{Bmatrix} p \\ q \\ r \end{Bmatrix}. \tag{2.17}$$

As previously mentioned, the quaternion notation is free of singularities. However, the interpretation of the results can be complex. This is why they will only be used in manoeuvres in which the *gimbal lock* can occur, thus using the Euler angles in the remaining manoeuvres, as their interpretation is more intuitive.

2.5 Aerodynamic model

With the *Bryan Equations* already presented in Section 2.3, it is left to analyse the acting forces and moments, and thereby be able to solve said equations. This section will focus on aerodynamic expressions, and thrust forces will be studied in the upcoming section.

The first step is to define the aerodynamic derivatives, which are essential to determine the dynamic behaviour of the aircraft. By applying small disturbances, it is possible to linearise the forces and moments equations by means of Taylor series and simplifying in such a way that an expression like follows is obtained.

$$f(x_1, x_2, \dots) = f(x_{1,0}, x_{2,0}, \dots) + \left. \frac{\partial f}{\partial x_1} \right|_0 \Delta x_1 + \left. \frac{\partial f}{\partial x_2} \right|_0 \Delta x_2 + \dots \tag{2.18}$$

Lastly, the notation is simplified taking into account Expression 2.19.

$$\frac{\partial f}{\partial x_1} = f_{x_1} \quad , \quad \Delta x \approx x \tag{2.19}$$

That way and applying drag polar of constant coefficients, the longitudinal derivatives are the following:

$$\begin{aligned}
C_D &= C_{D0} + KC_L^2 \\
C_L &= C_{L0} + C_{L\alpha}\alpha + C_{L\delta E}\delta E + C_{Lq}\frac{c_w}{2V}q + C_{L\dot{\alpha}}\frac{c_w}{2V}\dot{\alpha} \\
C_M &= C_{M0} + C_{M\alpha}\alpha + C_{M\delta E}\delta E + C_{Mq}\frac{c_w}{2V}q + C_{M\dot{\alpha}}\frac{c_w}{2V}\dot{\alpha}
\end{aligned} \tag{2.20}$$

As for the lateral-directional dynamics:

$$\begin{aligned}
C_Y &= C_{Y\beta}\beta + C_{Y\delta A}\delta A + C_{Y\delta R}\delta R + C_{Yp}\frac{b_w}{2V}p + C_{Yr}\frac{b_w}{2V}r + C_{Y\dot{\beta}}\frac{b_w}{2V}\dot{\beta} \\
C_l &= C_{l\beta}\beta + C_{l\delta A}\delta A + C_{l\delta R}\delta R + C_{lp}\frac{b_w}{2V}p + C_{lr}\frac{b_w}{2V}r + C_{l\dot{\beta}}\frac{b_w}{2V}\dot{\beta} \\
C_N &= C_{N\beta}\beta + C_{N\delta A}\delta A + C_{N\delta R}\delta R + C_{Np}\frac{b_w}{2V}p + C_{Nr}\frac{b_w}{2V}r + C_{N\dot{\beta}}\frac{b_w}{2V}\dot{\beta}
\end{aligned} \tag{2.21}$$

It is important to remark that the notation for both lift and roll moment is L , so in order to differentiate both coefficients, l will be used for the roll coefficient and its aerodynamic derivatives.

The resulting aerodynamic forces and moments are:

$$D = \frac{1}{2}\rho(z)S_wV^2C_D \quad Y = \frac{1}{2}\rho(z)S_wV^2C_Y \quad L = \frac{1}{2}\rho(z)S_wV^2C_L \tag{2.22}$$

$$l = \frac{1}{2}\rho(z)S_wb_wV^2C_l \quad M = \frac{1}{2}\rho(z)S_wc_wV^2C_M \quad N = \frac{1}{2}\rho(z)S_wb_wV^2C_N \tag{2.23}$$

As it has already been stated, both wind and body-fixed axes will be applied, so the forces have to be obtained for each coordinate system. Even though Equation 2.22 is expressed in wind axes, since they are related to the aerodynamic velocity, slip angle has to be taken into account. To do so, a rotation around the Z-axis will be performed (Equation 2.24).

$$\begin{aligned}
\begin{Bmatrix} C_{x,w} \\ C_{y,w} \\ C_{z,w} \end{Bmatrix} &= \begin{bmatrix} \cos \beta & -\sin \beta & 0 \\ \sin \beta & \cos \beta & 0 \\ 0 & 0 & 1 \end{bmatrix} \begin{Bmatrix} -C_D \\ -C_Y \\ -C_L \end{Bmatrix} \\
&= \begin{Bmatrix} -C_D \cos \beta + C_Y \sin \beta \\ -C_D \sin \beta - C_Y \cos \beta \\ -C_L \end{Bmatrix}
\end{aligned} \tag{2.24}$$

Regarding the body-fixed system, the transformation matrix from Equation 2.1 is applied, as seen in Equation 2.25.

$$\begin{aligned}
\begin{Bmatrix} C_{x,b} \\ C_{y,b} \\ C_{z,b} \end{Bmatrix} &= \begin{bmatrix} \cos \alpha \cos \beta & -\cos \alpha \sin \beta & -\sin \alpha \\ \sin \beta & \cos \beta & 0 \\ \cos \beta \sin \alpha & -\sin \alpha \sin \beta & \cos \alpha \end{bmatrix} \begin{Bmatrix} -C_D \\ -C_Y \\ -C_L \end{Bmatrix} \\
&= \begin{Bmatrix} -C_D \cos \alpha \cos \beta + C_L \sin \alpha + C_Y \cos \alpha \sin \beta \\ -C_D \sin \beta + C_Y \cos \beta \\ -C_L \cos \alpha - C_D \sin \alpha \cos \beta + C_Y \sin \alpha \sin \beta \end{Bmatrix}
\end{aligned} \tag{2.25}$$

Once the aerodynamic model has been established, it is possible to know the dynamic behaviour of the aircraft, as well as to study the stability. It is only left to define the thrust and a proper propulsion model.

2.6 Propulsion models

Analogously to the aerodynamic forces, a transformation is to be made in order to obtain the thrust in both coordinate systems. It should be noted that this force is already expressed in body axes, however, it is necessary to take into account the existence of torsion in the engine with respect to the velocity. That is to say, there may be cases in which the engine is not completely horizontal, but inclined, so the thrust vector will be broken down into vertical and horizontal coordinates. On the other hand, the thrust on the Y-axis shall be considered to be zero, so that the thrust on body axes will be as follows:

$$\begin{aligned} T_x &= T \cos \varepsilon \\ T_y &= 0 \\ T_z &= T \sin \varepsilon \end{aligned} \tag{2.26}$$

Additionally, there is the possibility that the engines are inclined towards the longitudinal axis of the aircraft, in which case, the angle of inclination would have to be taken into account.

In terms of wind axes, the procedure will consist of using the matrix from Equation 2.2. Once again, the torsion of the engine is to be taken into account, so substituting Equation 2.26 it is obtained:

$$\begin{aligned} \begin{Bmatrix} T_{x,w} \\ T_{y,w} \\ T_{z,w} \end{Bmatrix} &= \begin{bmatrix} \cos \alpha \cos \beta & -\cos \alpha \sin \beta & -\sin \alpha \\ \sin \beta & \cos \beta & 0 \\ \cos \beta \sin \alpha & -\sin \alpha \sin \beta & \cos \alpha \end{bmatrix}^T \begin{Bmatrix} T_x \\ T_y \\ T_z \end{Bmatrix} \\ &= \begin{Bmatrix} T \cos \varepsilon \cos \alpha \cos \beta + T \sin \varepsilon \cos \beta \sin \alpha \\ -T \cos \varepsilon \cos \alpha \sin \beta - T \sin \varepsilon \sin \alpha \sin \beta \\ -T \cos \varepsilon \sin \alpha + T \sin \varepsilon \cos \alpha \end{Bmatrix} \end{aligned} \tag{2.27}$$

The value for the thrust has not been yet defined. For this purpose, a number of propulsion models [8] will be available, from which the user will choose the one that best suits the engine of the aircraft of study. It must be kept in mind that the proposed models are for academic purposes and therefore have their limitations. Another important remark is that the existence of afterburner is not being considered in order to simplify the models.

1. J-C Wanner Model

$$T = k_f \sigma(z) V^{\lambda_f} \delta_P \tag{2.28}$$

Used for turboprops, simple flux jet engines and ramjets. k_f is a constant provided by the manufacturer, while λ_f is a constant that varies according the type of engine:

$$\lambda_f \approx -1 \text{ for turboprops}$$

$$\lambda_f \approx 0 \text{ for simple flux jet engines}$$

$$\lambda_f \approx 1 \text{ for simple flux engines with postcombustion}$$

$$\lambda_f \approx 2 \text{ for ramjets.}$$

2. Aérospatiale Model

$$T = T_0 \left(1 - M + \frac{M^2}{2} \right) \sigma(z) \delta_P \quad (2.29)$$

It is applied with engines whose bypass ratio ranges between 5 and 8.

3. J. Mattingly Model

$$T = T_0 [0.5687 + 0.25(1.2 - M)^3] \sigma(z)^{0.6} \delta_P \quad (2.30)$$

It is used when the bypass ratio of the engine varies between 5 and 8 and, in addition, the Mach number is lower than 0.9.

4. D. Hull Model

$$T = T_0 [\sigma(z)]^a \delta_P \quad (2.31)$$

Applicable when the bypass ratio is low, for turbojets or turbofan engines. a is a constant that depends on the layer of the atmosphere at which the aircraft is flying, and the type of engine, as seen in Table 2.6.1.

Turbojet	a
Troposphere ($z < 11\text{km}$)	1.2
Stratosphere ($z > 11\text{km}$)	1.0
Turbofan	a
Troposphere ($z < 11\text{km}$)	1.0
Stratosphere ($z > 11\text{km}$)	1.0

Table 2.6.1: Value of a according to altitude and type of engine

5. Howe Model

$$T = T_0 \left[1 + 0.4M(M - 2) \left(1 + \frac{BPR}{10} \right) \right] \sigma(z)^{0.9} \delta_P \quad (2.32)$$

Used for turbofan engines with wide range of bypass ratio.

6. Thrust Model for turbofan engines

$$T = T_0 n(z, BPR) \sigma(z) [k_1 + k_2 BPR + M(k_3 + k_4 BPR)] \delta_P \quad (2.33)$$

Applied with turbofan engines, being n a value dependent on bypass ratio and altitude, and k_1, k_2, k_3, k_4 being constants according to bypass ratio and Mach number. Its values can be consulted in the work of Luis Fajardo and Ruxandra Mihaela Botez [16].

Chapter 3

Methodology

The procedure for the development of the flight simulator will be explained below. The aircraft selected for the study is to be presented first, and the data involved will be introduced. Afterwards, the steps followed in the design of the simulator will be detailed, including a brief explanation of the several functions created in order to achieve the objective.

Given the fact that this is a project that will be used by the students, the software selected has been MATLAB, as it is an “easy-to-use” and well-known program.

3.1 Aircraft of study

First of all, an aircraft is going to be selected with which to test the correct performance of the simulator. Later, its behaviour will be analysed by performing a simulation of several manoeuvres.

The chosen aircraft is the F/A-18 Hornet (Figure 3.1.1), a twin-engine supersonic fighter developed in the 1970s by the McDonnell Douglas company.



Figure 3.1.1: McDonnell Douglas F/A-18 [5]

It is of conventional configuration, meaning that the main wing is forward of the horizontal stabiliser, and features two vertical stabilisers.

Geometrical data

The geometric data of the aircraft required for the study are shown in Table 3.1.1.

m	13273	[kg]	I_{xx}	30673.6	[kg · m ²]
b_w	11.43	[m]	I_{yy}	115752	[kg · m ²]
S_w	37.16	[m ²]	I_{zz}	431240	[kg · m ²]
c_w	3.02	[m]	I_{xz}	0	[kg · m ²]
L	17.07	[m]			

Table 3.1.1: Geometrical data of the F-18

It is important to highlight, that while the aircraft dimensions have been obtained from a manual [6], the reference mass has been calculated from the empty weight taking into account 50% of the fuel.

On the other hand, the moments of inertia have been computed from Equation 3.1.

$$\begin{aligned}
 I_{xx} &= m \left(\frac{b_w}{2} \right)^2 R_x^2 \\
 I_{yy} &= m \left(\frac{L}{2} \right)^2 R_y^2 \\
 I_{zz} &= m \left(\frac{b_w + L}{2} \right)^2 R_z^2
 \end{aligned} \tag{3.1}$$

where R_x , R_y and R_z are the radii of gyration. Its value is assumed to depend on the type of aircraft. It can be consulted in document [8]. For the chosen aircraft, the values are as follows.

$$\begin{aligned}
 R_x &= 0.266 \\
 R_y &= 0.346 \\
 R_z &= 0.400
 \end{aligned}$$

Lastly, the product of inertia will be considered null, as it is being assumed principal axes of inertia.

Thrust model

The F/A-18 is powered by two General Electric F-404-GE-402 turbofan engines with low bypass ratio, so the selected propulsion model will be the D. Hull model.

Consequently, and following Table 2.6.1, the parameters used in Equation 2.26 and Equation 2.27, as well as in Equation 2.31 will be, considering a single engine:

T_0	48900	[N]	C_e	$2.3 \cdot 10^{-5}$	[kg/N · s]
ε	0	[rad]	a	1	[—]

Table 3.1.2: Data for the thrust model of the F-18

Provided that there are two engines, the total thrust model will be such that:

$$T = 97800\sigma(z)\delta_P \tag{3.2}$$

Aerodynamic model

The aerodynamic derivatives used to define the aerodynamic model of the aircraft are shown below. Firstly, the longitudinal stability derivatives, calculated using the procedures of the *Mecánica del Vuelo* course [9], are shown in Table 3.1.3.

C_{D0}	0.0100593	$C_{L\alpha}$	4.24237	C_{Lq}	0.94699
K	0.10567	$C_{L\dot{\alpha}}$	0.48787	C_{Mq}	-0.543272
C_{L0}	0	$C_{M\alpha}$	-0.420158	$C_{L\delta E}$	0.82536
C_{M0}	0	$C_{M\dot{\alpha}}$	-0.279883	$C_{M\delta E}$	-0.473495

Table 3.1.3: Value of the longitudinal stability derivatives of the F-18

The derivatives of the lateral-directional dynamics, calculated according to the methods of Marcello R. Napolitano [12], are displayed as follows. They have been classified into stability derivatives in Table 3.1.4 and control derivatives in Table 3.1.5.

$C_{l\beta}$	-0.21195	$C_{l\dot{\beta}}$	0	C_{lr}	0.122386	C_{lp}	-0.258664
$C_{N\beta}$	0.0037412	$C_{N\dot{\beta}}$	0	C_{Nr}	-0.119257	C_{Np}	-0.0364167
$C_{Y\beta}$	-0.575519	$C_{Y\dot{\beta}}$	0	C_{Yr}	0.27852	C_{Yp}	-0.150519

Table 3.1.4: Value of the aerodynamic derivatives of the F-18

$C_{N\delta R}$	-0.147535	$C_{l\delta R}$	0.0443965	$C_{Y\delta R}$	0.352187
$C_{N\delta A}$	-0.001285	$C_{l\delta A}$	0.183164	$C_{Y\delta A}$	0

Table 3.1.5: Value of the control derivatives of the F-18

It should be kept in mind that, as the values of the aerodynamic model are specific for each aircraft, changing the aircraft of study would imply changing the values of the aerodynamic derivatives.

Atmospheric model

The characteristics of the atmosphere vary according to various factors, so it is necessary to define an atmospheric model. Consequently, the *International Standard Atmosphere* model, will be selected, allowing the estimation of average atmospheric properties. In addition, the atmospheric conditions at sea level, $z = 0$, will be defined [18]:

$$\begin{aligned}
 T_0 &= 288.15 \quad K \\
 P_0 &= 101325 \quad Pa \\
 \rho_0 &= 1.225 \quad kg/m^3
 \end{aligned}$$

3.2 Development of the flight simulator

The aim is to create an academic flight simulator from the equations that describe the dynamics of a rigid body. This will be done by means of the numerical integration of the *Bryan Equations* in order to obtain the behaviour of the aircraft. The MATLAB solver *ode45* will be used, being its expression described in Equation 3.3. It is a numerical solver that allows integration of differential equations using explicit Runge-Kutta methods of orders 4 and 5. The integration process can be found in the book [3].

$$[\vec{t}, \vec{F}] = \text{ode45}(\text{odefun}, \text{tspan}, F_0, \text{options}) \quad (3.3)$$

There are four inputs and two outputs. The first input represents the function containing the differential equations, i.e. the *Bryan Equations* for the corresponding case. The next input is the integration time, which will vary according to the case study. The third input, F_0 , is the vector of initial conditions, whose value will depend on each manoeuvre. There will be three different vectors, one for each reference system:

$$\begin{aligned} F_{0, \text{body}} &= [u_0, v_0, w_0, p_0, q_0, r_0, \phi_0, \theta_0, \psi_0, x_0, y_0, z_0, \dot{m}_0] \\ F_{0, \text{wind}} &= [V_0, \beta_0, \alpha_0, p_0, q_0, r_0, \mu_0, \gamma_0, \chi_0, x_0, y_0, z_0, \dot{m}_0] \\ F_{0, \text{quaternions}} &= [u_0, v_0, w_0, p_0, q_0, r_0, q_{0,0}, q_{1,0}, q_{2,0}, q_{3,0}, x_0, y_0, z_0, \dot{m}_0] \end{aligned}$$

Finally, the input *options*, although it is not necessary, will be used to specify the error tolerance. That will allow to indicate the total permissible error, the required accuracy. Thus, trying to make the solution as accurate as possible, the chosen tolerance is 10^{-10} , as can be seen in Equation 3.4.

$$\text{options} = \text{odeset}('RelTol', 1e - 10, 'AbsTol', 1e - 10) \quad (3.4)$$

On the other hand, the outputs will be \vec{t} , which is a vector with each of the integration instants, and \vec{F} , which will be the state vector obtained for each instant.

To assist in understanding the process, the step-by-step process is shown in the following flowchart:

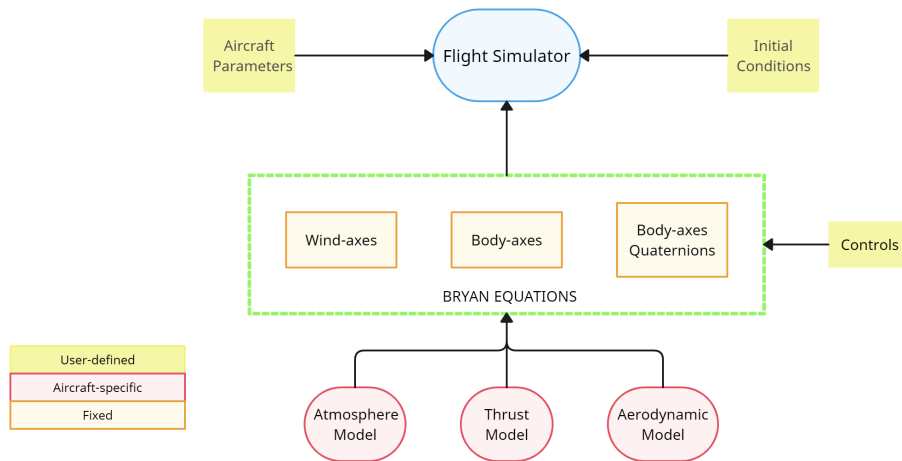


Figure 3.2.1: Flight simulator development

The first stage is to define the atmospheric model based on the ISA model, which will be given by the MATLAB function *atmosisa*. Its expression can be seen in Equation 3.5,

where the input will be the study altitude and the outputs will be the temperature, sound speed, pressure and density at the given altitude.

$$[T(z), a(z), P(z), \rho(z)] = \text{atmosisa}(z) \quad (3.5)$$

The thrust model will be given by the function *thrustmodel.m*. In it, the different propulsion models discussed in Section 2.6 have been introduced, in such a way that the user can select the preferred model. The generic expression can be seen in Equation 3.6:

$$[T, T_x, T_y, T_z, T_{x,w}, T_{y,w}, T_{z,w}] = \text{thrustmodel}(\delta_P, z, V, M, \alpha, \beta) \quad (3.6)$$

The six inputs refer to the conditions needed to calculate the thrust for each model and reference system. The outputs are, on the one hand, the thrust modulus, T , and, on the other hand, the thrust in body-fixed axes, T_x, T_y, T_z , and in wind axes, $T_{x,w}, T_{y,w}, T_{z,w}$, given by Equations 2.26 and 2.27, respectively.

Lastly, the aerodynamic model is provided by the function *coefficients.m*, whose expression can be seen in Equation 3.7.

$$[C_L, C_D, C_Y, C_l, C_M, C_N] = \text{coefficients}(V, \alpha, \dot{\alpha}, p, q, r, \beta, \dot{\beta}, \delta_E, \delta_A, \delta_R) \quad (3.7)$$

Therefore, the function developed allows the aerodynamic coefficients to be obtained from Equations 2.20 and 2.21.

Having defined the three necessary models, it proceeds to the implementation of the *Bryan Equations*, following the diagram in Figure 3.2.1. As a result, three functions will be created for each reference system: *BRYANBODY.m*, *BRYANWIND.m*, *BRYANBODYQUATERNIONS.m*.

For the case study of the body-fixed reference system, Equations 2.4, 2.5, 2.6 and 2.7 will be used. It is important to emphasise that they must be introduced in its explicit form. Equation 2.8 will also be included.

The same approach is adopted for the function relative to the coordinate system on wind axes. In this case, Equations 2.5, 2.9, 2.10 and 2.11 will be needed.

An additional equation has been taken into account when developing the functions related to the equations. It is not only intended to find the time evolution of the state variables, but also to calculate the fuel consumption during the manoeuvres. This will be performed from Equation 3.8.

$$\dot{m}_f = -C_e T \quad (3.8)$$

Whereas the process applied to obtain the functions relative to the body-fixed axes and wind axes coordinate systems is straightforward, a complication arises in the case related to quaternions.

First and foremost, Equations 2.4, 2.5, 2.7 and 2.17 are introduced. As discussed in Section 2.4, the substitution of the Euler angles for the quaternions has to be done, so the Equation 2.16 is also included. Nonetheless, a problem is encountered in the code, for there will be an instant when $\theta = \pm\pi/2$, while both azimuth and bank angle will undergo a sudden change of 180 degrees. In order to avoid said drawback, the

following algorithm is developed [14]:

$$\begin{aligned}
& \text{if } (q_0q_2 - q_1q_3 = 0.5) \\
& \quad \begin{pmatrix} \phi \\ \theta \\ \psi \end{pmatrix} = \begin{pmatrix} 2 \arcsin\left(\frac{q_1}{\cos(\pi/4)}\right) + \psi \\ \pi/2 \\ 0 \end{pmatrix} \\
& \text{elseif } (q_0q_2 - q_1q_3 = -0.5) \\
& \quad \begin{pmatrix} \phi \\ \theta \\ \psi \end{pmatrix} = \begin{pmatrix} 2 \arcsin\left(\frac{q_1}{\cos(\pi/4)}\right) - \psi \\ -\pi/2 \\ 0 \end{pmatrix} \\
& \text{else} \\
& \quad \begin{pmatrix} \phi \\ \theta \\ \psi \end{pmatrix} = \begin{pmatrix} \arctan\left(\frac{2(q_0q_1+q_2q_3)}{1-2q_1^2-2q_2^2}\right) \\ \arcsin(2(q_0q_2 - q_1q_3)) \\ \arctan\left(\frac{2(q_0q_3+q_1q_2)}{1-2q_2^2-2q_3^2}\right) \end{pmatrix}
\end{aligned} \tag{3.9}$$

The last step to complete the simulator consists of establishing the value of the controls. Two scenarios might be considered. Firstly, one can start from equilibrium, with the possibility of modifying the controls later. To do so, the aircraft has to be trimmed, considering cruise flight, i.e. rectilinear trajectory in the horizontal plane, with constant initial conditions. The alternative approach is to start from non-equilibrium conditions. In other words, the initial conditions specific to the manoeuvre to be studied would be introduced.

In this way, the system constituted by Equations 2.4 and 2.5 will be solved. In the event of studying manoeuvres in wind axes, the system to be solved will be the one formed by Equations 2.5 and 2.9.

There also exists the possibility of modifying the controls during the manoeuvres. In order to achieve that, Equation 3.10 shall be applied.

$$\text{unitstep} = t \geq \text{unitsteptime} \tag{3.10}$$

As a result, a unitary step will be introduced at the instant $t = \text{unitsteptime}$, previously defined by the user. Eventually the controls will be given by Equation 3.11.

$$\begin{aligned}
\delta_P &= \delta_{P,initial} + \text{unitstep} * (\delta_{P,final} - \delta_{P,initial}) \\
\delta_E &= \delta_{E,initial} + \text{unitstep} * (\delta_{E,final} - \delta_{E,initial}) \\
\delta_A &= \delta_{A,initial} + \text{unitstep} * (\delta_{A,final} - \delta_{A,initial}) \\
\delta_R &= \delta_{R,initial} + \text{unitstep} * (\delta_{R,final} - \delta_{R,initial})
\end{aligned} \tag{3.11}$$

If no modification in the controls is desired, it is sufficient to set the same final and initial values. It is important to stress that the only modifications allowed are to the controls, as they simulate the modifications made by the pilot should it be a real case.

The design of the simulator has been a process of trial and error, which has been gradually refined by adding the equations one at a time and carefully testing their correct operation. Moreover, it has been planned to be interactive, allowing the user to choose the coordinate system as well as the thrust model desired to be used. The final code developed in the current section can be found in Appendix C.

Chapter 4

Presentation of results

The present chapter provides an analysis of the performance of the McDonnell Douglas F-18 Hornet during the execution of different manoeuvres using the flight simulator previously developed. To begin with, the initial conditions introduced in the simulator for each case of study will be presented, as well as the reference frame established. It should be stressed that, despite presenting the results in a single reference system, the study has been carried out both in wind axes and in body-fixed axes, as well as with the Euler-Rodrigues quaternions.

Subsequently, the time evolution of the variables and the trajectory followed by the aircraft will be displayed. Finally, the fuel consumed during each manoeuvre will be estimated.

The initial flight conditions selected for the study of all scenarios are as follows:

- $z_0 = 3000$ m
- $V_0 = 175$ m/s.

Once the flight dynamics study of the McDonnell Douglas F-18 has been carried out, it will be proceeded to test the simulator operation for a commercial aircraft. For this purpose, data of the Airbus A320-200 will be applied and the vertical equilibrium and gliding flight manoeuvres will be simulated. As a result, it will be ensured that the simulator can be used independently of the aircraft under study.

4.1 Vertical plane equilibrium

The first manoeuvre will be the equilibrium in the vertical plane, studied in body-fixed axes. The manoeuvre is of interest since it allows to verify whether the equations are correct, as the attitude of the aircraft would be predictable. On this basis, the proper operation of the flight simulator will be ensured.

Vertical equilibrium is achieved in such a way that, starting from the controls applied, the aircraft will stabilise without the intervention of the pilot, while simultaneously maintaining the lateral-directional dynamic parameters null.

First of all, the initial conditions are summarised in Table 4.1.1, followed by the value of the aerodynamic angles and controls applied in Table 4.1.2.

u_0	174.55	[m/s]	p_0	0	[rad/s]	ϕ_0	0	[rad]	x_0	0	[m]
v_0	0	[m/s]	q_0	0	[rad/s]	θ_0	0.0713	[rad]	y_0	0	[m]
w_0	12.48	[m/s]	r_0	0	[rad/s]	ψ_0	0	[rad]	z_0	3000	[m]

Table 4.1.1: Value of the initial conditions for the vertical equilibrium

α_0	0.0713	[rad]	δ_E	-0.0633	[rad]
β_0	0	[rad]	δ_A	0	[rad]
δ_P	0.1192	[-]	δ_R	0	[rad]

Table 4.1.2: Value of the controls and the aerodynamic angles for the vertical equilibrium

The integration time is defined for $t_f = 300$ s. The results obtained are depicted as follows.

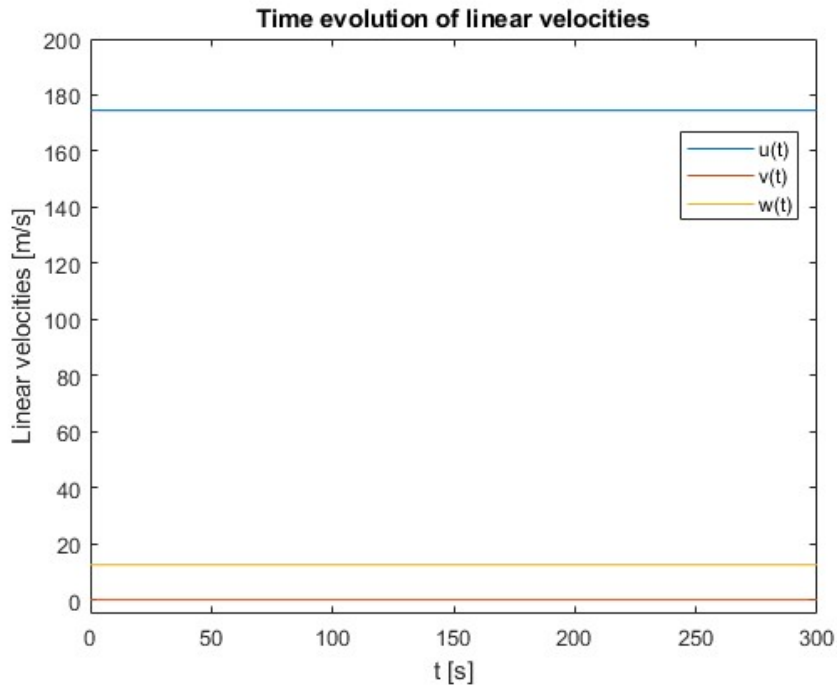


Figure 4.1.1: Plot of the time evolution of the linear velocities for vertical equilibrium

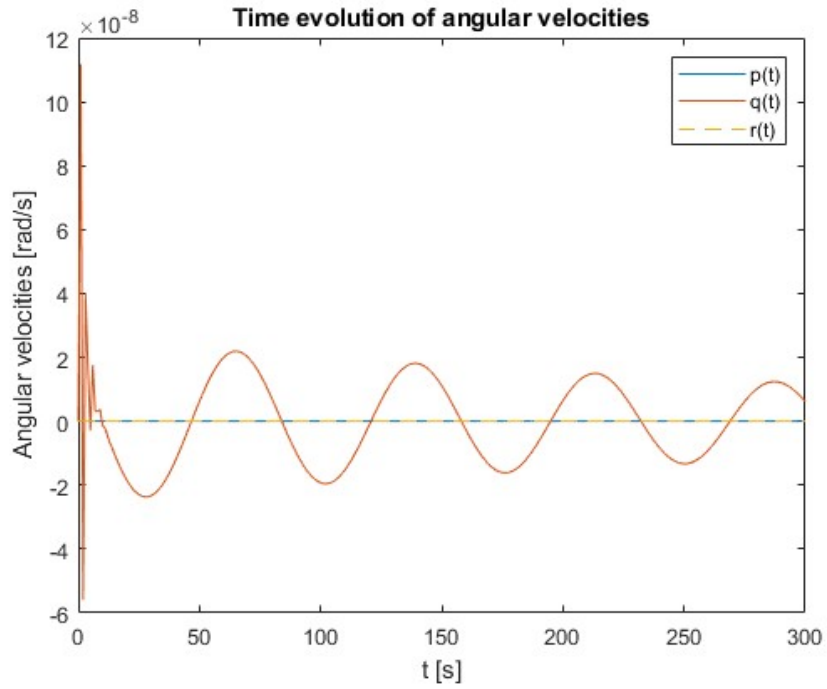


Figure 4.1.2: Plot of the time evolution of the angular velocities for vertical equilibrium

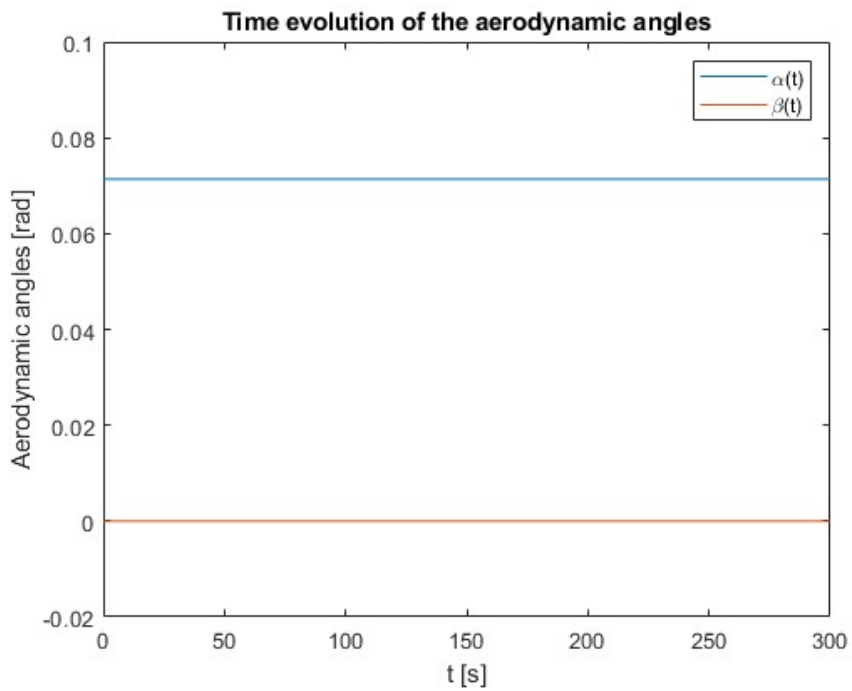


Figure 4.1.3: Plot of the time evolution of the aerodynamic angles for vertical equilibrium

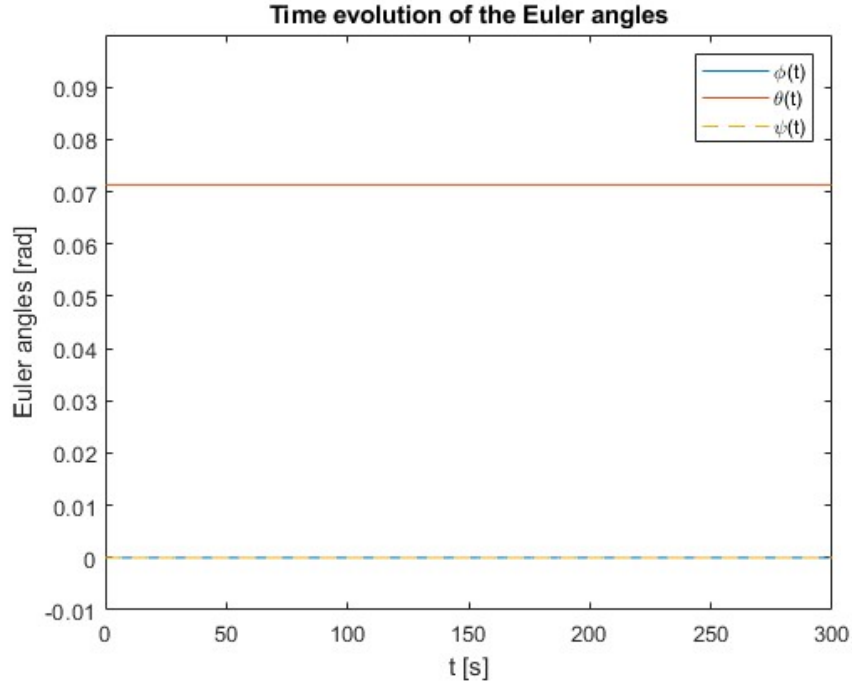


Figure 4.1.4: Plot of the time evolution of the Euler angles for vertical equilibrium

It is noticeable that the variables are constant with time, while the parameters that may perturb the vertical trajectory remain null in time. In other words, on the one hand, the lateral velocity $v(t)$ is null (Figure 4.1.1), indicating that the plane does not move laterally. The null angular velocities $p(t)$ and $q(t)$ (Figure 4.1.2) imply that there is no motion around the X, Z axes, respectively. This statement is supported by Figure 4.1.4, where the bank angle, $\phi(t)$ and azimuth angle, $\psi(t)$ are null. Thus it is confirmed that the aircraft follows a rectilinear trajectory in the vertical plane.

Nevertheless, it is clear from Figure 4.1.2 that one of the variables, the angular velocity $q(t)$, is oscillating. This is mainly a consequence of numerical error, either due to the solution or to lack of precision in the conditions introduced. However, the order of magnitude of said oscillation is 10^{-8} rad/s, so it therefore may be considered invariant. A further distinction is made between short period and phugoid, both of which are characteristic modes of longitudinal dynamics. On the other hand, the reduction of the amplitude indicates that, after a certain period of time, the aircraft will stabilise in an equilibrium position, which would be clear if the integration time were increased by several minutes.

To conclude, Figure 4.1.5 illustrates the two-dimensional trajectory of the aircraft, confirming what was previously stated.

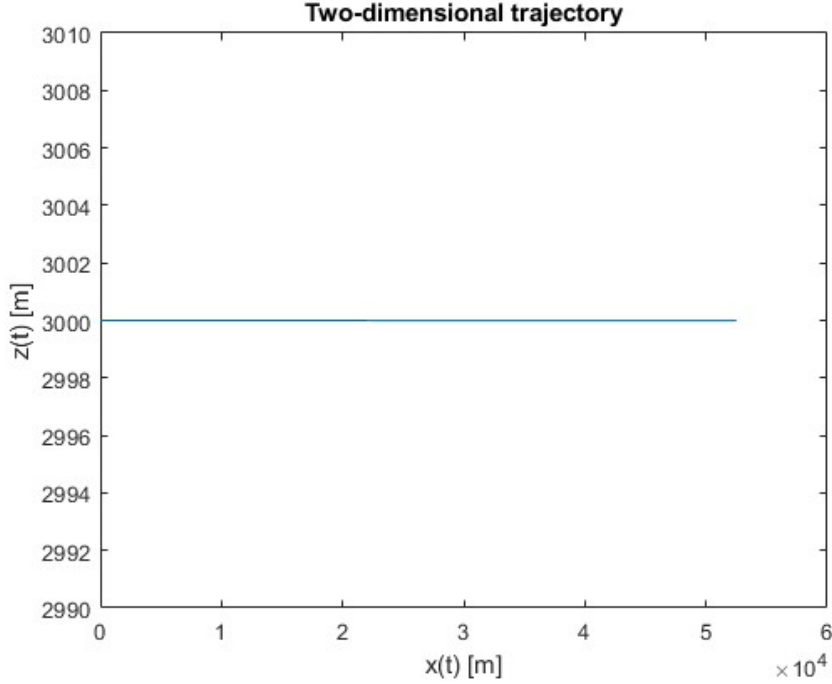


Figure 4.1.5: Plot of the two-dimensional trajectory of the vertical equilibrium

Fuel consumption during the manoeuvre is $m_f = 59.71$ kg.

4.2 Vertical turn

The following manoeuvre to be analysed is the vertical turn, also referred to as a loop. This consists of a 360-degree turn in the vertical plane. In this sort of exercise, the gimbal lock phenomenon occurs, hence, as mentioned in the Section 2.4, it will be studied in body-fixed axes through the application of the Euler-Rodrigues quaternions.

To perform the manoeuvre, the aircraft will start from steady flight in the vertical plane and afterwards, the loop will be executed. The initial controls will be those seen in Table 4.1.2, and then modified to reach the values in Table 4.2.1. The values for the controls were computed assuming maximum throttle in order to be able to complete the turn. Once the loop is initiated, constant controls will be assumed for the entire turn, although this is not standard for this type of manoeuvre, as the pilot will normally vary the controls to suit the conditions of the turn. It will be done in this configuration in order to simplify the calculations.

δ_E	-0.2968	[rad]	δ_A	0	[rad]
δ_P	1	[-]	δ_R	0	[rad]

Table 4.2.1: Value of the controls for the vertical loop manoeuvre

As the starting point is a vertical equilibrium, the initial conditions shall be those provided in Table 4.1.1. The initial values of the quaternions according to Table 4.2.2 shall also be taken into account.

$q_{0,0}$	0.9994	$q_{2,0}$	0.0357
$q_{1,0}$	0	$q_{3,0}$	0

Table 4.2.2: Initial value of the quaternions for the loop manoeuvre

The integration time for the manoeuvre will be $t_f = 40$ s, whilst the turn will commence at the instant $t = 10$ s. The results obtained are presented as follows.

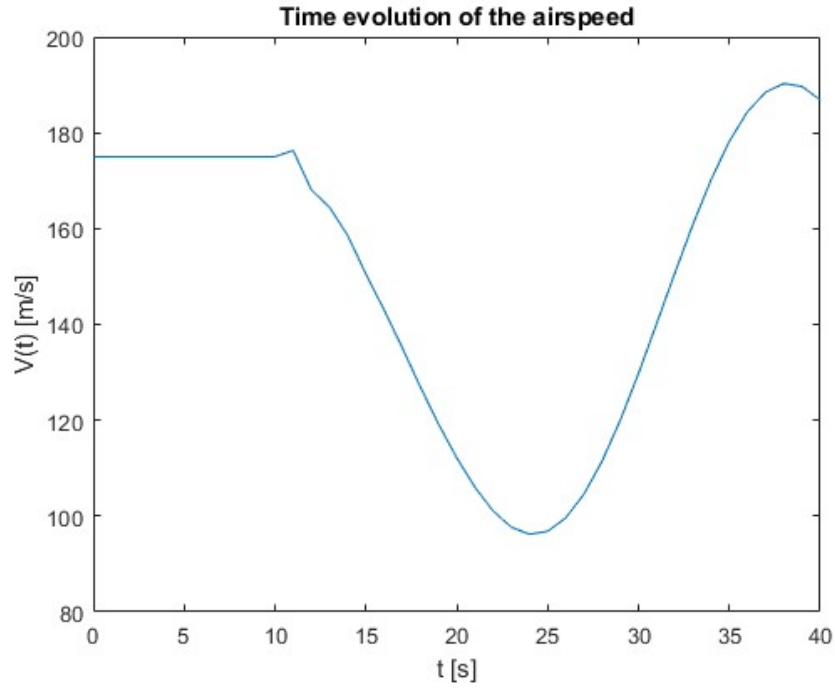


Figure 4.2.1: Plot of the time evolution of the airspeed for the loop

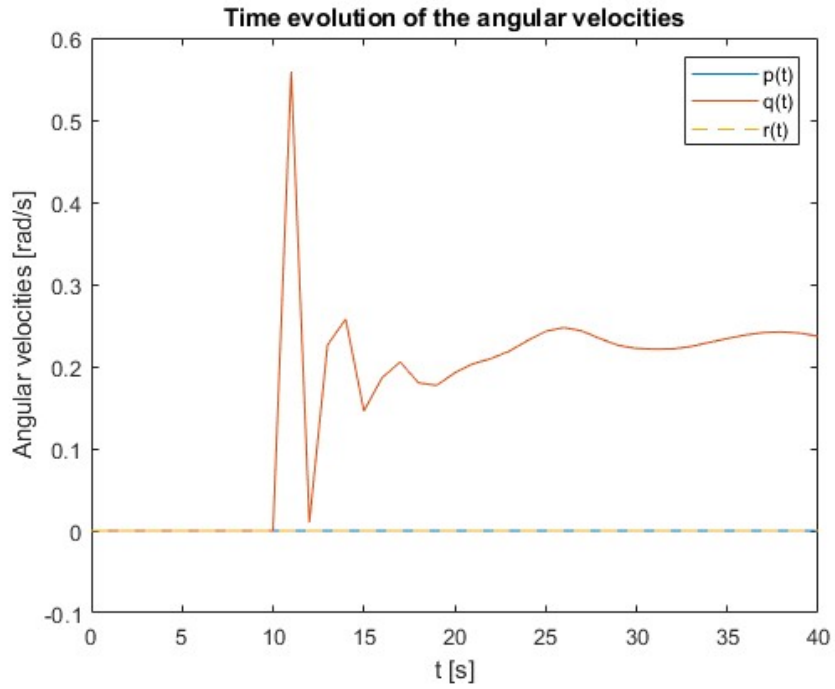


Figure 4.2.2: Plot of the time evolution of the angular velocities for the loop

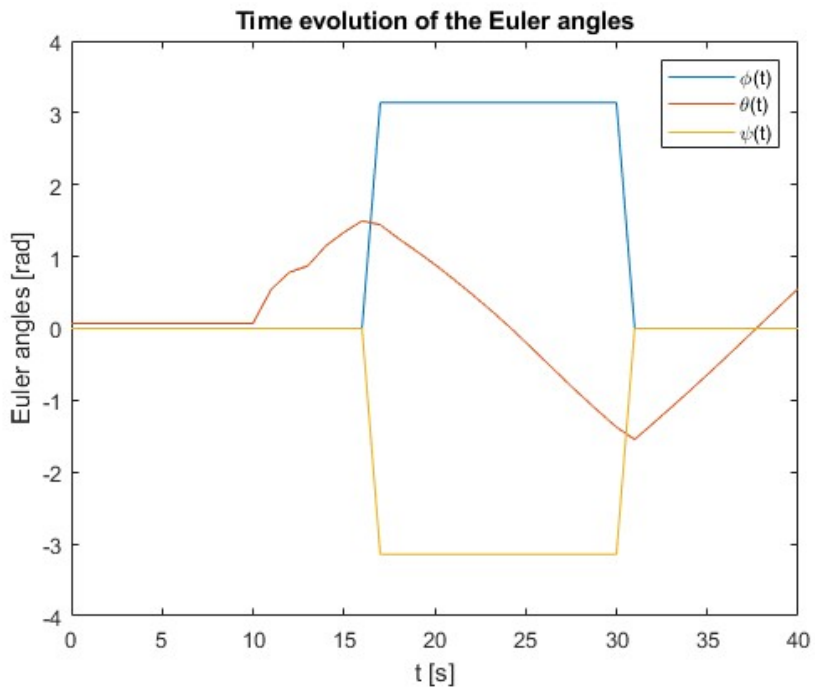


Figure 4.2.3: Plot of the time evolution of the Euler angles for the loop

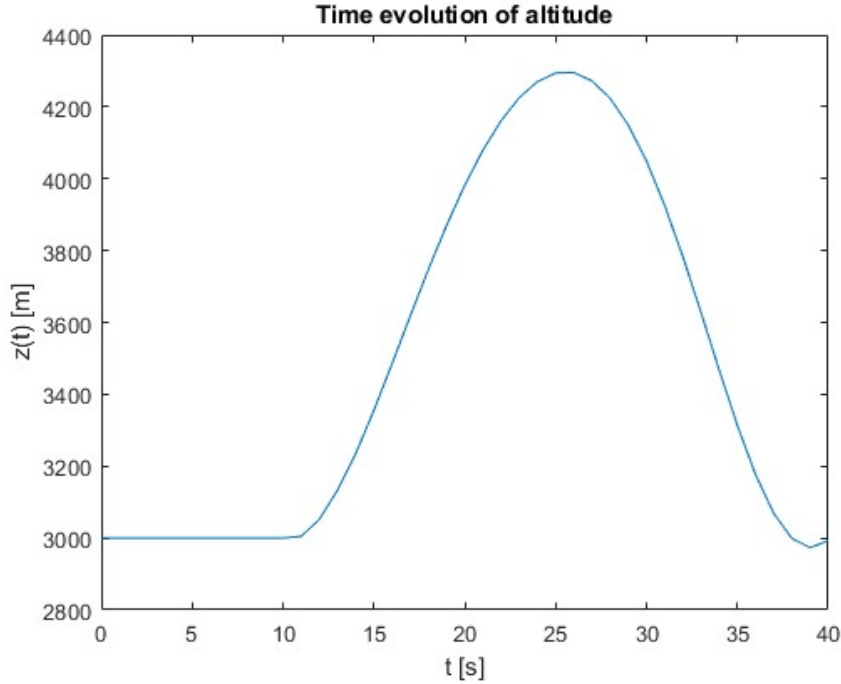


Figure 4.2.4: Plot of the time evolution of the altitude for the loop

Within the first ten seconds, the proper behaviour of the aircraft in the steady flight in the vertical plane is observed, as explained in the previous section. As soon as the controls are modified, a significant change in the variables becomes apparent. However, in Figure 4.2.2 the angular velocities $p(t)$ and $r(t)$ confirm yet again that this is a manoeuvre contained in the vertical plane. On the other hand, the angular velocity $q(t)$ oscillates around a positive value until it finally stabilises, indicating that the aircraft is moving around the Y-axis in upward direction. This is consistent with the type of manoeuvre that is being carried out by the F-18.

Figure 4.2.3 illustrates the time evolution of the Euler angles, which has a complex interpretation. Analysing the evolution of the elevation angle, $\theta(t)$, it can be seen that it does not exceed certain values. This is because it is confined to the interval $[-\pi/2, \pi/2]$ rad. Once the maximum value is reached, a roll of $\phi = \pi$ rad and a yaw of $\psi = -\pi$ rad are produced, thus turning the aircraft inverted, mathematically speaking. By doing so, the manoeuvre can be completed without going out of range, while at the same time avoiding the *gimbal lock* as discussed in Section 2.4.

Now comparing Figures 4.2.1 and 4.2.4, related to velocity and altitude, correspondingly, a clear relationship can be observed. As the aircraft ascends the velocity decreases, reaching its maximum and minimum value respectively at $t = 25$ s, while as the aircraft descends, the velocity increases. This is due to the fact that during the ascent, the force of gravity acts contrary to the movement, so that, even though there is enough thrust to carry out the manoeuvre, speed is still reduced. The opposite occurs when descending, considering also that potential energy is being lost and therefore kinetic energy is gained.

Lastly, the trajectory followed by the aircraft is shown in Figure 4.2.5. It is interesting to highlight that although it is a turn, it is not describing a circle. This is mainly because the radius of the turn will depend on the speed, which, as previously seen, will vary throughout the manoeuvre.

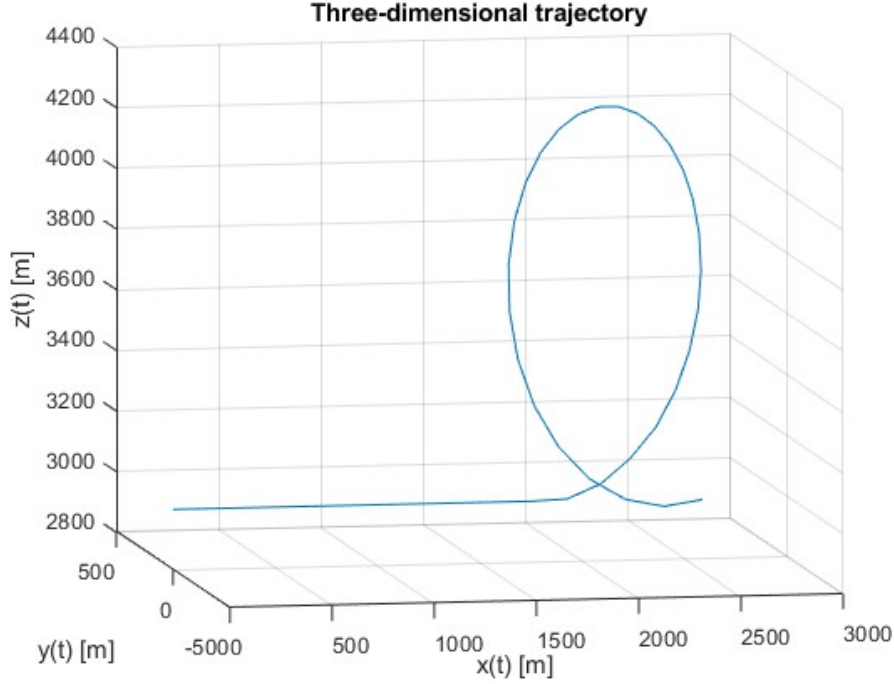


Figure 4.2.5: Plot of the three-dimensional trajectory of the loop

The fuel consumed during the operation is $m_f = 48.79$ kg.

4.3 Gliding flight

Despite the fact that there exist aircraft specifically designed for this purpose, gliding flight can be performed by any fixed-wing aircraft. It occurs when there is a lack of thrust, either caused by a sudden failure of all engines or fuel exhaustion. In order to perform the manoeuvre it will be assumed that the aircraft suddenly suffers an irreversible engine failure, departing from the conditions presented in Table 4.3.1. On the other hand, the controls entered by the pilot are shown in Table 4.3.2. The study will be performed in wind axes.

V_0	175	[m/s]	p_0	0	[rad/s]	μ_0	0	[rad]	x_0	0	[m]
β_0	0	[rad]	q_0	0	[rad/s]	γ_0	-0.0665	[rad]	y_0	0	[m]
α_0	0.0715	[rad]	r_0	0	[rad/s]	χ_0	0	[rad]	z_0	3000	[m]

Table 4.3.1: Value of the initial conditions for the gliding flight manoeuvre

δ_P	0	[-]	δ_A	0	[rad]
δ_E	-0.0635	[rad]	δ_R	0	[rad]

Table 4.3.2: Value of the controls for the gliding flight

The integration time will be $t_f = 316$ s, the time it takes to impact. The response obtained during the manoeuvre can be seen below.

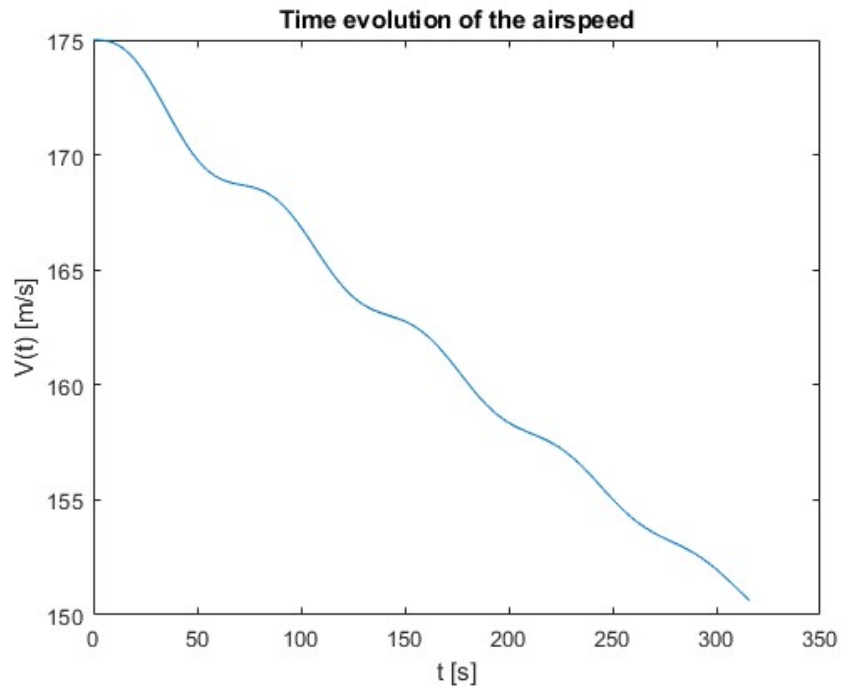


Figure 4.3.1: Plot of the time evolution of the airspeed for the gliding flight

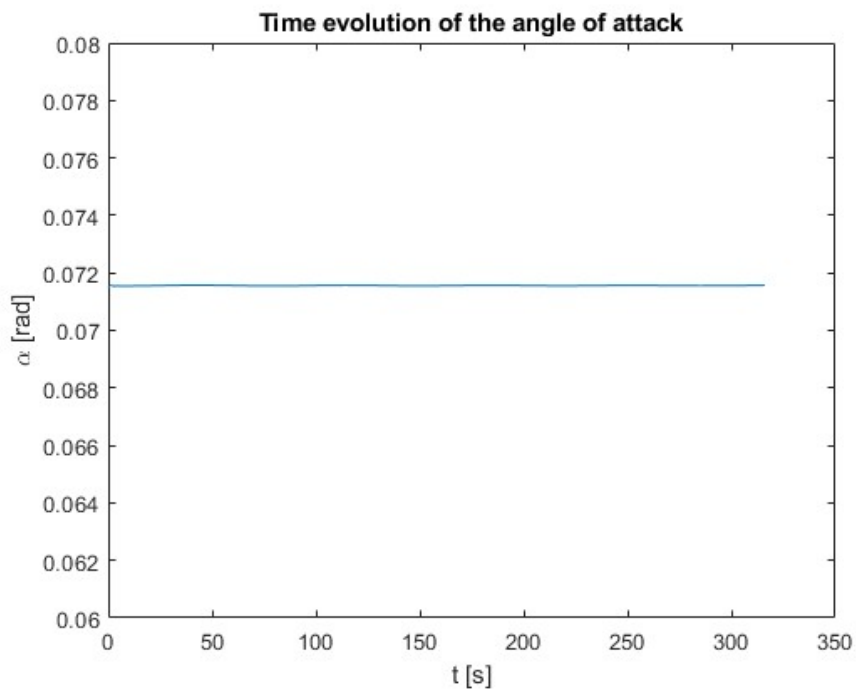


Figure 4.3.2: Plot of the time evolution of the angle of attack for the gliding flight

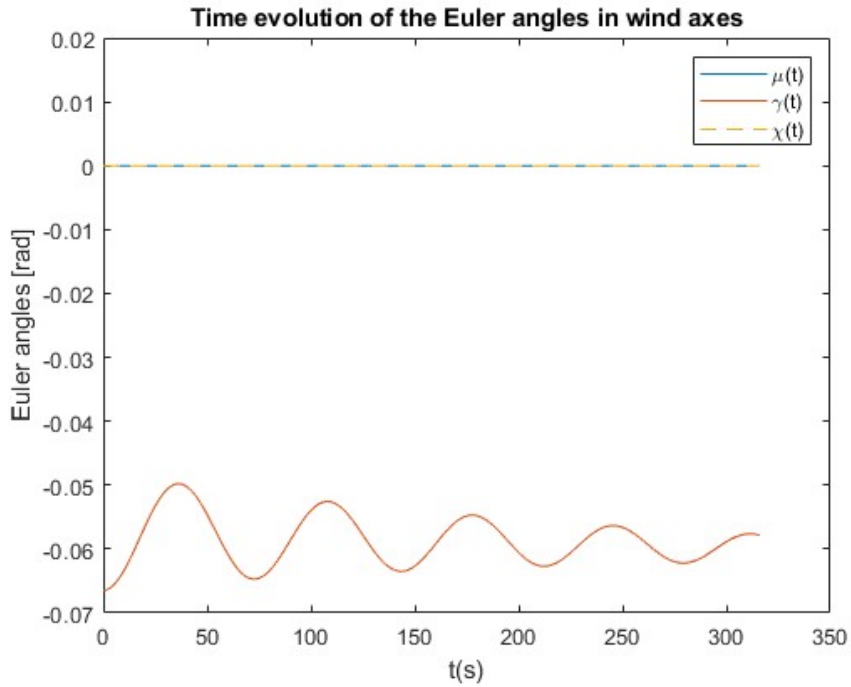


Figure 4.3.3: Plot of the time evolution of the Euler angles for the gliding flight

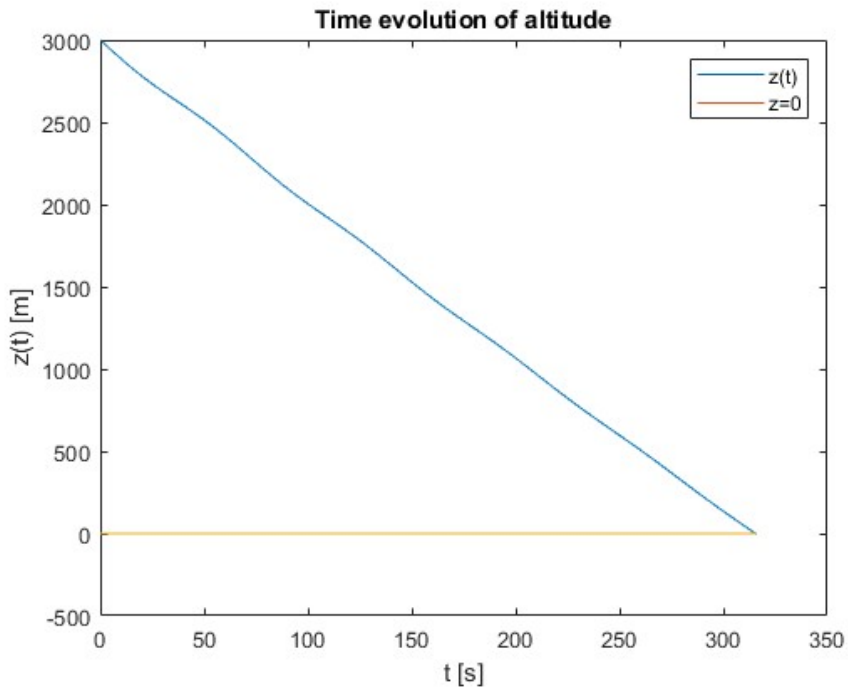


Figure 4.3.4: Plot of the time evolution of the altitude for the gliding flight

In gliding flight the airspeed is established by the deflection of the elevator. In other words, the pilot adjusts the elevator so that the aircraft tends to fly at an specific angle of attack which will determine the airspeed. However, in the scenario under study, the deflection is constant, so the angle of attack will remain invariant over time, as shown in Figure 4.3.2. According to this reasoning, it could be concluded that the velocity would also remain constant, but in Figure 4.3.1 it is noticed that the velocity diminishes.

That is due to the fact that since thrust is null, drag is the only force acting on the longitudinal axis, thus slowing down the aircraft. If both elevator deflection and angle of attack remain constant, and the speed decreases, the lift generated by the aircraft will be reduced, so it will not be able to compensate for the weight. Consequently the altitude will decrease as shown in Figure 4.3.4, until subsequent impact.

Lastly, Figure 4.3.3 represents the time evolution of the Euler angles in wind axes. It is of particular interest the angle of the slope, $\gamma(t)$, which keeps oscillating around a negative value, indicating that the aircraft is descending. On the other hand, the bank angle $\mu(t)$ and the heading angle $\chi(t)$ confirm that the manoeuvre has been performed in the vertical plane.

The trajectory followed by the aircraft is represented in Figure 4.3.5, where a surface has also been plotted in reference to the ground in order to show the impact more effectively. The distance travelled before hitting the ground is 50 km.

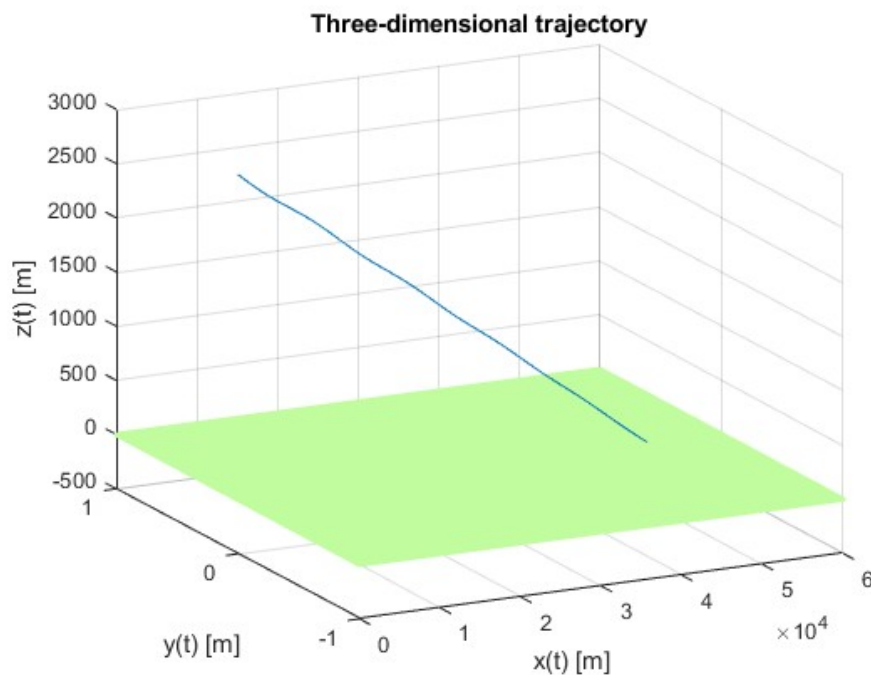


Figure 4.3.5: Plot of the three-dimensional trajectory of the gliding flight

Being the thrust non-existent, no fuel has been consumed during the glide flight, so $m_f = 0$ kg.

4.4 Dive recovery

The following manoeuvre consists of a dive recovery, meaning that the aircraft will initially fly in vertical position with the nose pointing downwards, known as nosedive, so the pilot has to reach null slope. In order to achieve so, it will be assumed that the pilot applies maximum thrust and the proper controls to obtain the maximum lift coefficient, and therefore analysing how long it takes to recover and the altitude at which it occurs. The study will be carried out in the wind axes coordinate system. The initial conditions can be seen in Table 4.4.1, while the controls entered shall be those shown in Table 4.4.2.

V_0	175	[m/s]	p_0	0	[rad/s]	μ_0	0	[rad]	x_0	0	[m]
β_0	0	[rad]	q_0	0	[rad/s]	γ_0	-1.5708	[rad]	y_0	0	[m]
α_0	0.001	[rad]	r_0	0	[rad/s]	χ_0	0	[rad]	z_0	3000	[m]

Table 4.4.1: Value of the initial conditions for the dive recovery manoeuvre

δ_E	-0.2968	[rad]	δ_A	0	[rad]
δ_P	1	[-]	δ_R	0	[rad]

Table 4.4.2: Value of the controls for the dive recovery manoeuvre

An integration time $t_f = 10$ s will be established. The response obtained is displayed hereunder.

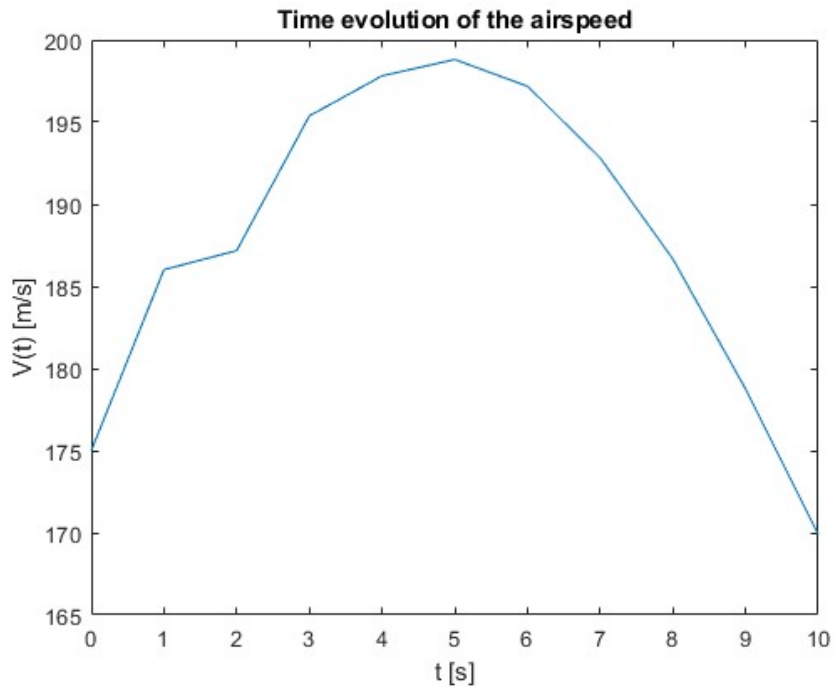


Figure 4.4.1: Plot of the time evolution of the airspeed for the dive recovery manoeuvre

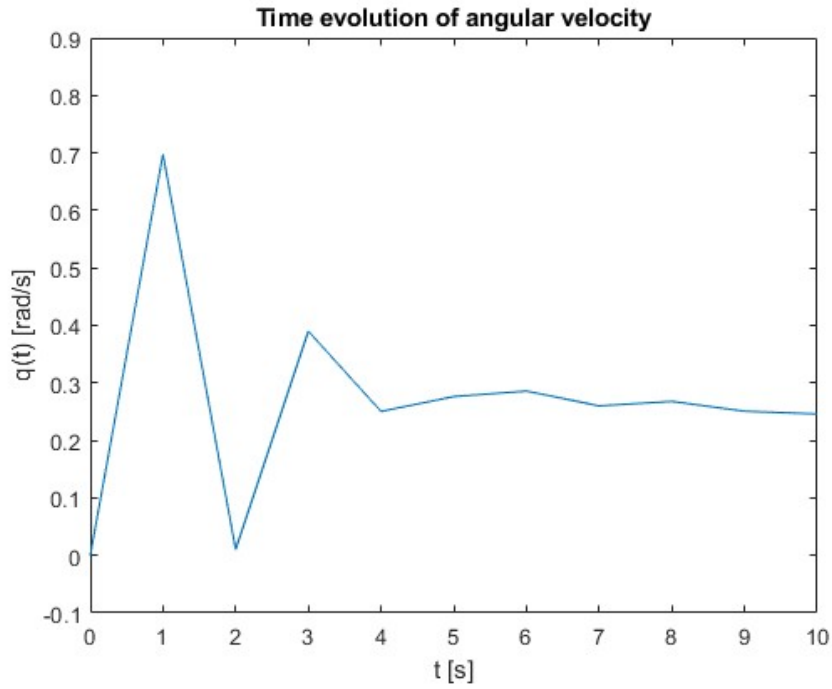


Figure 4.4.2: Plot of the time evolution of the angular velocity q for the dive recovery manoeuvre

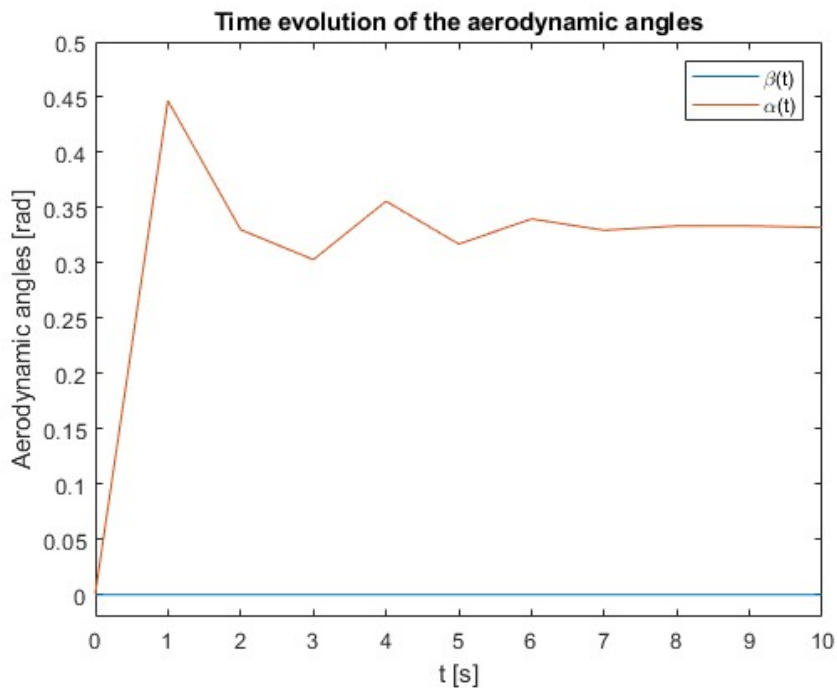


Figure 4.4.3: Plot of the aerodynamic angles for the dive recovery manoeuvre

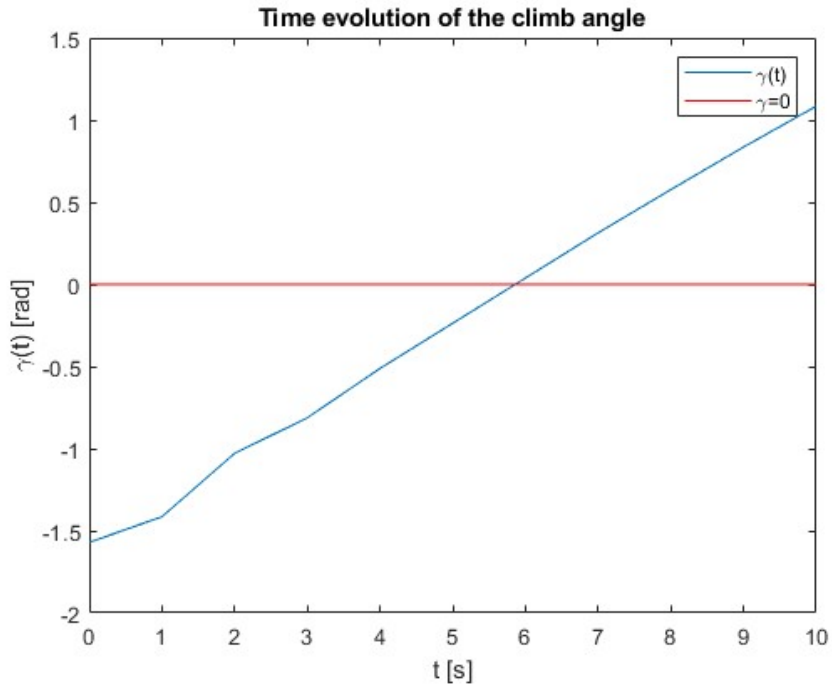


Figure 4.4.4: Plot of the time evolution of the climb angle for the dive recovery manoeuvre

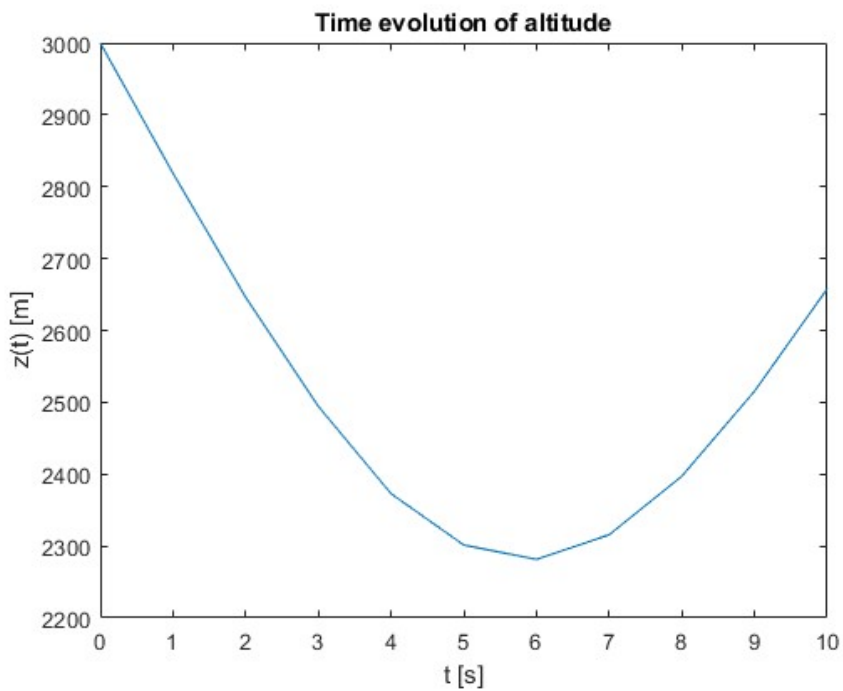


Figure 4.4.5: Plot of the time evolution of the altitude for the dive recovery manoeuvre

The performance of the aircraft in the current manoeuvre under study is similar to that obtained during the vertical turn. Comparing Figures 4.4.1 and 4.4.5 it can be appreciated that as the aircraft loses altitude, the airspeed increases. This is due to the fact that not only is maximum thrust being applied, but as the altitude diminishes,

the thrust will increase, and therefore the speed will be higher. Consequently, the lift will increase, so the nose of the aircraft will progressively rise. This movement will be reflected in the evolution of the slope (Figure 4.4.4), as it gradually increases from an initial value $\gamma = -90^\circ$ until it reaches zero slope at $t = 6$ s. It is from this moment that the aircraft begins to climb. Thus, as it gains altitude, the speed is reduced because, even with maximum thrust, the force of gravity acts contrary to the movement, so the aircraft will decelerate.

On the other hand, Figure 4.4.3 shows the evolution of the aerodynamic angles. It can be noticed how the angle of attack augments at the commencement of the manoeuvre, primarily due to the controls that have been introduced. That is to say, as the necessary controls are applied to obtain the maximum lift coefficient, the angle of attack will adopt the corresponding value. Furthermore, Figure 4.4.2 confirms that the pitch-up movement performed by the aircraft, as a positive value indicates a positive movement about the Y-axis.

Figure 4.4.5 additionally illustrates the loss of altitude suffered by the aircraft, eventually reaching $z = 2300$ m.

The trajectory followed by the aircraft during recovery is shown in Figure 4.4.6.

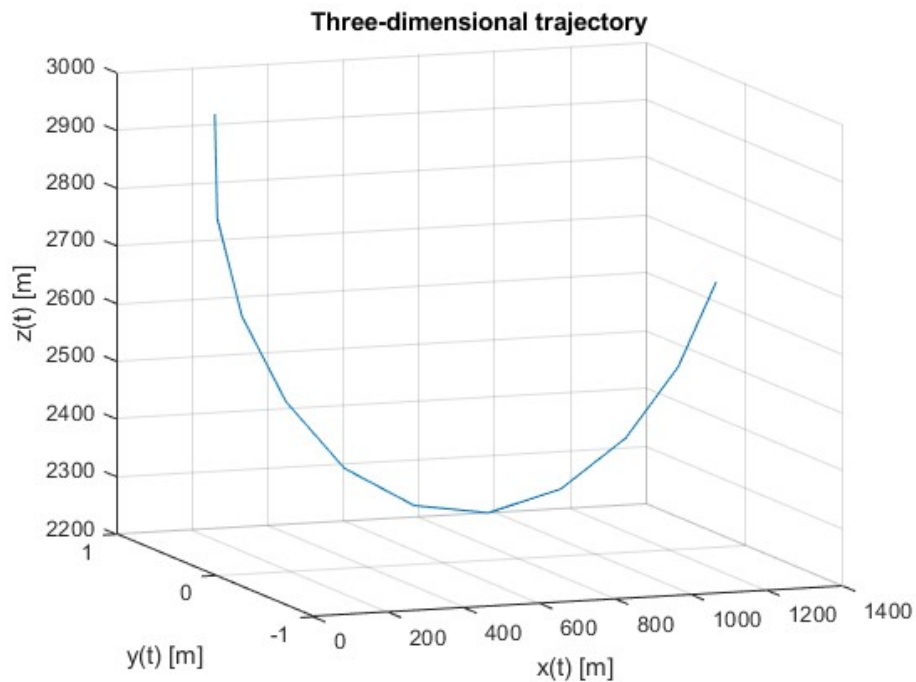


Figure 4.4.6: Plot of the three-dimensional trajectory of the dive recovery manoeuvre

Lastly, fuel consumption during dive recovery has been $m_f = 17.58$ kg.

4.5 Horizontal turn

The performance of the F-18 Hornet during a turn in the horizontal plane will now be analysed. The standard procedure when performing a turn would be to bank the aircraft, as this is the most efficient approach. However, for the case study, null roll will be imposed. The manoeuvre will be studied in wind axes. The initial conditions

considered are presented in Table 4.5.1. Table 4.5.2 contains the value of the controls. The angular velocity of the turn shall be further defined as: $\Omega = 0.0343$ rad/s.

V_0	175	[m/s]	p_0	-0.0024	[rad/s]	μ_0	0	[rad]	x_0	0	[m]
β_0	0.3637	[rad]	q_0	0	[rad/s]	γ_0	0	[rad]	y_0	0	[m]
α_0	0.0698	[rad]	r_0	0.0342	[rad/s]	χ_0	0	[rad]	z_0	3000	[m]

Table 4.5.1: Value of the initial conditions for the horizontal turn

δ_E	-0.0620	[rad]	δ_A	0.4189	[rad]
δ_P	0.6811	[-]	δ_R	0.0047	[rad]

Table 4.5.2: Value of the controls for the horizontal turn

The integration time is defined as $t_f = 100$ s, resulting in the response displayed as follows.

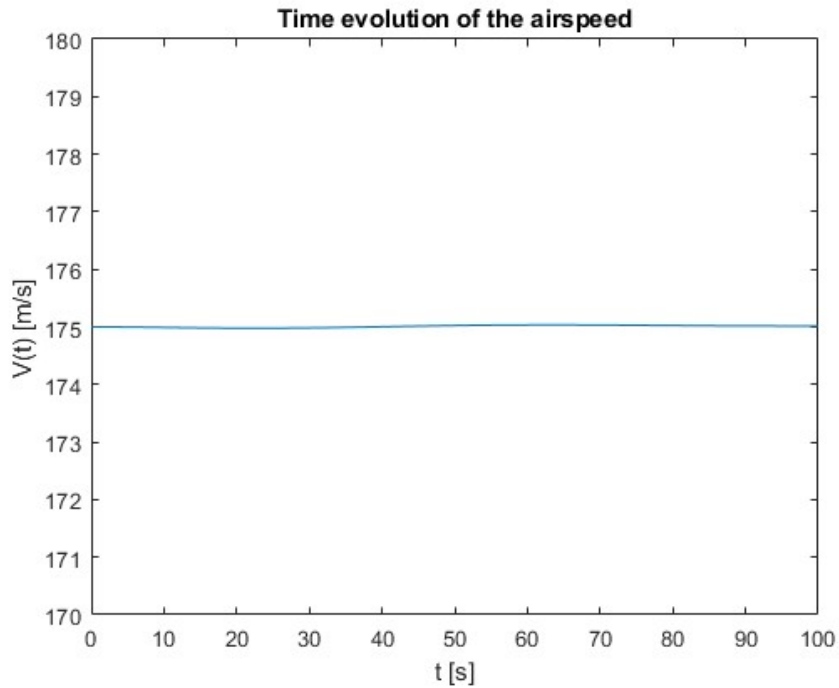


Figure 4.5.1: Plot of the time evolution of the airspeed for the horizontal turn

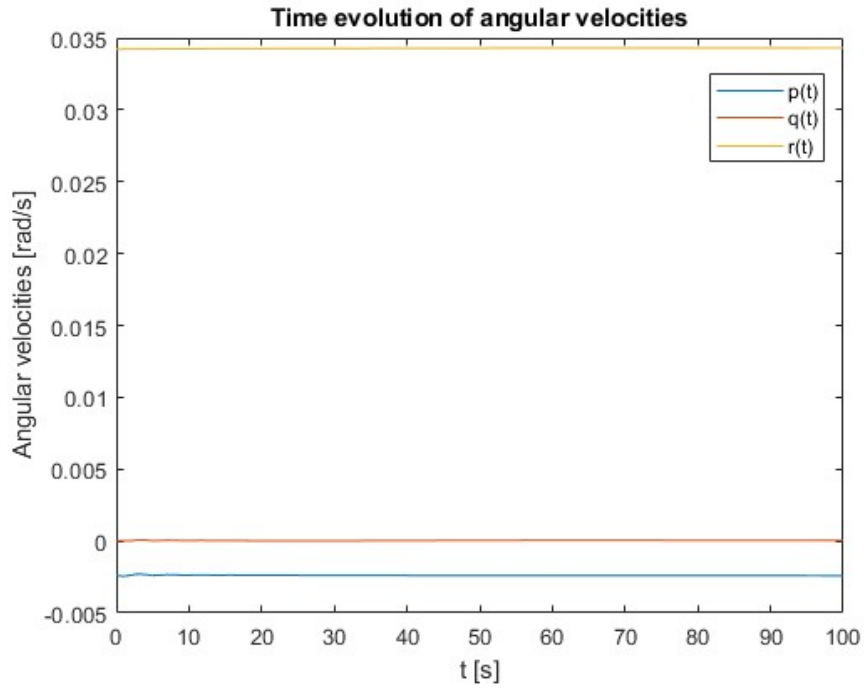


Figure 4.5.2: Plot of the time evolution of the angular velocities for the horizontal turn

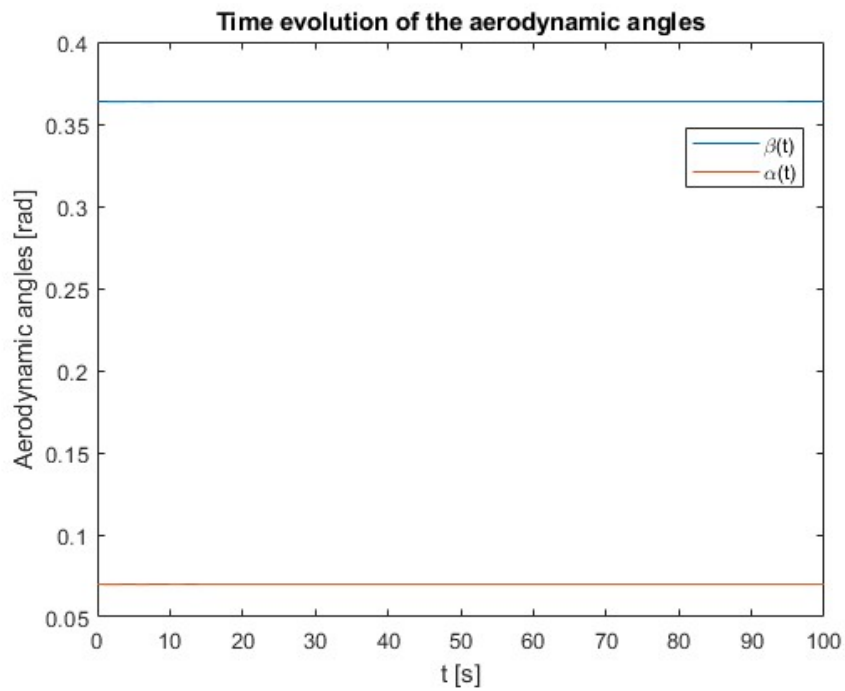


Figure 4.5.3: Plot of the time evolution of the aerodynamic angles for the horizontal turn

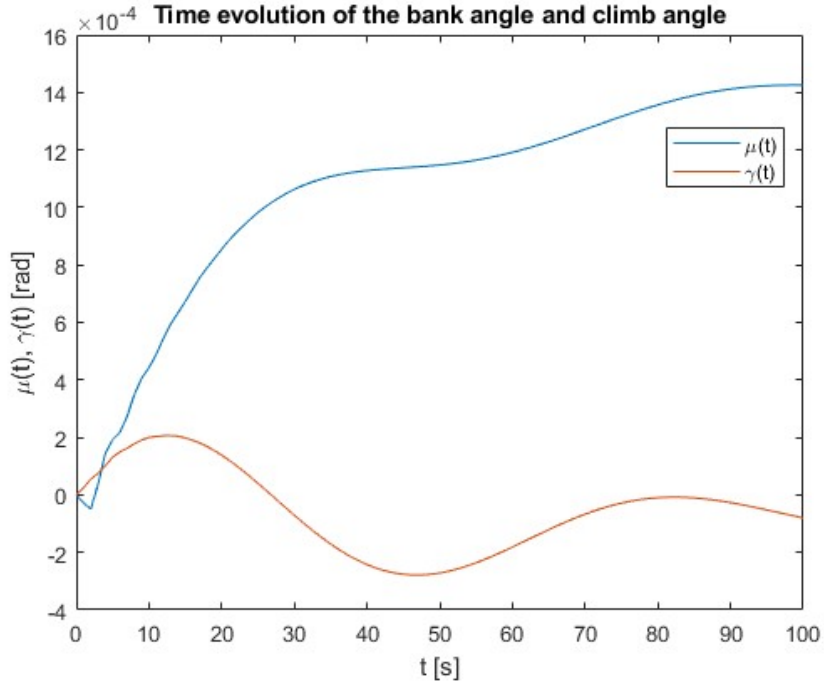


Figure 4.5.4: Plot of the time evolution of the bank angle and the climb angle for the horizontal turn

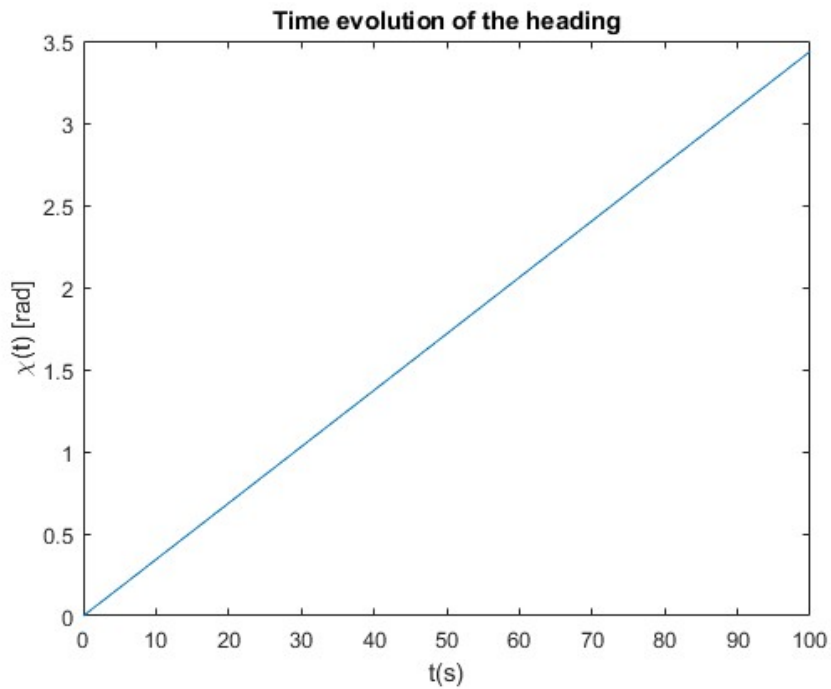


Figure 4.5.5: Plot of the time evolution of the heading angle for the horizontal turn

In the first place, it can be observed that most of the parameters remain invariant over time. However, in Figure 4.5.4 there exists a variation of the bank and slope angles. Nevertheless, such variation is of the order of 10^{-4} rad, mostly due to numerical error, so they shall be considered to be negligible. In this way, it is confirmed that a manoeuvre without roll is being performed in the horizontal plane. On the other

hand, Figure 4.5.5 shows how the heading angle has a linear variation with time, so it can be deduced that the rate of turn is constant. Consequently, this implies that the airspeed is constant, as demonstrated in Figure 4.5.1. Furthermore, since the heading is positive, the turn executed by the aircraft would be rightwards.

Now examining Figure 4.5.2 several conclusions can be drawn. To begin with, the angular velocity $r(t)$ confirms that a clockwise movement around the Z-axis is taking place, in other words, a right-hand turn. The angular velocity $q(t)$ remains zero, so there is no movement about the Y-axis, whereas $p(t)$ indicates that there is a slight movement about the X-axis, which does not imply roll, but will be given by the angle of attack (Figure 4.5.3).

It is interesting in this case to analyse the controls introduced regarding lateral-directional dynamics. Firstly, a positive aileron deflection, δ_A , considering that the right aileron moves upwards and the left aileron moves downwards, implies a negative yaw, due to lift asymmetry. On the other hand, a positive rudder deflection, δ_R , generates also a negative yaw moment. This phenomenon is known as adverse yaw, and occurs when the nose of the aircraft is facing away from the trajectory it is following. This is in turn confirmed by the positive slip angle, $\beta(t)$, which indicates that the nose is pointing to the left, while the turn is performed in a clockwise direction.

Lastly, Figure 4.5.6 illustrates the trajectory followed by the aircraft. It is important to highlight that although a left turn is being portrayed, it has to be taken into account that the trihedron described in Section 2.2 implies that the Y-axis is positive towards the right, while MATLAB considers it to be positive towards the left. Keeping this in mind, it is therefore safe to conclude that there is a rotation in the horizontal plane described in a clockwise direction.

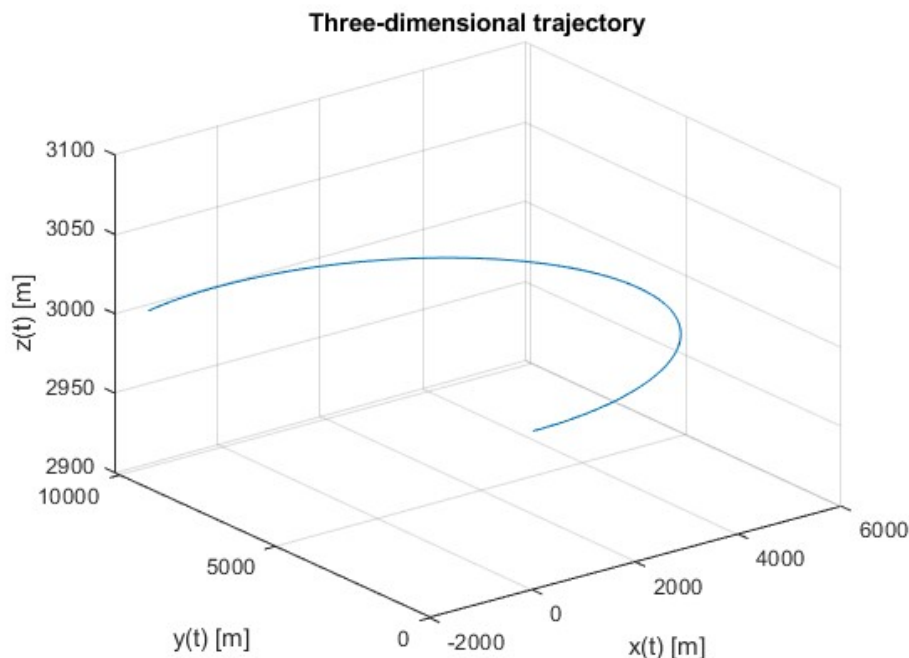


Figure 4.5.6: Plot of the three-dimensional trajectory of the horizontal turn

The fuel consumed by the aircraft in the execution of the turn is $m_f = 113.71$ kg.

4.6 Helical turn

The last manoeuvre of study shall consist of an upward helical turn. The study is to be performed on body axes, starting from the initial conditions shown in Table 4.6.1. Additionally, Table 4.6.2 shows the controls applied in the manoeuvre. The angular velocity considered will be $\Omega = 0.0262$ rad/s.

u_0	173.90	[m/s]	p_0	-0.0045	[rad/s]	ϕ_0	0.2618	[rad]	x_0	0	[m]
v_0	-14.47	[m/s]	q_0	0.0067	[rad/s]	θ_0	0.1745	[rad]	y_0	0	[m]
w_0	13.24	[m/s]	r_0	0.0249	[rad/s]	ψ_0	0	[rad]	z_0	3000	[m]

Table 4.6.1: Value of the initial conditions for the helical turn

α	0.0760	[rad]	δ_E	-0.0675	[rad]
β	-0.0828	[rad]	δ_A	-0.0961	[rad]
δ_P	0.4015	[-]	δ_R	-0.0019	[rad]

Table 4.6.2: Value of the controls for the helical turn

The duration of the manoeuvre is defined for $t_f = 300$ s. The results obtained are shown below.

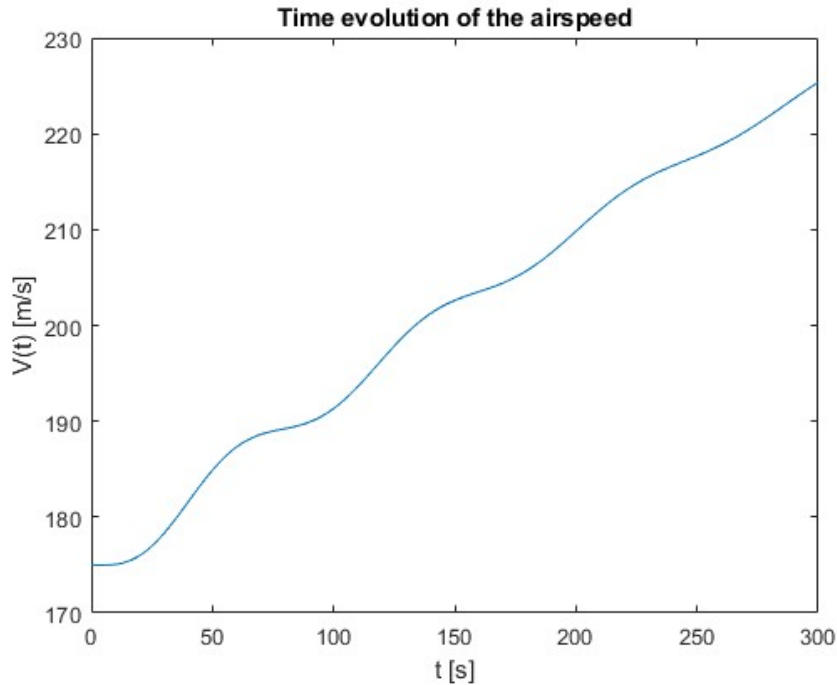


Figure 4.6.1: Plot of the time evolution of the airspeed for the helical turn

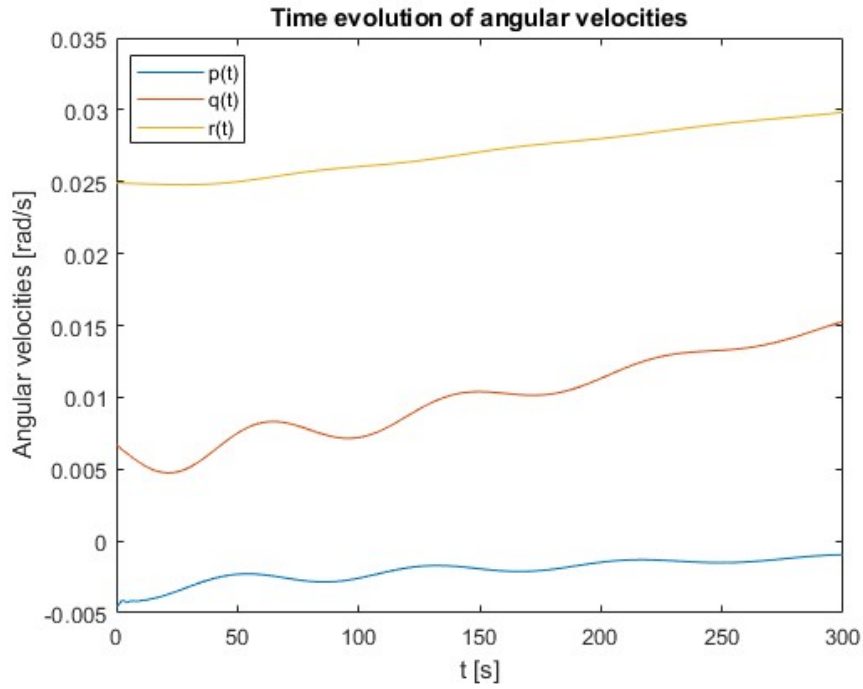


Figure 4.6.2: Plot of the time evolution of the angular velocities for the helical turn

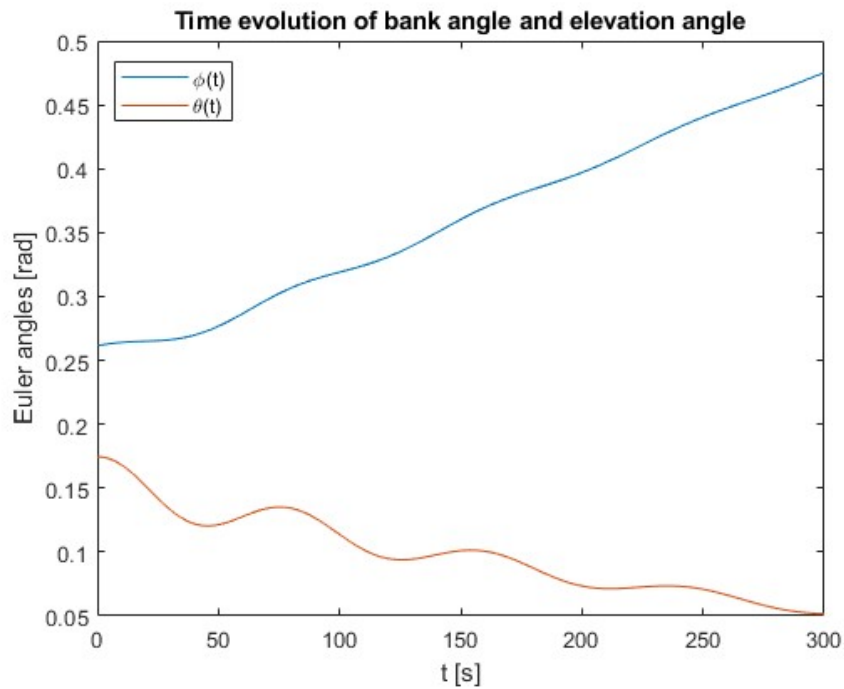


Figure 4.6.3: Plot of the time evolution of the bank angle and the elevation angle for the helical turn

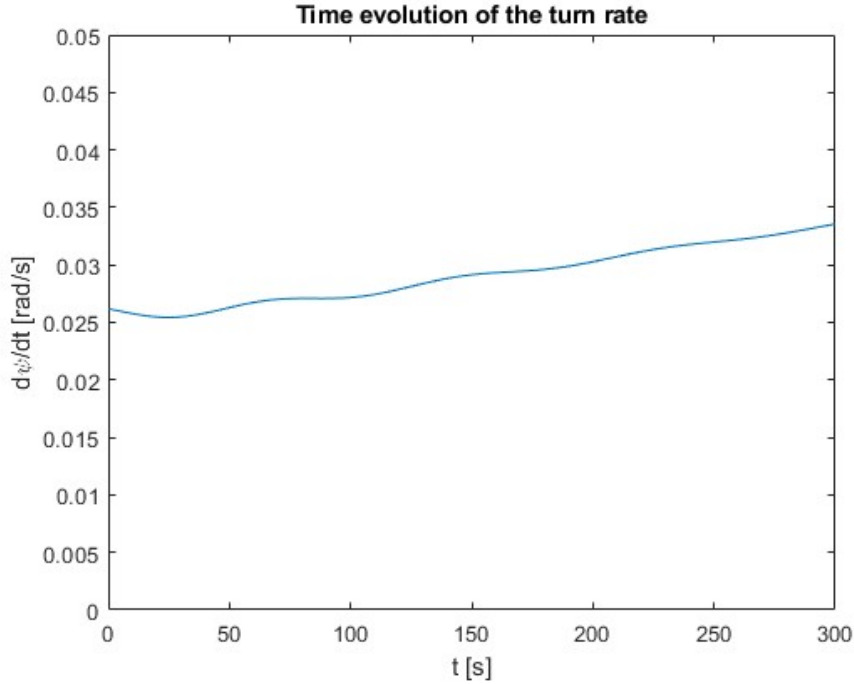


Figure 4.6.4: Plot of the time evolution of the turn rate for the helical turn

Before carrying out the analysis, it must be taken into account that, when rolling an aircraft, the lift vector is inclined, so it will be broken down into a vertical component, $L \cos \phi$, and a horizontal component, $L \sin \phi$. During an climbing turn, as the altitude increases, both the density and the relative density decrease. This implies that, on the one hand, the thrust is reduced, so that the speed would have to be increased in order to have enough thrust to make the ascent. Additionally, if the density decreases, the vertical component of lift will also decrease, which would imply an increase in speed to cope with the weight and avoid a loss of altitude. Thus, said increase in velocity is depicted in Figure 4.6.1.

On the other hand, one of the consequences of a change of direction is the appearance of centrifugal force. In this way, the higher the speed, the greater the centrifugal force, so the turning radius would increase, thereby decreasing the turn rate. However, if the roll increases (Figure 4.6.3), the horizontal component of lift would increase, so the turn radius would decrease, resulting in an increase in the turn rate.

Figure 4.6.4 shows the time evolution of the turn rate. A slight increase can be seen, implying that the horizontal component of lift is slightly larger than the centrifugal force. However, this is a minimal variation compared to the elapsed time, so a constant turn rate can be considered.

Now analysing Figure 4.6.2, it can be concluded that a rightward turn is performed, as a positive angular velocity $r(t)$ indicates a positive motion about the Z axis. Furthermore, the angular velocities $p(t)$ and $q(t)$ reflect the decrease of the pitch angle (Figure 4.6.3), as indicated by Equation 2.6.

Finally, Figure 4.6.5 shows the trajectory followed by the aircraft. Analogous to the case of the horizontal turn, it should be noted that MATLAB considers the Y-axis positive to the right, whereas throughout the current project it has been considered positive to the left. As a result, it can be seen that a clockwise upward turn is indeed described.

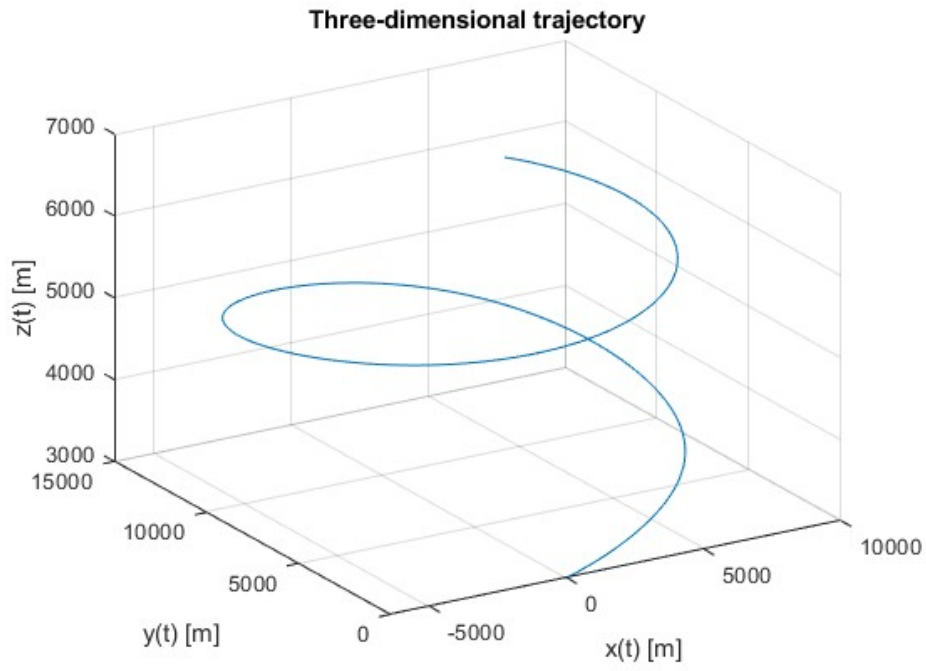


Figure 4.6.5: Plot of the three-dimensional trajectory of the helical turn

The fuel consumed by the aircraft during the manoeuvre is $m_f = 163.81$ kg.

4.7 Verification with the Airbus A320-200

In the current section the verification of the simulator with the Airbus A320-200 will be presented. It is important to highlight that as this is a checking, the results will not be analysed as extensively as previously done with the F-18 Hornet. The initial conditions chosen to perform the manoeuvres are as follows:

- $z_0 = 5000$ m
- $V_0 = 175$ m/s

4.7.1 Equilibrium in the vertical plane

In the first place, the initial conditions are presented in Table 4.7.1. Additionally, the controls introduced for the execution of the manoeuvre can be consulted in Table 4.7.2. The chosen reference frame is body-fixed axes.

u_0	174.28	[m/s]	p_0	0	[rad/s]	ϕ_0	0	[rad]	x_0	0	[m]
v_0	0	[m/s]	q_0	0	[rad/s]	θ_0	0.0907	[rad]	y_0	0	[m]
w_0	15.8586	[m/s]	r_0	0	[rad/s]	ψ_0	0	[rad]	z_0	5000	[m]

Table 4.7.1: Value of the initial conditions for the vertical equilibrium of the A320

α_0	0.0907	[rad]	δ_E	-0.0577	[rad]
β_0	0	[rad]	δ_A	0	[rad]
δ_P	0.6653	[-]	δ_R	0	[rad]

Table 4.7.2: Value of the controls and the aerodynamic angles for the vertical equilibrium of the A320

The integration time shall be defined as $t_f = 1000$ s. The obtained results are presented hereunder.

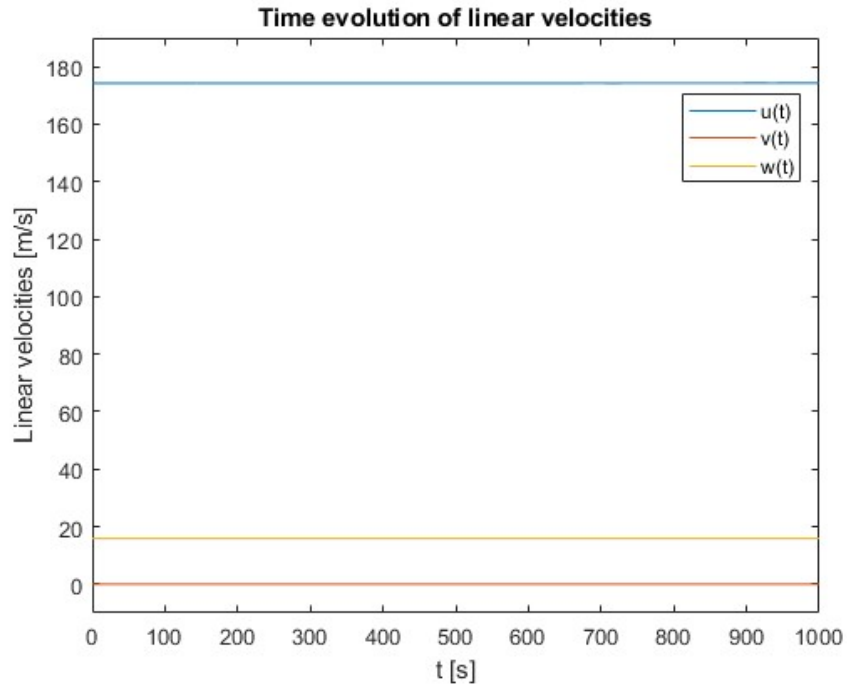


Figure 4.7.1: Plot of the time evolution of the linear velocities for the vertical equilibrium of the A320

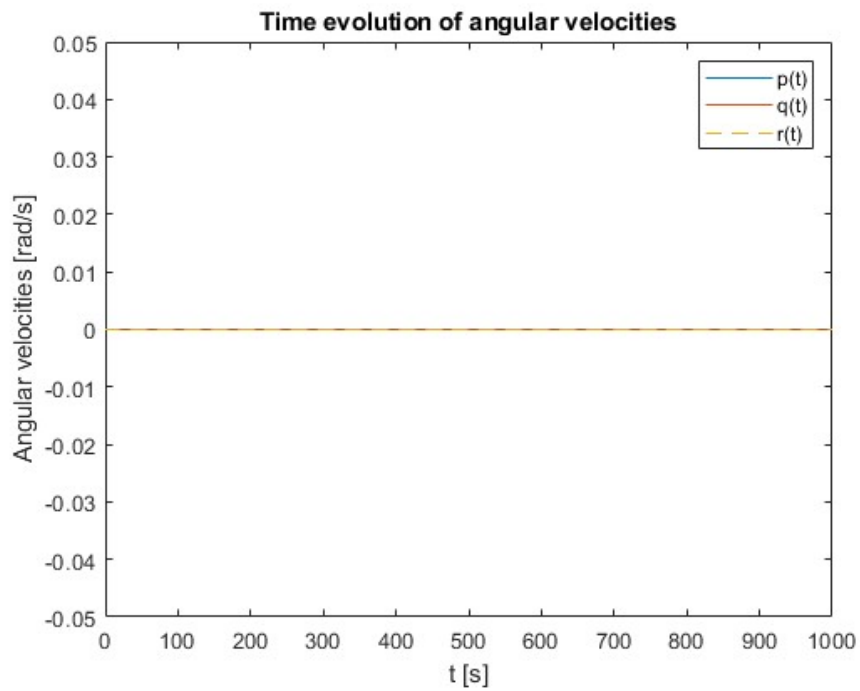


Figure 4.7.2: Plot of the time evolution of the angular velocities for the vertical equilibrium of the A320

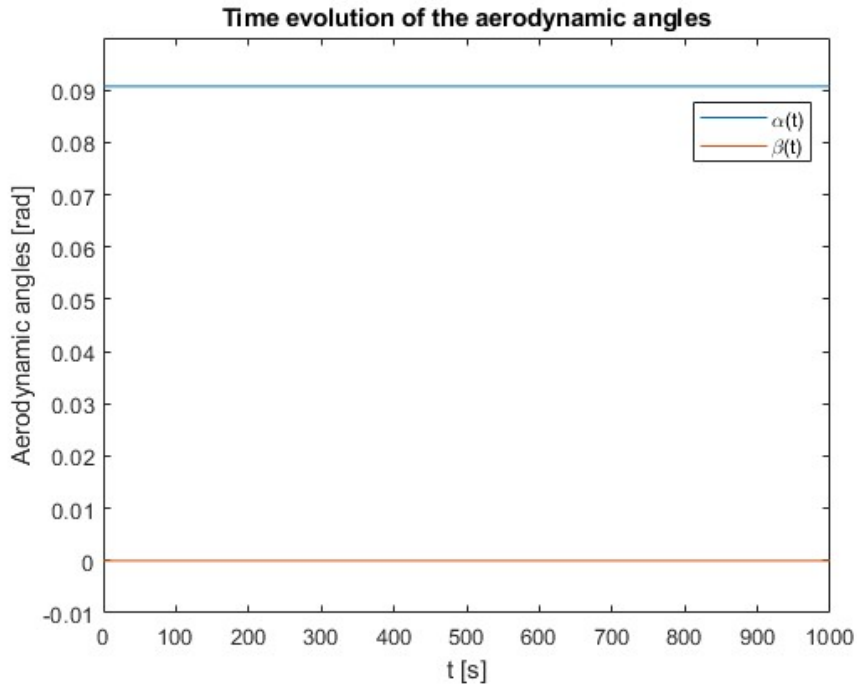


Figure 4.7.3: Plot of the time evolution of the aerodynamic angles for the vertical equilibrium of the A320

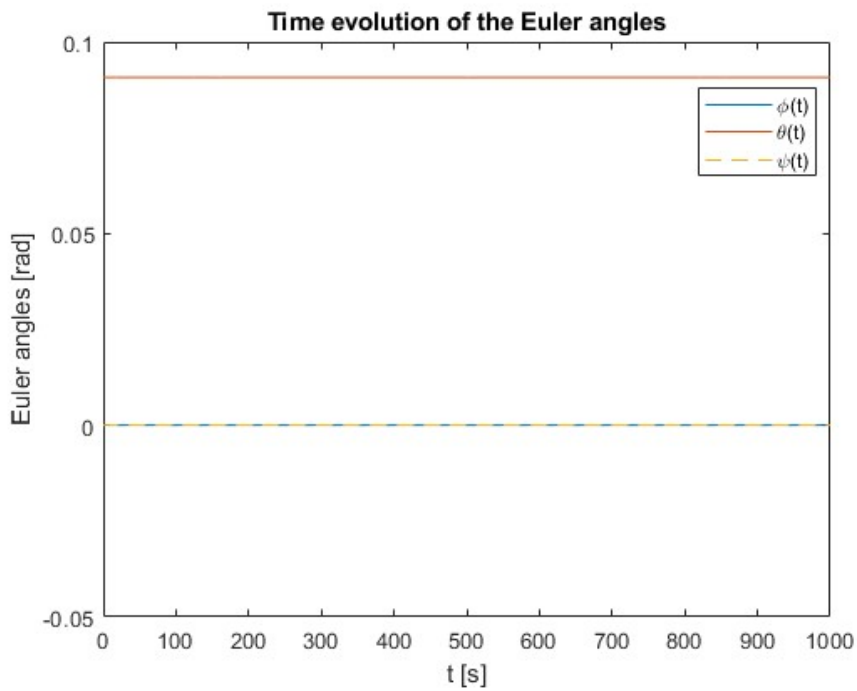


Figure 4.7.4: Plot of the time evolution of the Euler angles for the vertical equilibrium of the A320

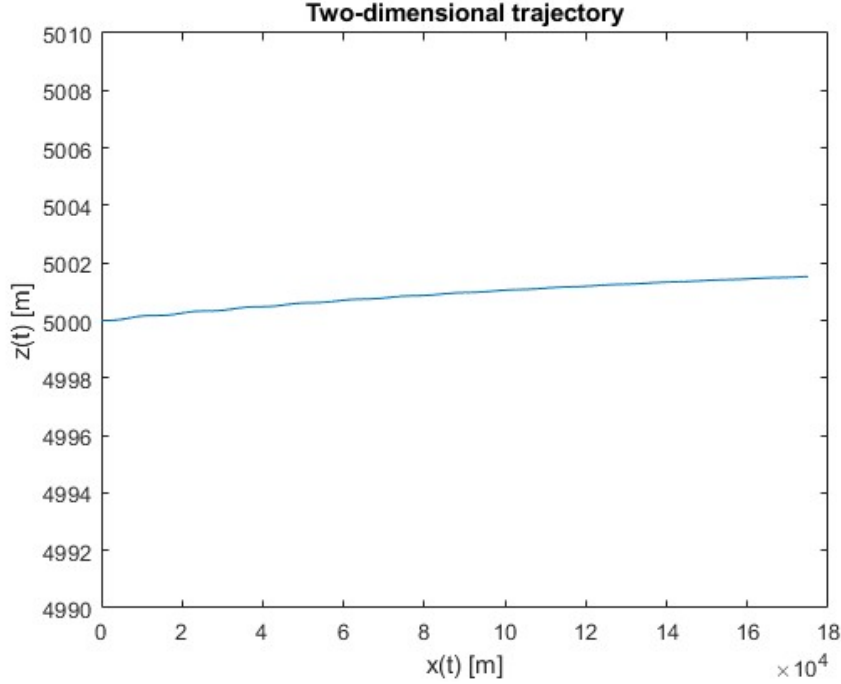


Figure 4.7.5: Plot of the two-dimensional trajectory of the aerodynamic angles for the vertical equilibrium of the A320

As it can be seen, the variables are stabilised after a period of time, with the parameters related to the lateral-directional dynamics remaining null. It is interesting to have a look at Figure 4.7.5, which shows the two-dimensional trajectory followed by the aircraft. It can be seen that the altitude increases with time. However, it can be seen that the curve tends to stabilise, so it is confirmed that the results obtained are correct.

4.7.2 Gliding flight

The initial conditions considered in the execution of the manoeuvre are given in Table 4.7.3, whereas Table 4.7.4 lists the controls introduced. The simulation has been tested using the wind axis coordinate system.

V_0	175	[m/s]	p_0	0	[rad/s]	μ_0	0	[rad]	x_0	0	[m]
β_0	0	[rad]	q_0	0	[rad/s]	γ_0	-0.0481	[rad]	y_0	0	[m]
α_0	0.0910	[rad]	r_0	0	[rad/s]	χ_0	0	[rad]	z_0	5000	[m]

Table 4.7.3: Value of the initial conditions for the gliding flight manoeuvre for the A320

δ_P	0	[-]	δ_A	0	[rad]
δ_E	-0.0579	[rad]	δ_R	0	[rad]

Table 4.7.4: Value of the controls for the gliding flight for the A320

The integration time is defined as $t_f = 761$ s, the time it takes to hit the ground. The time evolution obtained is displayed below.

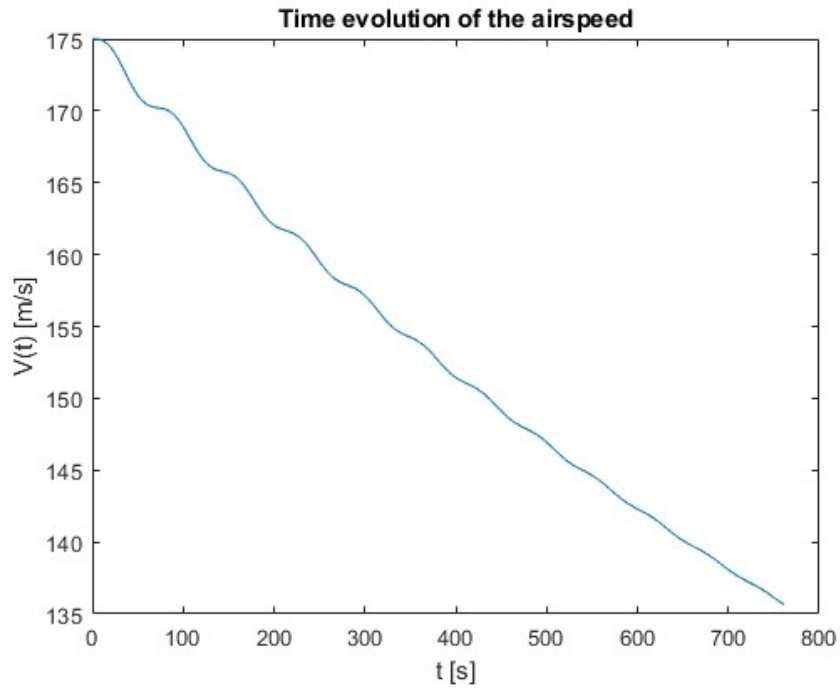


Figure 4.7.6: Plot of the time evolution of the airspeed for the gliding flight for the A320

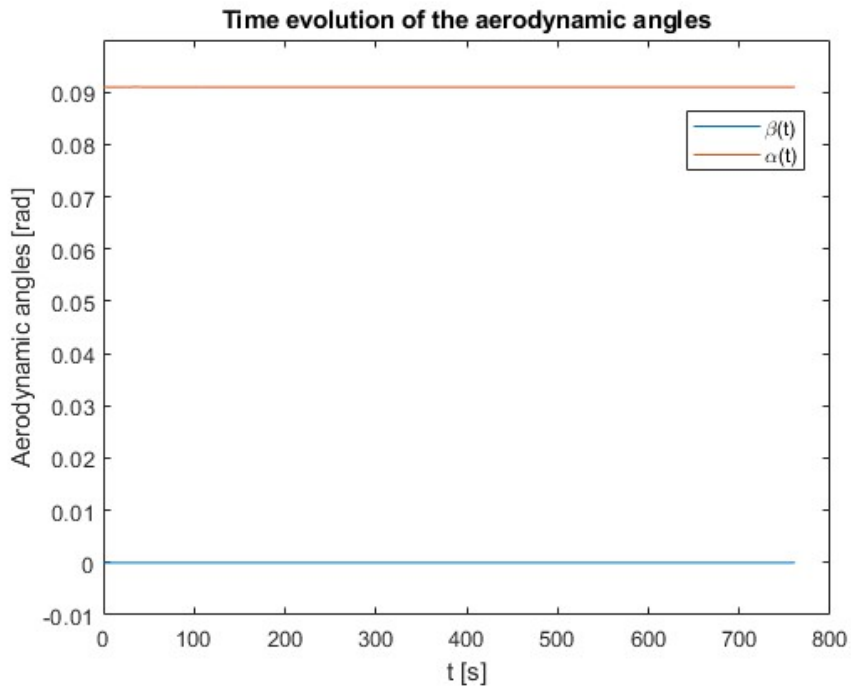


Figure 4.7.7: Plot of the time evolution of the aerodynamic angles for the gliding flight for the A320

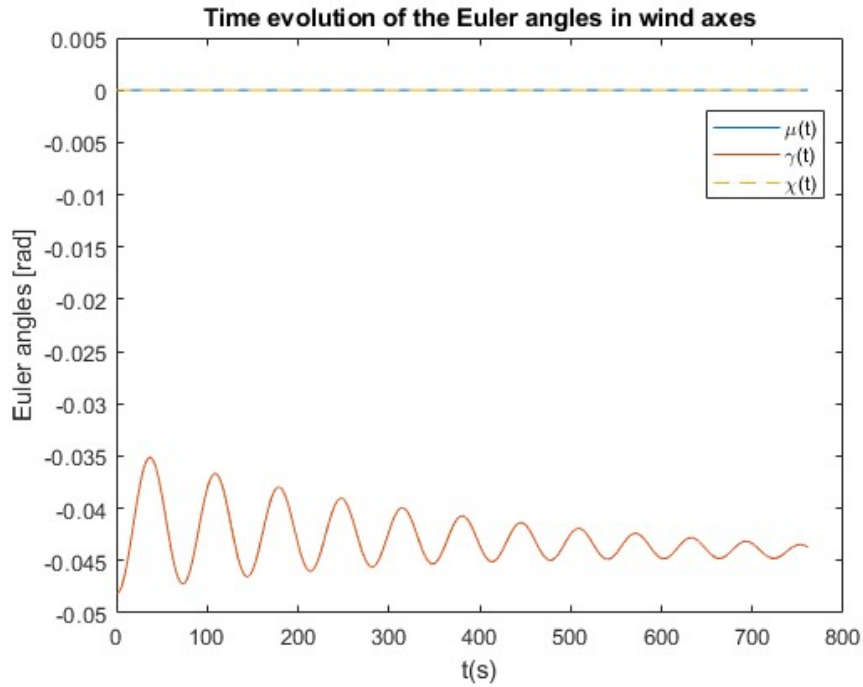


Figure 4.7.8: Plot of the time evolution of the Euler angles for the gliding flight for the A320

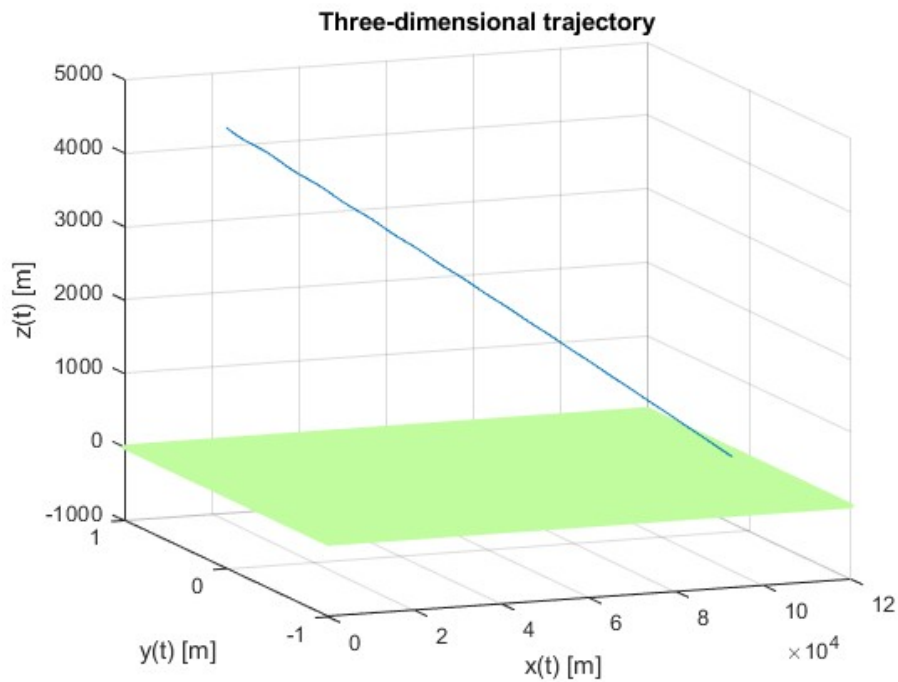


Figure 4.7.9: Plot of the three-dimensional trajectory of the gliding flight for the A320

As it can be seen, the performance of the aircraft is similar to the one obtained in Section 4.3, as expected. Thereby, it can be confirmed that the simulator can be operated regardless of the aircraft under study.

Chapter 5

Conclusions

After completing the study of the flight dynamics of the F-18 Hornet during a variety of manoeuvres, it can be stated that the proposed objectives have been achieved.

One of the main objectives was to develop an academic flight simulator that could be used to analyse the performance of conventional configuration aircraft. For this purpose, use was made of the *Bryan Equations*, expressed in both body-fixed axes and wind axes. Problems such as the *gimbal lock* have also been solved through the application of quaternions, so it can be stated that not only has the knowledge acquired during the courses of *Mecánica del Vuelo* and *Ampliación de Mecánica del Vuelo* been applied, but it has also been extended through the exhaustive study of the Euler-Rodrigues quaternions.

Additionally, the aerodynamic model, obtained from the aerodynamic derivatives of the aircraft, was implemented, as well as the thrust model, to which the different propulsive models that have been studied were introduced. It was ensured that the user could choose the desired model for greater convenience.

It was also intended to use the simulator developed to analyse the performance of an aircraft, the McDonnell Douglas F-18 Hornet, during a series of operations. By applying the simulator to a specific aircraft, it has not only been possible to draw satisfactory conclusions from the performance of the aircraft, but also to check the correct functioning and ensure the validity of the simulator in question. Furthermore, it has been possible to ensure its proper operation independently of the aircraft.

To conclude, and taking into account the limitations of the models and the assumptions made, it can be confirmed that the numerical methods satisfactorily resolve the flight dynamics. It is worth highlight that all of the objectives have been successfully fulfilled, thus providing future students with an analytical tool to facilitate their understanding of the concepts they have learned and from which they can complete their own case studies.

5.1 Future work

Having completed the project, different ideas are proposed in order to continue the development of the simulator in a more complete and accurate way. Some of these improvements imply the total modification of the equations used in the programming, so they could only be implemented if more time was available.

Firstly, one of the hypotheses applied in obtaining the *Bryan Equations* adapted to the literature of the *Ampliación de Mecánica del Vuelo* course consists of assuming

constant mass. This hypothesis may be feasible in manoeuvres of short duration; however, in manoeuvres in which fuel consumption is high, regardless of the flight time, it may lead to inaccurate results. It is therefore proposed to discard this hypothesis, so that the dependence on aircraft mass should be added in several terms of the equations and in certain data.

It is also proposed to extend the study of the actions to include the possibility of engine failure. In the performance of a manoeuvre with engine failure, the moments generated must be taken into account, as well as the decrease in thrust. This would imply the modification of the *Bryan Equations*, having to include an extra term referring to the moments. The propulsion models would also have to be modified, including the thrust reduction, also taking into account the number of engines in the aircraft.

Finally, as far as the format is concerned, a dynamic interface can be developed in order to obtain the temporal evolution in real time. This will make it easier for the user to understand the results, allowing them to observe the evolution at every moment and facilitating the comparison between mutually influencing parameters.

Chapter 6

Relation of the project to the Sustainable Development Goals of the Agenda 2030

The Sustainable Development Goals are a set of 17 goals established by the United Nations in 2015. They are part of the 2030 Agenda with the aim of achieving sustainable development, seeking to improve the quality of life, reduce inequalities and fight climate change, among others.

Table 6.0.1 below summarises the 17 objectives, indicating their degree of relationship with the current project.

Sustainable Development Goals	High	Medium	Low	Not applicable
1. No poverty				X
2. Zero hunger				X
3. Good health and well-being				X
4. Quality education		X		
5. Gender Equality				X
6. Clean water and sanitation				X
7. Affordable and clean energy				X
8. Decent work and economic growth				X
9. Industry, innovation and infrastructure		X		
10. Reduced inequalities				X
11. Sustainable cities and communities				X
12. Responsible consumption and production				X
13. Climate action				X
14. Life below water				X
15. Life on land				X
16. Peace, justice and strong institutions				X
17. Partnership for the goals				X

Table 6.0.1: Degree of relationship with the Sustainable Development Goals

It can be noted that two of the objectives (Figure 6.0.1) are fairly related to the developed project.

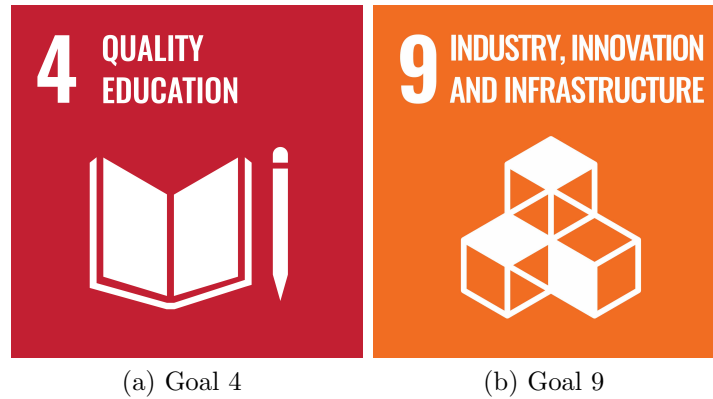


Figure 6.0.1: SDGs with higher degree of relationship

Firstly, SDG 4 (Figure 6.0.1a) aims to achieve quality education. As it has been already discussed, the present project is focused on the academic field, being one of the principal objectives to provide students with a tool to complete their analysis carried out in the *Ampliación de Mecánica del Vuelo* course. By doing so, it will allow them to deepen the knowledge they have acquired and facilitate their understanding of it, thus constituting an upgrade in the received education.

On the other hand, SDG 9 (Figure 6.0.1b) focuses on industry, innovation and infrastructure. The present project has involved the introduction of improvements in the field of simulation due to the lack of simulators dedicated to the academic field and hence the necessity to develop one. The innovations introduced could be applied not only for educational purposes, but also for experimental purposes.

Chapter 7

Scope Statement

The purpose of the current section is to explain the correct fulfilment of the requirements and criteria concerning health and safety during the development of the End of Degree Project.

7.1 Standard regulations

The legislation governing the minimum health and safety provisions to be adopted for adequate worker protection is set out below. They are established by the *Real Decreto 488/1997, de 14 de abril* [2].

Artículo 1. *Objeto.*

1. *El presente Real Decreto establece las disposiciones mínimas de seguridad y de salud para la utilización por los trabajadores de equipos que incluyan pantallas de visualización.*
2. *Las disposiciones de la Ley 31/1995, de 8 de noviembre, de Prevención de Riesgos Laborales, se aplicarán plenamente al conjunto del ámbito contemplado en el apartado anterior*
3. *Quedan excluidos del ámbito de aplicación de este Real Decreto:*
 - (a) *Los puestos de conducción de vehículos o máquinas.*
 - (b) *Los sistemas informáticos embarcados en un medio de transporte.*
 - (c) *Los sistemas informáticos destinados prioritariamente a ser utilizados por el público.*
 - (d) *Los sistemas llamados portátiles, siempre y cuando no se utilicen de modo continuado en un puesto de trabajo.*
 - (e) *Las calculadoras, cajas registradoras y todos aquellos equipos que tengan un pequeño dispositivo de visualización de datos o medidas necesario para la utilización directa de dichos equipos.*
 - (f) *Las calculadoras, cajas registradoras y todos aquellos equipos que tengan un pequeño dispositivo de visualización de datos o medidas necesario para la utilización directa de dichos equipos.*
 - (g) *Las máquinas de escribir de diseño clásico, conocidas como máquinas de ventanilla.*

Artículo 2. *Definiciones.*

1. *A efectos de este Real Decreto se entenderá por:*

- (a) *Pantalla de visualización: una pantalla alfanumérica o gráfica, independientemente del método de representación visual utilizado.*
- (b) *Puesto de trabajo: el constituido por un equipo con pantalla de visualización provisto, en su caso, de un teclado o dispositivo de adquisición de datos, de un programa para la interconexión persona/máquina, de accesorios ofimáticos y de un asiento y mesa o superficie de trabajo, así como el entorno laboral inmediato.*
- (c) *Trabajador: cualquier trabajador que habitualmente y durante una parte relevante de su trabajo normal utilice un equipo con pantalla de visualización.*

Artículo 3. *Obligaciones generales del empresario.*

1. *El empresario adoptará las medidas necesarias para que la utilización por los trabajadores de equipos con pantallas de visualización no suponga riesgos para su seguridad o salud o, si ello no fuera posible, para que tales riesgos se reduzcan al mínimo.*

En cualquier caso, los puestos de trabajo a que se refiere el presente Real Decreto deberán cumplir las disposiciones mínimas establecidas en el anexo del mismo.

2. *A efectos de lo dispuesto en el primer párrafo del apartado anterior, el empresario deberá evaluar los riesgos para la seguridad y salud de los trabajadores, teniendo en cuenta en particular los posibles riesgos para la vista y los problemas físicos y de carga mental, así como el posible efecto añadido o combinado de los mismos. La evaluación se realizará tomando en consideración las características propias del puesto de trabajo y las exigencias de la tarea y entre éstas, especialmente, las siguientes:*

- (a) *El tiempo promedio de utilización diaria del equipo.*
- (b) *El tiempo máximo de atención continua a la pantalla requerido por la tarea habitual.*
- (c) *El grado de atención que exija dicha tarea.*

3. *Si la evaluación pone de manifiesto que la utilización por los trabajadores de equipos con pantallas de visualización supone o puede suponer un riesgo para su seguridad o salud, el empresario adoptará las medidas técnicas u organizativas necesarias para eliminar o reducir el riesgo al mínimo posible. En particular, deberá reducir la duración máxima del trabajo continuado en pantalla, organizando la actividad diaria de forma que esta tarea se alterne con otras o estableciendo las pausas necesarias cuando la alternancia de tareas no sea posible o no baste para disminuir el riesgo suficientemente.*

4. *En los convenios colectivos podrá acordarse la periodicidad, duración y condiciones de organización de los cambios de actividad y pausas a que se refiere el apartado anterior.*

Artículo 4. *Vigilancia de la salud.*

1. *El empresario garantizará el derecho de los trabajadores a una vigilancia adecuada de su salud, teniendo en cuenta en particular los riesgos para la vista y los problemas físicos y de carga mental, el posible efecto añadido o combinado de los mismos, y la eventual patología acompañante. Tal vigilancia será realizada por personal sanitario competente y según determinen las autoridades sanitarias en las pautas y protocolos que se elaboren, de conformidad con lo dispuesto en el apartado 3 del artículo 37 del Real Decreto 39/1997, de 17 de enero, por el que se aprueba el Reglamento de los servicios de prevención. Dicha vigilancia deberá ofrecerse a los trabajadores en las siguientes ocasiones:*
 - (a) *Antes de comenzar a trabajar con una pantalla de visualización.*
 - (b) *Posteriormente, con una periodicidad ajustada al nivel de riesgo a juicio del médico responsable.*
 - (c) *Cuando aparezcan trastornos que pudieran deberse a este tipo de trabajo.*
2. *Cuando los resultados de la vigilancia de la salud a que se refiere el apartado 1 lo hiciese necesario, los trabajadores tendrán derecho a un reconocimiento oftalmológico.*
3. *El empresario proporcionará gratuitamente a los trabajadores dispositivos correctores especiales para la protección de la vista adecuados al trabajo con el equipo de que se trate, si los resultados de la vigilancia de la salud a que se refieren los apartados anteriores demuestran su necesidad y no pueden utilizarse dispositivos correctores normales.*

Artículo 5. *Obligaciones en materia de información y formación.*

1. *De conformidad con los artículos 18 y 19 de la Ley de Prevención de Riesgos Laborales, el empresario deberá garantizar que los trabajadores y los representantes de los trabajadores reciban una formación e información adecuadas sobre los riesgos derivados de la utilización de los equipos que incluyan pantallas de visualización, así como sobre las medidas de prevención y protección que hayan de adoptarse en aplicación del presente Real Decreto.*
2. *El empresario deberá informar a los trabajadores sobre todos los aspectos relacionados con la seguridad y la salud en su puesto de trabajo y sobre las medidas llevadas a cabo de conformidad con lo dispuesto en los artículos 3 y 4 de este Real Decreto.*
3. *El empresario deberá garantizar que cada trabajador reciba una formación adecuada sobre las modalidades de uso de los equipos con pantallas de visualización, antes de comenzar este tipo de trabajo y cada vez que la organización del puesto de trabajo se modifique de manera apreciable.*

Artículo 6. *Consulta y participación de los trabajadores.*

La consulta y participación de los trabajadores o sus representantes sobre las cuestiones a que se refiere este Real Decreto se realizarán de conformidad con lo dispuesto en el apartado 2 del artículo 18 de la Ley de Prevención de Riesgos Laborales.

Anexos.

1. Equipo.

(a) *Observación general.*

La utilización en sí misma del equipo no debe ser una fuente de riesgo para los trabajadores.

(b) *Pantalla.*

Los caracteres de la pantalla deberán estar bien definidos y configurados de forma clara, y tener una dimensión suficiente, disponiendo de un espacio adecuado entre los caracteres y los renglones.

La imagen de la pantalla deberá ser estable, sin fenómenos de destellos, centelleos u otras formas de inestabilidad.

El usuario de terminales con pantalla deberá poder ajustar fácilmente la luminosidad y el contraste entre los caracteres y el fondo de la pantalla, y adaptarlos fácilmente a las condiciones del entorno.

La pantalla deberá ser orientable e inclinable a voluntad, con facilidad para adaptarse a las necesidades del usuario.

Podrá utilizarse un pedestal independiente o una mesa regulable para la pantalla.

La pantalla no deberá tener reflejos ni reverberaciones que puedan molestar al usuario.

(c) *Teclado.*

El teclado deberá ser inclinable e independiente de la pantalla para permitir que el trabajador adopte una postura cómoda que no provoque cansancio en los brazos o las manos.

Tendrá que haber espacio suficiente delante del teclado para que el usuario pueda apoyar los brazos y las manos.

La superficie del teclado deberá ser mate para evitar los reflejos.

La disposición del teclado y las características de las teclas deberán tender a facilitar su utilización.

Los símbolos de las teclas deberán resaltar suficientemente y ser legibles desde la posición normal de trabajo.

(d) *Mesa o superficie de trabajo.*

La mesa o superficie de trabajo deberán ser poco reflectantes, tener dimensiones suficientes y permitir una colocación flexible de la pantalla, del teclado, de los documentos y del material accesorio.

El soporte de los documentos deberá ser estable y regulable y estará colocado de tal modo que se reduzcan al mínimo los movimientos incómodos de la cabeza y los ojos.

El espacio deberá ser suficiente para permitir a los trabajadores una posición cómoda.

(e) *Asiento de trabajo.*

El asiento de trabajo deberá ser estable, proporcionando al usuario libertad de movimiento y procurándole una postura confortable.

La altura del mismo deberá ser regulable.

El respaldo deberá ser reclinable y su altura ajustable.

Se pondrá un reposapiés a disposición de quienes lo deseen.

2. Entorno.

(a) *Espacio.*

El puesto de trabajo deberá tener una dimensión suficiente y estar acondicionado de tal manera que haya espacio suficiente para permitir los cambios de postura y movimientos de trabajo.

(b) *Iluminación.*

La iluminación general y la iluminación especial (lámparas de trabajo), cuando sea necesaria, deberán garantizar unos niveles adecuados de iluminación y unas relaciones adecuadas de luminancias entre la pantalla y su entorno, habida cuenta del carácter del trabajo, de las necesidades visuales del usuario y del tipo de pantalla utilizado.

El acondicionamiento del lugar de trabajo y del puesto de trabajo, así como la situación y las características técnicas de las fuentes de luz artificial, deberán coordinarse de tal manera que se eviten los deslumbramientos y los reflejos molestos en la pantalla u otras partes del equipo.

(c) *Reflejos y deslumbramientos.*

Los puestos de trabajo deberán instalarse de tal forma que las fuentes de luz, tales como ventanas y otras aberturas, los tabiques transparentes o translúcidos y los equipos o tabiques de color claro no provoquen deslumbramiento directo ni produzcan reflejos molestos en la pantalla.

Las ventanas deberán ir equipadas con un dispositivo de cobertura adecuado y regulable para atenuar la luz del día que ilumine el puesto de trabajo.

(d) *Ruido.*

El ruido producido por los equipos instalados en el puesto de trabajo deberá tenerse en cuenta al diseñar el mismo, en especial para que no se perturbe la atención ni la palabra.

(e) *Calor.*

Los equipos instalados en el puesto de trabajo no deberán producir un calor adicional que pueda ocasionar molestias a los trabajadores.

(f) *Emisiones.*

Toda radiación, excepción hecha de la parte visible del espectro electromagnético, deberá reducirse a niveles insignificantes desde el punto de vista de la protección de la seguridad y de la salud de los trabajadores.

(g) *Humedad.*

Deberá crearse y mantenerse una humedad aceptable.

3. Interconexión ordenador/persona.

Para la elaboración, la elección, la compra y la modificación de programas, así como para la definición de las tareas que requieran pantallas de visualización, el empresario tendrá en cuenta los siguientes factores:

(a) *El programa habrá de estar adaptado a la tarea que deba realizarse.*

- (b) *El programa habrá de ser fácil de utilizar y deberá, en su caso, poder adaptarse al nivel de conocimientos y de experiencia del usuario; no deberá utilizarse ningún dispositivo cuantitativo o cualitativo de control sin que los trabajadores hayan sido informados y previa consulta con sus representantes.*
- (c) *Los sistemas deberán proporcionar a los trabajadores indicaciones sobre su desarrollo.*
- (d) *Los sistemas deberán mostrar la información en un formato y a un ritmo adaptados a los operadores.*
- (e) *Los principios de ergonomía deberán aplicarse en particular al tratamiento de la información por parte de la persona.*

7.2 Specific regulations

The current project has been carried out in a suitable environment, which follows the stipulations set out above. It has also required trained personnel, equipment, an office, stationery, prior knowledge, computer skills and access to bibliographic material.

7.2.1 Resource specifications

- Personnel
The project will be carried out by a person in charge of the work, as well as by additional personnel with the necessary knowledge. In this case, they will be the tutor and co-tutor and will have the function of guiding and supervising the development of the project.
- Hardware The development of the project does not require particularly complex equipment, so a laptop was chosen. In addition, a tablet was used to consult the teaching material used and to make diagrams, and a mouse to work more comfortably.
- Software The software employed in the Final Degree Project has been provided by the *Universitat Politècnica de València*. It comprises the following programmes:
 - MATLAB R2022b
 - Wolfram Mathematica 12.0
 - Microsoft Office 365
 - Overleaf
- Office The environment was suitable, quiet, illuminated and free of distractions. All that was required was a desk with the appropriate space and an ergonomic armchair for greater comfort. Moreover, electricity, water and internet supplies were indispensable for the realisation of the project.
- Stationery Stationery should be available in case it is necessary to take notes, make diagrams, structure the different sections or plan the implemented code.

- Prior knowledge As this is such a specialised subject, it is necessary to have the appropriate knowledge. These are mainly those acquired in the courses of *Mecánica del Vuelo* and *Ampliación de Mecánica del Vuelo*. In addition, knowledge of programming and mathematics is required, as a numerical computer programme is used.
- Additional material Access to material related to the subject matter has been needed.

7.2.2 Quality requirements

The quality of the final product must be guaranteed. It shall be taken into account that the company is in possession of the ISO-9001 quality certificate.

Tests will be carried out during the development of the project in order to mitigate errors. The correct functionality of the product will also be checked.

The entire process shall be properly documented and a record shall be kept of all tests carried out with their description, date, results and possible assessments.

7.2.3 Warranty and maintenance requirements

The company contracted for the development of the project guarantees the product for a period of two years, starting at the time of purchase. In the event of a problem with the product, the company is committed to solving it and will also provide a user support service. The guarantee will cease to be valid in the event of improper use of the product.

Regarding the maintenance of the product, none is required. Improper use of the product can permanently alter its functionality.

7.2.4 Legal and contractual requirements

If the contracting party wishes to extend the contract to other deliveries, a new quotation will be drawn up for these. In the event of a suspension of supplies or a delay in delivery, an extension is possible before the expiry of the term of the contract.

7.2.5 Revision of costs

No modifications will be made to the prices submitted.

7.2.6 Deposit

In order to ensure the fulfilment of the obligations stipulated in the contract, the contractor undertakes to provide a guarantee in favour of the purchaser, as a deposit, amounting to 10 % of the total contract amount. It will be maintained from the beginning of the project until the end of the guarantee period, at which time it will be returned.

Chapter 8

Budget of the project

The costs of carrying out the Final Degree Project will be shown below. The resources used will be divided by their nature according to personnel, equipment - software and hardware-, installations and office material. The unit price of each of these will be determined in order to finally obtain the final budget.

Before the cost breakdown, the amortisation cost and hourly rate as well as the annual hours worked shall be defined.

1. Amortization cost:

$$a = \frac{AV - RV}{n} \quad (8.1)$$

where:

a: amortisation, in €/year

AV: acquisition value, in €

RV: residual value, in €

n: amortisation period, in years.

2. Hourly rate:

$$h_r = \frac{a}{h} \quad (8.2)$$

where:

h_r : hourly rate, in euros/h

h: annual hours worked, in h/year.

3. Annual hours worked:

$$h = \left(\frac{week}{year} - \frac{week_{holiday}}{year} \right) \frac{hours\ worked}{week}. \quad (8.3)$$

8.1 Cost calculation

Personnel

The cost of the personnel involved in the development of the project is now estimated.

- University professor

$$\begin{aligned} \text{Gross annual salary} &= 32000 \text{ €/year} \\ \text{Hourly rate} &= \frac{32000}{1760} = 18.18 \text{ €/h} \end{aligned} \tag{8.4}$$

- Junior aerospace engineer

$$\begin{aligned} \text{Gross annual salary} &= 21000 \text{ €/year} \\ \text{Hourly rate} &= \frac{21000}{1760} = 11.93 \text{ €/h} \end{aligned} \tag{8.5}$$

Equipment

- Hardware

- Personal computer: HP Laptop 15-bs1xx

With an acquisition value of 690 €, it is assumed a depreciation period of 6 years and a residual value of 20%.

$$\begin{aligned} a &= \frac{690 - 138}{6} = 92 \text{ €/year} \\ t_h &= \frac{92}{1760} = 0.052 \text{ €/h} \end{aligned} \tag{8.6}$$

- Mouse

$$\text{Acquisition value} = 11.90 \text{ €} \tag{8.7}$$

- Tablet: Lenovo Tab P11 With an acquisition price of 279 €, it has been assumed a depreciation period of 5 years and a residual value of 20%.

$$\begin{aligned} a &= \frac{279 - 55.8}{5} = 44.64 \text{ €/year} \\ t_h &= \frac{44.64}{1760} = 0.025 \text{ €/h} \end{aligned} \tag{8.8}$$

- Software

- Overleaf licence. The free plan has been used.

- MATLAB R2022b licence.

The price for a standard annual licence is 860 €.

$$t_h = \frac{860}{1760} = 0.489 \text{ €/h} \tag{8.9}$$

- Wolfram Mathematica 12.0 licence.
The cost of an annual academic licence is 1523.55 €.

$$t_h = \frac{1523.55}{1760} = 0.866 \text{ €/h} \quad (8.10)$$

- Microsoft Office 365 licence.
The value of an annual personal licence amounts to 69 €.

$$t_h = \frac{69}{1760} = 0.039 \text{ €/h} \quad (8.11)$$

Office

The location of development of the project has been the residence of the student. The costs of utilities, including electricity, water and internet, were obtained from an invoice.

The total price of supplies amounts to 30.53 €.

Stationery

- Notebook: 1.50 €.
- Pens: 3 €.

8.2 Overall budget

Finally, both the breakdown of costs and the total budget are presented.

Specification	Unit	Cost per unit	Total cost
Personnel			
Supervisor	30	18.18	545.40
Graduate	360	11.93	4294.80
		Total	4840.20 €
Hardware			
Laptop	360	0.052	18.72
Mouse	1	11.90	11.90
Tablet	60	0.025	1.50
		Total	32.12 €
Software			
MATLAB licence	200	0.489	97.80
Wolfram Mathematica licence	50	0.866	43.30
Microsoft Office licence	70	0.039	2.73
Overleaf licence	100	0.00	0.00
		Total	143.83 €
Stationery			
Notebook	1	1.50	1.50
Pens	2	1.50	3
		Total	4.50 €
Office			
Supplies	1	30.53	30.53
		Total	30.53 €
		Raw total	5051.18 €

Table 8.2.1: Budget breakdown

Raw total	5051.18 €
6% Industrial benefit	303.07
Raw total	5354.25 €
21% V.A.T	1124.39
Overall budget	6478.64 €

Table 8.2.2: Overall budget

The total cost of the project amounts to:

**SIX THOUSAND, FOUR HUNDRED AND SEVENTY-EIGHT WITH
SIXTY-FOUR CENTS**

Bibliography

- [1] AllDrawings (2014). Northrop F-18 Hornet aircraft. <https://alldrawings.ru/en/pictures/item/northrop-f-18-hornet-aircraft-drawings-dimensions-figures>.
- [2] Arenas Bocanegra, J. (1997). Real decreto 488/1997 de 14 de abril sobre disposiciones mínimas de seguridad y salud para la utilización por los trabajadores de equipos que incluyan pantallas de visualización. <https://www.boe.es/buscar/act.php?id=BOE-A-1997-8671>.
- [3] Blanes Zamora, S., Ginestar Peiró, D., and Roselló Ferragud, M. D. (2020). *Introducción a los métodos numéricos para ecuaciones diferenciales*. Académica. Universitat Politècnica de València, Valencia, 3rd edition.
- [4] Bzuk (2010). Link trainer. [https://commons.wikimedia.org/wiki/File:Link_Trainer_\(WCAM\).JPG](https://commons.wikimedia.org/wiki/File:Link_Trainer_(WCAM).JPG).
- [5] Ejército del Aire y del Espacio Ministerio de Defensa (2017). McDonnell Douglas F-18 Hornet. <https://www.flickr.com/photos/ejercitoaire/36529327554/in/album-72157682593521854/>.
- [6] Hunter, J. (2008). *Jane's aircraft upgrades 2008-2009*. Jane's Information Group, Coulsdon.
- [7] Magraner Rullan, J. and Martinez Val, R. (2014). The birth of airplane stability theory. *Proceedings of the Institution of Mechanical Engineers, Part G: Journal of Aerospace engineering*. 228(9):1498-1506. DOI: 10.1177/0954410013494139.
- [8] Magraner Rullan, J., Martí Gómez-Aldaraví, P., and Carreres Talens, M. (2022a). *Flight Mechanics*. Chapter 0.
- [9] Magraner Rullan, J., Martí Gómez-Aldaraví, P., and Carreres Talens, M. (2022b). *Flight Mechanics*. Notes of the course.
- [10] Martí Gómez-Aldaraví, P. and Carreres Talens, M. (2022a). *Ampliación de Mecánica del Vuelo*. Dinámica de un avión rígido. Parte A.
- [11] Martí Gómez-Aldaraví, P. and Carreres Talens, M. (2022b). *Ampliación de Mecánica del Vuelo*. Dinámica de un avión rígido. Parte B.
- [12] Napolitano, M. R. (2012). *Aircraft dynamics : from modeling to simulation*. John Wiley & Sons, Hoboken.

- [13] Patrol, S. (2021). Sandglass patrol. <https://blog.sandglasspatrol.com/un-barril-partido-en-dos-para-aprender-a-volar/>.
- [14] Phillips, W. F. (2010). *Mechanics of flight*. John Wiley & Sons, Hoboken, New Jersey, 2nd edition.
- [15] Phillips, W. F., Hailey, C. E., and Gerbert, G. A. (2001). Review of Attitude Representations used for Aircraft Kinematics. *Journal of Aircraft*, Vol. 38, No. 4.
- [16] Rodriguez, L. and Botez, R. (2012). Civil turbofan engines thrust generic model. pages 5444–5450.
- [17] Smith, H. (2022). Aircraft Flight Mechanics. Axes Transformations. <https://aircraftflightmechanics.com/EoMs/EulerTransforms.html>.
- [18] Talay, T. A. (1975). *Introduction to the Aerodynamics of Flight*. NASA Langley Research Center.

Appendix A

Orientation methods

A.1 Euler Axis

One of the existing methods of orientation is the Euler axis. It states that the orientation of a reference frame can be described by a rotation around an axis, known as the Euler axis. This rotation will be given by the angle η , while the axis will be characterised by the vector $\{\xi, \zeta, \chi\}$. It is easy to realise that there are three degrees of freedom, so to eliminate redundancy, the vector will be considered unitary (Equation A.1):

$$\xi^2 + \zeta^2 + \chi^2 = 1 \quad (\text{A.1})$$

Any vector in body-fixed coordinates can be expressed from the same vector in Earth-fixed axes, as seen in Section 2.2, giving the Equation A.2.

$$R_\eta = \begin{bmatrix} \xi^2(1 - \cos \eta) + \cos \eta & \xi\zeta(1 - \cos \eta) + \chi \sin \eta & \xi\chi(1 - \cos \eta) - \zeta \sin \eta \\ \xi\zeta(1 - \cos \eta) - \chi \sin \eta & \zeta^2(1 - \cos \eta) + \cos \eta & \zeta\chi(1 - \cos \eta) + \xi \sin \eta \\ \xi\chi(1 - \cos \eta) + \zeta \sin \eta & \zeta\chi(1 - \cos \eta) - \xi \sin \eta & \chi^2(1 - \cos \eta) + \cos \eta \end{bmatrix} \quad (\text{A.2})$$

Another relationship to be taken into account is that between the angular velocities and the rate of change of the Euler axis parameters [15]:

$$\begin{Bmatrix} \dot{\eta} \\ \dot{\xi} \\ \dot{\zeta} \\ \dot{\chi} \end{Bmatrix} = \frac{1}{2} \begin{bmatrix} 2\xi & 2\zeta & 2\chi \\ E'_{\xi\xi} + \frac{\cos \eta/2}{\sin \eta/2} & E'_{\xi\zeta} - \chi & E'_{\xi\chi} + \zeta \\ E'_{\xi\zeta} + \chi & E'_{\zeta\zeta} + \frac{\cos \eta/2}{\sin \eta/2} & E'_{\zeta\chi} - \xi \\ E'_{\xi\chi} - \zeta & E'_{\zeta\chi} + \xi & E'_{\chi\chi} + \frac{\cos \eta/2}{\sin \eta/2} \end{bmatrix} \begin{Bmatrix} p \\ q \\ r \end{Bmatrix} \quad (\text{A.3})$$

where the following notation is considered for simplicity:

$$E'_{ij} = -E_i E_j \frac{\cos(\eta/2)}{\sin(\eta/2)} \quad (\text{A.4})$$

The Euler axis formulation has a great drawback: a singularity occurs when η reaches zero or 180 degrees, which is when the aircraft is directed north or south. As these positions are pretty common, the above singularity can cause a variety of problems in flight simulators. Consequently, the above formulation will only be used to relate the Euler angles to the quaternions.

A.2 Quaternions Formulation

Quaternions are parameters that define the orientation of a rigid body from a rotation around an axis. They are strongly related to the Euler axis, so once it has been described, it is possible to develop the formulation of the quaternions. First, the transformation matrix will be obtained. For this, it is necessary to apply the following trigonometric identities, substituting them in the Equation A.2:

$$\begin{aligned}\sin \eta &= 2 \sin \frac{\eta}{2} \cos \frac{\eta}{2} \\ \cos \eta &= \cos^2 \frac{\eta}{2} - \sin^2 \frac{\eta}{2} \\ 1 - \cos \eta &= 2 \sin^2 \frac{\eta}{2}\end{aligned}\tag{A.5}$$

Thus, the matrix is such that:

$$R_\eta = \begin{bmatrix} E_{\xi\xi} + \cos^2 \frac{\eta}{2} - \sin^2 \frac{\eta}{2} & E_{\xi\zeta} + \chi 2 \sin \frac{\eta}{2} \cos \frac{\eta}{2} & E_{\xi\chi} - \zeta 2 \sin \frac{\eta}{2} \cos \frac{\eta}{2} \\ E_{\xi\zeta} - \chi 2 \sin \frac{\eta}{2} \cos \frac{\eta}{2} & E_{\zeta\zeta} + \cos^2 \frac{\eta}{2} - \sin^2 \frac{\eta}{2} & E_{\chi\zeta} + \xi 2 \sin \frac{\eta}{2} \cos \frac{\eta}{2} \\ E_{\xi\chi} + \zeta 2 \sin \frac{\eta}{2} \cos \frac{\eta}{2} & E_{\chi\zeta} - \xi 2 \sin \frac{\eta}{2} \cos \frac{\eta}{2} & E_{\chi\chi} + \cos^2 \frac{\eta}{2} - \sin^2 \frac{\eta}{2} \end{bmatrix}\tag{A.6}$$

with $E_{ij} = E_i E_j 2 \sin^2 \eta/2$ [15].

Equation 2.14 is then substituted into Equation A.6. The following relation is applied, recalling Equation A.1:

$$\sin^2 \eta/2 = (\xi^2 + \zeta^2 + \chi^2) \sin^2 \eta/2\tag{A.7}$$

Performing a series of simplifications, the transformation matrix as a function of the quaternions is finally reached:

$$R_q = \begin{bmatrix} q_1^2 + q_0^2 - q_2^2 - q_3^2 & 2(q_1 q_2 + q_0 q_3) & 2(q_1 q_3 - q_0 q_2) \\ 2(q_1 q_2 - q_0 q_3) & q_2^2 + q_0^2 - q_1^2 - q_3^2 & 2(q_2 q_3 + q_0 q_1) \\ 2(q_1 q_3 + q_0 q_2) & 2(q_2 q_3 - q_0 q_1) & q_3^2 + q_0^2 - q_1^2 - q_2^2 \end{bmatrix}\tag{A.8}$$

The relationship between the quaternions and the Euler angles must now be established. For this purpose, a comparison will be made between the transformation matrices expressed in terms of both parameters. Hence, taking into account Equation 2.3 and Equation A.8, the following system based on the diagonals of each matrix is reached. As four degrees of freedom are needed, an extra relationship is to be established.

$$\begin{aligned}q_1^2 + q_0^2 - q_2^2 - q_3^2 &= \cos \psi \cos \theta \\ q_2^2 + q_0^2 - q_1^2 - q_3^2 &= \cos \psi \cos \phi + \sin \psi \sin \theta \sin \phi \\ q_3^2 + q_0^2 - q_1^2 - q_2^2 &= \cos \phi \cos \theta \\ q_0^2 + q_1^2 + q_2^2 + q_3^2 &= 1\end{aligned}\tag{A.9}$$

Solving Equation A.9, the relation between quaternions and Euler angles is finally obtained, as seen in Equation 2.15.

Comparing once again both transformation matrices (Equation 2.3 and Equation A.8), the upcoming system of equations is obtained, from which it is easy to deduce Equation 2.16.

$$\begin{aligned}
-\sin \theta &= 2(q_1 q_3 - q_0 q_2) \\
\sin \phi \cos \theta &= 2(q_2 q_3 + q_0 q_1) \\
\cos \phi \cos \theta &= q_3^2 + q_0^2 - q_1^2 - q_2^2 \\
\sin \psi \cos \theta &= 2(q_1 q_2 + q_0 q_3) \\
\cos \psi \cos \theta &= q_1^2 + q_0^2 - q_2^2 - q_3^2
\end{aligned} \tag{A.10}$$

Finally, by deriving with respect to time Equation 2.14:

$$\begin{aligned}
\dot{q}_0 &= -\frac{\dot{\eta}}{2} \sin \frac{\eta}{2} \\
\dot{q}_1 &= \dot{\xi} \sin \frac{\eta}{2} + \xi \frac{\dot{\eta}}{2} \cos \frac{\eta}{2} \\
\dot{q}_2 &= \dot{\zeta} \sin \frac{\eta}{2} + \zeta \frac{\dot{\eta}}{2} \cos \frac{\eta}{2} \\
\dot{q}_3 &= \dot{\chi} \sin \frac{\eta}{2} + \chi \frac{\dot{\eta}}{2} \cos \frac{\eta}{2}
\end{aligned} \tag{A.11}$$

and replacing Equation A.3, it is reached:

$$\begin{Bmatrix} \dot{q}_0 \\ \dot{q}_1 \\ \dot{q}_2 \\ \dot{q}_3 \end{Bmatrix} = \frac{1}{2} \begin{bmatrix} -\xi \sin \frac{\eta}{2} & -\zeta \sin \frac{\eta}{2} & -\chi \sin \frac{\eta}{2} \\ \cos \frac{\eta}{2} & -\chi \sin \frac{\eta}{2} & \zeta \sin \frac{\eta}{2} \\ \chi \sin \frac{\eta}{2} & \cos \frac{\eta}{2} & -\xi \sin \frac{\eta}{2} \\ -\zeta \sin \frac{\eta}{2} & \xi \sin \frac{\eta}{2} & \cos \frac{\eta}{2} \end{bmatrix} \begin{Bmatrix} p \\ q \\ r \end{Bmatrix} \tag{A.12}$$

Substituting the definition given by Equation 2.14, it is not difficult to obtain Equation 2.17.

Appendix B

Three-view of the aircraft

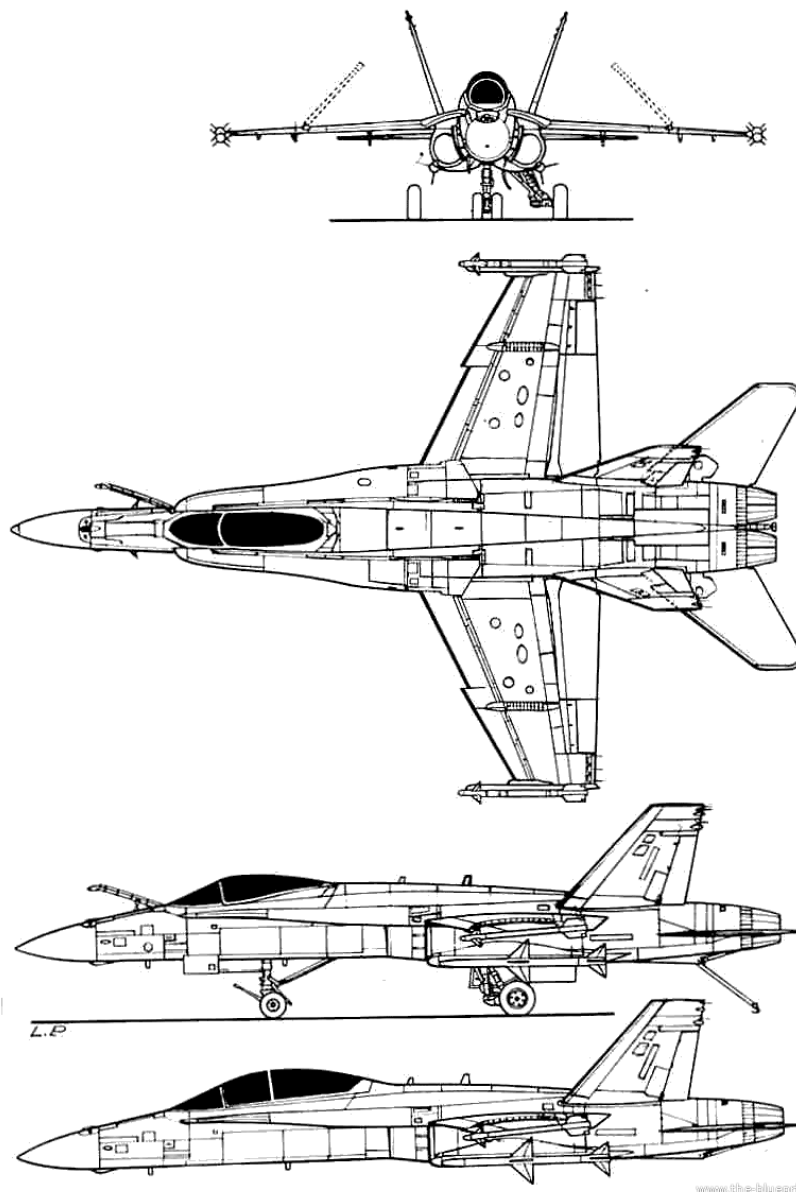


Figure B.0.1: Three-view of the McDonnell Douglas F-18 Hornet[1]

Appendix C

MATLAB code

C.1 Aircraft Parameters

```
1  %Aircraft: F-18
2
3  g = 9.8067;
4
5  %% Geometrical data
6  bw = 11.43;           % COMPLETE
7  % Main wing span. Units: m
8  Sw = 37.16;         % COMPLETE
9  % Wing surface. Units: m^2
10 ARw = 3.51574;      % COMPLETE
11 % Aspect ratio
12 m = 13273;          % COMPLETE
13 % Reference mass. Units: kg
14 xCoG = 1.85;        % COMPLETE
15 % Center of gravity. Units: m
16 cw = 3.02228;      % COMPLETE
17 % Mean aerodynamic chord. Units: m
18 e = 0;              % COMPLETE
19 % Inclination of thrust with respect to the airspeed
    vector. Units: rad
20
21 %% Thrust
22 ThrustSL = 97800;   % COMPLETE
23 % Total thrust (all engines) at sea level. Units: N
24 Ce = 2.3e-05;      % COMPLETE
25 % Specific Fuel Consumption. Units: kg/N*s
26
27 % Thrust Model. When having chosen the model, uncomment the
    corresponding
28 % data and complete.
29 model = 4;         % COMPLETE
30
31
```

```

32 % model = 1 -> J-C Wanner
33     % kf = ;                               % COMPLETE
34     % lambdaf = ;                           % COMPLETE
35
36 % model = 2 -> Aeroespatiale
37
38 % model = 3 -> J. Mattingly
39
40 % model = 4 -> D. Hull
41     a = 1;                                  % COMPLETE
42
43 % model = 5 -> Howe
44     % BPR = ;                               % COMPLETE
45
46 % model = 6 -> Thrust model for turbofan engines (FaRux)
47     % nparameter = ;                       % COMPLETE
48     % BPR = ;                               % COMPLETE
49     % k1 = ;                                 % COMPLETE
50     % k2 = ;                                 % COMPLETE
51     % k3 = ;                                 % COMPLETE
52     % k4 = ;                                 % COMPLETE
53
54
55 %% Inertia
56 Ixx = 30673.6;                              % COMPLETE
57 Iyy = 115752;                                % COMPLETE
58 Izz = 431240;                                % COMPLETE
59 Ixz = 0;                                     % COMPLETE
60
61 %% Aerodynamic coefficients
62
63 % Longitudinal
64 K = 0.10567;                                  % COMPLETE
65 CD0 = 0.0100593;                              % COMPLETE
66
67 CL0 = 0;                                       % COMPLETE
68 CLalpha = 4.24237;                             % COMPLETE
69 CLdE = 0.82536;                                % COMPLETE
70 CLalphaDot = 0.48787;                          % COMPLETE
71 CLq = 0.94699;                                 % COMPLETE
72
73 CMO = 0;                                       % COMPLETE
74 CMalpha = -0.420158;                            % COMPLETE
75 CMdE = -0.473495;                              % COMPLETE
76 CMalphaDot = -0.279883;                        % COMPLETE
77 CMq = -0.543272;                              % COMPLETE
78
79 % Lateral

```

```

80 CYbeta = -0.575519;           % COMPLETE
81 CYbetaDot = 0;               % COMPLETE
82 CYp = -0.150519;            % COMPLETE
83 CYr = 0.27852;              % COMPLETE
84 CYdA = 0;                    % COMPLETE
85 CYdR = 0.352187;            % COMPLETE
86
87 Clbeta = -0.21195;           % COMPLETE
88 ClbetaDot = 0;               % COMPLETE
89 Clp = -0.258664;             % COMPLETE
90 Clr = 0.122386;              % COMPLETE
91 CldA = 0.183164;             % COMPLETE
92 CldR = 0.0443965;           % COMPLETE
93
94 CNbeta = 0.0037412;          % COMPLETE
95 CNbetaDot = 0;               % COMPLETE
96 CNp = -0.0364167;           % COMPLETE
97 CNr = -0.119257;            % COMPLETE
98 CNdA = -0.001285;           % COMPLETE
99 CNdR = -0.147535;           % COMPLETE

```

C.2 Function for the thrust model

```

1 function [T,Tx,Ty,Tz,Txw,Tyw,Tzw] = THRUSTMODEL(dP,z,V,mach
   ,alpha,beta)
2     run('AircraftParameters.m')
3
4 % Atmosphere model
5     [~,~,~,rhoat]=atmosisa(z);
6     rho0 = 1.225;              % density at sea level
7     sigmaat=rhoat/rho0;        % relative density
8
9 % Magnitude of thrust according to the selected model
10 if model == 1 % JCWanner
11     T = kf*sigmaat*V^lambdaf*dP;
12
13 elseif model == 2 % Aerospatiale
14     T = ThrustSL*(1-mach+(mach^2)/2)*sigmaat*dP;
15
16 elseif model == 3 % JMattingly
17     T = ThrustSL*(0.568+0.25*(1.2-mach)^3)*sigmaat^0.6*dP;
18
19 elseif model == 4 % Hull
20     T = ThrustSL*sigmaat^a*dP;
21
22 elseif model == 5 % Howe

```

```

23     T = ThrustSL*(1+0.4*mach*(mach-2)*(1+BPR/10))*sigmaat
        ^0.9*dP;
24
25 elseif model == 6 % FaRux
26     T = ThrustSL*nparameter*sigmaat*(k1+k2*BPR+mach*(k3+k4*
        BPR))*dP;
27
28 end
29
30 % Thrust in body-fixed axes
31     Tx = T*cos(e);
32     Ty = 0;
33     Tz = T*sin(e);
34 % Thrust in wind axes
35     Txw = T*cos(e)*cos(alpha)*cos(beta)+T*sin(e)*cos(beta)*
        sin(alpha);
36     Tyw = -T*cos(e)*cos(alpha)*sin(beta)-T*sin(e)*sin(alpha)
        *sin(beta);
37     Tzw = -T*cos(e)*sin(alpha)+T*sin(e)*cos(alpha);
38
39 end

```

C.3 Function for the aerodynamic model

```

1     function [CL,CD,CY,Cl,CM,CN] = coefficients(V,alpha,
        alphaDot,p,q,r,beta,betaDot,dE,dA,dR)
2
3 % Function to calculate the coefficients of the aerodynamic
        model
4
5 run('AircraftParameters.m')
6
7     CL = CL0 + CLalpha*alpha + CLdE*dE + CLq*cw/(2*V)*q +
        CLalphaDot*cw/(2*V)*alphaDot;
8     CD = CD0 + K*CL^2;
9     CM = CM0 + CMalpha*alpha + CMdE*dE + CMq*cw/(2*V)*q +
        CMalphaDot*cw/(2*V)*alphaDot;
10
11     CY = CYbeta*beta + CYbetaDot*bw/(2*V)*betaDot + CYdA*dA
        + CYdR*dR + CYr*bw/(2*V)*r + CYp*bw/(2*V)*p;
12     Cl = Clbeta*beta + ClbetaDot*bw/(2*V)*betaDot + CldA*dA
        + CldR*dR + Clr*bw/(2*V)*r + Clp*bw/(2*V)*p;
13     CN = CNbeta*beta + CNbetaDot*bw/(2*V)*betaDot + CNdA*dA
        + CNdR*dR + CNr*bw/(2*V)*r + CNp*bw/(2*V)*p;
14
15 end

```

C.4 Function for the *Bryan Equations* in body-fixed axes

```

1 function dFdt= BRYANBODY(t,F)
2
3 global manoeuvre
4 run('InitialConditionsBody.m')
5 run('AircraftParameters.m')
6
7 % Atmosphere model
8 [Tat,aat,Pat,rhoat] = atmosisa(F(12)); % Function to
   obtain the atmosphere model as a function of
   altitude
9
10 rho0 = 1.225; % Density at z = 0
11 T0 = 288.16; % Temperature at z = 0
12 P0 = 101325; % Pressure at z = 0
13
14 thetaat = Tat/T0; % Relative temperature
15 sigmaat = rhoat/rho0; % Relative density
16 deltaat = Pat/P0; % Relative pressure
17
18 % Value of the controls
19 unitstep = t>=unitstep*time; % Variation of the controls
20 dP = dPinitial+unitstep*(dPfinal-dPinitial);
21 dEO = dEinitial+unitstep*(dEfinal-dEinitial);
22 dAO = dAinitial+unitstep*(dAfinal-dAinitial);
23 dRO = dRinitial+unitstep*(dRfinal-dRinitial);
24
25 % Aerodynamic Angles
26 alpha = atan(F(3)/F(1));
27 beta = asin(F(2)/(sqrt(F(1)^2+F(2)^2+F(3)^2)));
28 alphaDot = 0;
29 betaDot = 0;
30
31 % Thrust
32 % THRUSTMODEL(dP,z,V,mach,alpha,beta)
33 [T,Tx,Ty,Tz,~,~,~] = THRUSTMODEL(dP,F(12),sqrt(F(1)^2+F
   (2)^2+F(3)^2),sqrt(F(1)^2+F(2)^2+F(3)^2)/aat,alpha,
   beta);
34
35 % Aerodynamic coefficients
36 % coefficients(V,alpha,alphaDot,p,q,r,beta,betaDot,dE,
   dA,dR)
37 [CL,CD,CY,C1,CM,CN] = coefficients(sqrt(F(1)^2+F(2)^2+F
   (3)^2),alpha,alphaDot,F(4),F(5),F(6),beta,betaDot,
   dEO,dAO,dRO);

```

```

38
39
40 % [1] [2] [3]
41 % uDot=(Tx+1/2*rhoat*Sw*(u^2+v^2+w^2)*(-CD*cos(alpha)*
      cos(beta)+CL*sin(alpha)+CY*cos(alpha)*sin(beta))-m*g
      *sin(theta))/m-q*w+r*v;
42 % vDot=(Ty+1/2*rhoat*Sw*(u^2+v^2+w^2)*(-CD*sin(beta)+CY
      *cos(beta))+m*g*cos(theta)*sin(phi))/m-r*u+p*w;
43 % wDot=(Tz+1/2*rhoat*Sw*(u^2+v^2+w^2)*(-CL*cos(alpha)-
      CD*cos(beta)*sin(alpha)+CY*sin(alpha)*sin(beta))+m*g
      *cos(theta)*cos(phi))/m-p*v+q*u;
44
45 % [4] [5] [6]
46 % pDot=Izz/(Ixx*Izz-Ixz^2)*L+Ixz/(Ixx*Izz-Ixz^2)*N+((
      Ixz*(Ixx-Iyy+Izz))/(Ixx*Izz-Ixz^2))*p*q+((Izz*(Iyy-
      Izz)-Ixz^2)/(Ixx*Izz-Ixz^2))*r*q;
47 % qDot=MA/Iyy+((Izz-Ixx)/Iyy)*p*r+Ixz/Iyy*(r^2-p^2);
48 % rDot=Ixx/(Ixx*Izz-Ixz^2)*N+Ixz/(Ixx*Izz-Ixz^2)*L+((
      Ixx*(Ixx-Iyy)+Ixz^2)/(Ixx*Izz-Ixz^2))*p*q+((Ixz*(Iyy
      -Ixx-Izz))/(Ixx*Izz-Ixz^2))*r*q;
49
50 % [7bis] [8bis] [9bis]
51 % phiDot=p+(q*sin(phi)+r*cos(phi))*tan(theta);
52 % thetaDot=q*cos(phi)-r*sin(phi);
53 % psiDot=(q*sin(phi)+r*cos(phi))/cos(theta);
54
55 % [10] [11] [12]
56 % xDot=u*cos(psi)*cos(theta)+v*(cos(psi)*sin(theta)*sin
      (phi)-cos(phi)*sin(psi))+w*(sin(theta)*cos(phi)*cos(
      psi)+sin(phi)*sin(psi));
57 % yDot=u*cos(theta)*sin(psi)+v*(cos(phi)*cos(psi)+sin(
      theta)*sin(phi)*sin(psi))+w*(-cos(psi)*sin(phi)+cos(
      phi)*sin(theta)*sin(psi));
58 % -zDot=-u*sin(theta)+v*cos(theta)*sin(phi)+w*cos(theta
      )*cos(phi);
59
60
61 % Variables
62 % u = F(1)          uDot = dFdt(1)
63 % v = F(2)          vDot = dFdt(2)
64 % w = F(3)          wDot = dFdt(3)
65 % p = F(4)          pDot = dFdt(4)
66 % q = F(5)          qDot = dFdt(5)
67 % r = F(6)          rDot = dFdt(6)
68 % phi = F(7)        phiDot = dFdt(7)
69 % theta = F(8)      thetaDot = dFdt(8)
70 % psi = F(9)        psiDot = dFdt(9)
71 % x = F(10)         xDot = dFdt(10)

```

```

72     % y = F(11)       yDot = dFdt(11)
73     % z = F(12)       zDot = dFdt(12)
74
75 % Bryan Equations
76 % Traslation Equations
77 % [1] [2] [3]
78 uDot = (Tx+1/2*rhoat*Sw*(F(1)^2+F(2)^2+F(3)^2)*(-CD*cos
      (alpha)*cos(beta)+CL*sin(alpha)+CY*cos(alpha)*sin(
      beta))-m*g*sin(F(8)))/m - F(5)*F(3) + F(6)*F(2);
79 vDot = (Ty+1/2*rhoat*Sw*(F(1)^2+F(2)^2+F(3)^2)*(-CD*sin
      (beta)+CY*cos(beta))+m*g*cos(F(8))*sin(F(7)))/m - F
      (6)*F(1) + F(4)*F(3);
80 wDot = (Tz+1/2*rhoat*Sw*(F(1)^2+F(2)^2+F(3)^2)*(-CL*cos
      (alpha)-CD*cos(beta)*sin(alpha)+CY*sin(alpha)*sin(
      beta))+m*g*cos(F(8))*cos(F(7)))/m - F(4)*F(2) + F(5)
      *F(1);
81
82 % Rotation Equations
83 % [4] [5] [6]
84 pDot = Izz/(Ixx*Izz-Ixz^2)*(1/2*rhoat*bw*(F(1)^2+F(2)
      ^2+F(3)^2)*Sw*Cl) + Ixz/(Ixx*Izz-Ixz^2)*(1/2*rhoat*
      bw*(F(1)^2+F(2)^2+F(3)^2)*Sw*CN) + ((Ixz*(Ixx-Iyy+
      Izz))/(Ixx*Izz-Ixz^2))*F(4)*F(5) + ((Izz*(Iyy-Izz)-
      Ixz^2)/(Ixx*Izz-Ixz^2))*F(6)*F(5);
85 qDot = (1/2*rhoat*cw*(F(1)^2+F(2)^2+F(3)^2)*Sw*CM)/Iyy
      + ((Izz-Ixx)/Iyy)*F(4)*F(6) + Ixz/Iyy*(F(6)^2-F(4)
      ^2);
86 rDot = Ixx/(Ixx*Izz-Ixz^2)*(1/2*rhoat*bw*(F(1)^2+F(2)
      ^2+F(3)^2)*Sw*CN) + Ixz/(Ixx*Izz-Ixz^2)*(1/2*rhoat*
      bw*(F(1)^2+F(2)^2+F(3)^2)*Sw*Cl) + ((Ixx*(Ixx-Iyy)+
      Ixz^2)/(Ixx*Izz-Ixz^2))*F(4)*F(5) + ((Ixz*(Iyy-Ixx-
      Izz))/(Ixx*Izz-Ixz^2))*F(6)*F(5);
87
88 % Euler
89 % [7bis] [8bis] [9bis]
90 phiDot = F(4) + (F(5)*sin(F(7))+F(6)*cos(F(7)))*tan(F
      (8));
91 thetaDot = F(5)*cos(F(7)) - F(6)*sin(F(7));
92 psiDot = (F(5)*sin(F(7))+F(6)*cos(F(7)))/cos(F(8));
93
94 % Kinematic Equations
95 % [10] [11] [12]
96 xDot = F(1)*cos(F(9))*cos(F(8)) + F(2)*(cos(F(9))*sin(F
      (8))*sin(F(7))-cos(F(7))*sin(F(9))) + F(3)*(sin(F(8)
      )*cos(F(7))*cos(F(9))+sin(F(7))*sin(F(9)));
97 yDot = F(1)*cos(F(8))*sin(F(9)) + F(2)*(cos(F(7))*cos(F
      (9))+sin(F(8))*sin(F(7))*sin(F(9))) + F(3)*(-cos(F
      (9))*sin(F(7))+cos(F(7))*sin(F(8))*sin(F(9)));

```



```

98     zDot = -(-F(1)*sin(F(8)) + F(2)*cos(F(8))*sin(F(7)) + F
          (3)*cos(F(8))*cos(F(7)));
99
100
101 % Fuel mass consumption
102     fuelDot = -Ce*T;
103
104 % Integration vector
105     dFdt = [uDot; vDot; wDot; pDot; qDot; rDot; phiDot;
             thetaDot; psiDot; xDot; yDot; zDot; fuelDot];
106
107 end

```

C.5 Function for the *Bryan Equations* in wind axes

```

1  function dFdt = BRYANWIND(t,F)
2
3  global manoeuvre
4  run('InitialConditionsWind.m')
5  run('AircraftParameters.m')
6
7
8  % Atmosphere model
9  [Tat,aat,Pat,rhoat] = atmosisa(F(12)); % Function to
          obtain the atmosphere model as a function of
          altitude
10
11     rho0 = 1.225;           % Density at z = 0
12     T0 = 288.16;          % Temperature at z = 0
13     P0 = 101325;         % Pressure at z = 0
14
15     thetaat = Tat/T0;     % Relative temperature
16     sigmaat = rhoat/rho0; % Relative density
17     deltaat = Pat/P0;    % Relative pressure
18
19 % Value of the controls
20     unitstep = t>=unitsteptime;
21     dP = dPinitial+unitstep*(dPfinal-dPinitial);
22     dE = dEinitial+unitstep*(dEfinal-dEinitial);
23     dA = dAinitial+unitstep*(dAfinal-dAinitial);
24     dR = dRinitial+unitstep*(dRfinal-dRinitial);
25
26 % Thrust
27     % THRUSTMODEL(dP,z,V,mach,alpha,beta)
28     [T,~,~,~,Txw,Tyw,Tzw] = THRUSTMODEL(dP,F(12),F(1),F(1)/
          aat,F(3),F(2));
29

```

```

30
31 % [1] [2] [3]
32 % VDot=(Txw+1/2*rhoat*Sw*V^2*CXw-m*g*sin(gamma))/m
33 % V*m*rw=(Tyw+1/2*rhoat*Sw*V^2*CYw+m*g*cos(gamma)*sin(
34 % -V*m*qw=(Tzw+1/2*rhoat*Sw*V^2*CZw+m*g*cos(gamma)*cos(
35 %
36 % rw=r*cos(alpha)-p*sin(alpha)+betaDot
37 % qw=-sin(beta)*(p*cos(alpha)+r*sin(alpha))+cos(beta)*(
38 % q-alphaDot)
39 % Substituting:
40 % V*m*(r*cos(alpha)-p*sin(alpha)+betaDot)=(-T*cos(alpha
41 % )*sin(beta)+1/2*rhoat*Sw*V^2*CYw+m*g*cos(gamma)*sin(
42 % mu))
43 % -V*m*(-sin(beta)*(p*cos(alpha)+r*sin(alpha))+cos(beta
44 % )*(q-alphaDot))=(-T*sin(alpha)+1/2*rhoat*Sw*V^2*CZw+
45 % m*g*cos(gamma)*cos(mu))
46
47
48 % [4] [5] [6]
49 % pDot=Izz/(Ixx*Izz-Ixz^2)*L+Ixz/(Ixx*Izz-Ixz^2)*N+((
50 % Ixz*(Ixx-Iyy+Izz))/(Ixx*Izz-Ixz^2))*p*q+((Izz*(Iyy-
51 % Izz)-Ixz^2)/(Ixx*Izz-Ixz^2))*r*q;
52 % qDot=MA/Iyy+((Izz-Ixx)/Iyy)*p*r+Ixz/Iyy*(r^2-p^2);
53 % rDot=Ixx/(Ixx*Izz-Ixz^2)*N+Ixz/(Ixx*Izz-Ixz^2)*L+((
54 % Ixx*(Ixx-Iyy)+Ixz^2)/(Ixx*Izz-Ixz^2))*p*q+((Ixz*(Iyy
55 % -Ixx-Izz))/(Ixx*Izz-Ixz^2))*r*q;
56
57
58 % [7bis] [8bis] [9bis]
59 % muDot=pw+(qw*sin(mu)+rw*cos(mu))*tan(gamma)
60 % gammaDot=qw*cos(mu)-rw*sin(mu);
61 % chiDot=(qw*sin(mu)+rw*cos(mu))/cos(gamma)
62
63
64 % [10] [11] [12]
65 % xDot=V*cos(gamma)*cos(chi);
66 % yDot=V*cos(gamma)*sin(chi);
67 % -zDot=-V*sin(gamma);
68
69
70 % Variables
71 % V = F(1)          VDot = dFdt(1)
72 % beta = F(2)      betaDot = dFdt(2)
73 % alpha = F(3)     alphaDot = dFdt(3)
74 % p = F(4)         pDot = dFdt(4)
75 % q = F(5)         qDot = dFdt(5)
76 % r = F(6)         rDot = dFdt(6)
77 % mu = F(7)        muDot = dFdt(7)
78 % gamma = F(8)     gammaDot = dFdt(8)

```

```

67 % chi = F(9)          chiDot = dFdt(9)
68 % x = F(10)         xDot = dFdt(10)
69 % y = F(11)         yDot = dFdt(11)
70 % z = F(12)         zDot = dFdt(12)
71
72
73 % Bryan Equations
74 % Traslation Equations
75 % [1] [2] [3]
76 VDot = (1/(4*F(1)^2*m*(4*m + CLalphaDot*cw*rhoat*Sw*sec
(F(2)))^2))*(-16*CD0*CLalphaDot*cw*F(1)^4*m*rhoat^2*
Sw^2 + 64*F(1)^2*m^2*Twx - 32*CL0*CLalphaDot*cw*F(1)
^2*K*m*rhoat*Sw*Tzw - 32*CLalphaDot*CLdE*cw*dE*F(1)
^2*K*m*rhoat*Sw*Tzw - 32*CLalpha*CLalphaDot*cw*F(1)
^2*F(3)*K*m*rhoat*Sw*Tzw - 16*CLalphaDot^2*cw^2*F(1)
*F(5)*K*m*rhoat*Sw*Tzw - 16*CLalphaDot*CLq*cw^2*F(1)
*F(5)*K*m*rhoat*Sw*Tzw - 8*F(1)^2*(4*CD0*F(1)^2 +
(2*CL0*F(1) + 2*CLdE*dE*F(1) + 2*CLalpha*F(1)*F(3) +
CLalphaDot*cw*F(5) + CLq*cw*F(5))^2*K)*m^2*rhoat*Sw
*cos(F(2)) - 2*CD0*CLalphaDot^2*cw^2*F(1)^4*rhoat^3*
Sw^3*sec(F(2)) + ...
77 32*CLalphaDot*cw*F(1)^2*m*rhoat*Sw*Twx*sec(F(2)) -
8*CLalphaDot^2*cw^2*K*rhoat*Sw*Tzw^2*sec(F(2)) -
8*CLalphaDot^2*cw^2*g^2*K*m^2*rhoat*Sw*cos(F(7)
)^2*cos(F(8))^2*sec(F(2)) + 4*CLalphaDot^2*cw^2*
F(1)^2*rhoat^2*Sw^2*Twx*sec(F(2))^2 + 32*CYdA*dA
*F(1)^4*m^2*rhoat*Sw*sin(F(2)) + 32*CYdR*dR*F(1)
^4*m^2*rhoat*Sw*sin(F(2)) + 32*CYbeta*F(1)^4*F
(2)*m^2*rhoat*Sw*sin(F(2)) + 16*bw*CYp*F(1)^3*F
(4)*m^2*rhoat*Sw*sin(F(2)) + 16*bw*CYr*F(1)^3*F
(6)*m^2*rhoat*Sw*sin(F(2)) + 32*CL0*CLalphaDot*
cw*F(1)^3*F(4)*K*m^2*rhoat*Sw*cos(F(3))*sin(F(2)
) + 32*CLalphaDot*CLdE*cw*dE*F(1)^3*F(4)*K*m^2*
rhoat*Sw*cos(F(3))*sin(F(2)) + 32*CLalpha*
CLalphaDot*cw*F(1)^3*F(3)*F(4)*K*m^2*rhoat*Sw*
cos(F(3))*sin(F(2)) + 16*CLalphaDot^2*cw^2*F(1)
^2*F(4)*F(5)*K*m^2*rhoat*Sw*cos(F(3))*sin(F(2))
+ 16*CLalphaDot*CLq*cw^2*F(1)^2*F(4)*F(5)*K*m^2*
rhoat*Sw*cos(F(3))*sin(F(2)) + 32*CL0*CLalphaDot
*cw*F(1)^3*F(6)*K*m^2*rhoat*Sw*sin(F(2))*sin(F
(3)) + 32*CLalphaDot*CLdE*cw*dE*F(1)^3*F(6)*K*m
^2*rhoat*Sw*sin(F(2))*sin(F(3)) + 32*CLalpha*
CLalphaDot*cw*F(1)^3*F(3)*F(6)*K*m^2*rhoat*Sw*
sin(F(2))*sin(F(3)) + 16*CLalphaDot^2*cw^2*F(1)
^2*F(5)*F(6)*K*m^2*rhoat*Sw*sin(F(2))*sin(F(3))
+ 16*CLalphaDot*CLq*cw^2*F(1)^2*F(5)*F(6)*K*m^2*
rhoat*Sw*sin(F(2))*sin(F(3)) - 64*F(1)^2*g*m^3*
sin(F(8)) - 32*CLalphaDot*cw*F(1)^2*g*m^2*rhoat*

```

$$\begin{aligned}
& Sw \cdot \sec(F(2)) \cdot \sin(F(8)) - 4 \cdot CLalphaDot^2 \cdot cw^2 \cdot F(1)^2 \cdot g \cdot m \cdot rhoat^2 \cdot Sw^2 \cdot \sec(F(2))^2 \cdot \sin(F(8)) + \\
& 16 \cdot CLalphaDot \cdot cw \cdot CYdA \cdot dA \cdot F(1)^4 \cdot m \cdot rhoat^2 \cdot Sw^2 \cdot \tan(F(2)) + 16 \cdot CLalphaDot \cdot cw \cdot CYdR \cdot dR \cdot F(1)^4 \cdot m \cdot rhoat^2 \cdot Sw^2 \cdot \tan(F(2)) + 16 \cdot CLalphaDot \cdot cw \cdot CYbeta \cdot F(1)^4 \cdot F(2) \cdot m \cdot rhoat^2 \cdot Sw^2 \cdot \tan(F(2)) + \dots
\end{aligned}$$

78

$$\begin{aligned}
& 8 \cdot bw \cdot CLalphaDot \cdot cw \cdot CYp \cdot F(1)^3 \cdot F(4) \cdot m \cdot rhoat^2 \cdot Sw^2 \cdot \tan(F(2)) + 8 \cdot bw \cdot CLalphaDot \cdot cw \cdot CYr \cdot F(1)^3 \cdot F(6) \cdot m \cdot rhoat^2 \cdot Sw^2 \cdot \tan(F(2)) + 16 \cdot CLalphaDot^2 \cdot cw^2 \cdot F(1) \cdot F(4) \cdot K \cdot m \cdot rhoat \cdot Sw \cdot Tzw \cdot \cos(F(3)) \cdot \tan(F(2)) + \\
& 2 \cdot CLalphaDot^2 \cdot cw^2 \cdot CYdA \cdot dA \cdot F(1)^4 \cdot rhoat^3 \cdot Sw^3 \cdot \sec(F(2)) \cdot \tan(F(2)) + 2 \cdot CLalphaDot^2 \cdot cw^2 \cdot CYdR \cdot dR \cdot F(1)^4 \cdot rhoat^3 \cdot Sw^3 \cdot \sec(F(2)) \cdot \tan(F(2)) + 2 \cdot CLalphaDot^2 \cdot cw^2 \cdot CYbeta \cdot F(1)^4 \cdot F(2) \cdot rhoat^3 \cdot Sw^3 \cdot \sec(F(2)) \cdot \tan(F(2)) + bw \cdot CLalphaDot^2 \cdot cw^2 \cdot CYp \cdot F(1)^3 \cdot F(4) \cdot rhoat^3 \cdot Sw^3 \cdot \sec(F(2)) \cdot \tan(F(2)) + \\
& bw \cdot CLalphaDot^2 \cdot cw^2 \cdot CYr \cdot F(1)^3 \cdot F(6) \cdot rhoat^3 \cdot Sw^3 \cdot \sec(F(2)) \cdot \tan(F(2)) - 8 \cdot CLalphaDot^2 \cdot cw^2 \cdot F(1)^2 \cdot F(4)^2 \cdot K \cdot m^2 \cdot rhoat \cdot Sw \cdot \cos(F(3))^2 \cdot \sin(F(2)) \cdot \tan(F(2)) + 16 \cdot CLalphaDot^2 \cdot cw^2 \cdot F(1) \cdot F(6) \cdot K \cdot m \cdot rhoat \cdot Sw \cdot Tzw \cdot \sin(F(3)) \cdot \tan(F(2)) - 8 \cdot CLalphaDot^2 \cdot cw^2 \cdot F(1)^2 \cdot F(4) \cdot F(6) \cdot K \cdot m^2 \cdot rhoat \cdot Sw \cdot \sin(F(2)) \cdot \sin(F(3))^2 \cdot \tan(F(2)) - 8 \cdot CLalphaDot^2 \cdot cw^2 \cdot F(1)^2 \cdot F(4) \cdot F(6) \cdot K \cdot m^2 \cdot rhoat \cdot Sw \cdot \sin(F(2)) \cdot \sin(2 \cdot F(3)) \cdot \tan(F(2)) - 16 \cdot CLalphaDot \cdot cw \cdot g \cdot K \cdot m \cdot rhoat \cdot Sw \cdot \cos(F(7)) \cdot \cos(F(8)) \cdot (CLalphaDot \cdot cw \cdot Tzw \cdot \sec(F(2)) + F(1) \cdot m \cdot (2 \cdot CL0 \cdot F(1) + 2 \cdot CLdE \cdot dE \cdot F(1) + 2 \cdot CLalpha \cdot F(1) \cdot F(3) + CLalphaDot \cdot cw \cdot F(5) + CLq \cdot cw \cdot F(5) - CLalphaDot \cdot cw \cdot F(4) \cdot \cos(F(3)) \cdot \tan(F(2)) - CLalphaDot \cdot cw \cdot F(6) \cdot \sin(F(3)) \cdot \tan(F(2)))));
\end{aligned}$$

79

$$\begin{aligned}
betaDot = & -(1 / (4 \cdot F(1)^3 \cdot m \cdot (4 \cdot m + CLalphaDot \cdot cw \cdot rhoat \cdot Sw \cdot \sec(F(2)))^2)) \cdot (16 \cdot CLalphaDot \cdot cw \cdot CYdA \cdot dA \cdot F(1)^4 \cdot m \cdot rhoat^2 \cdot Sw^2 + 16 \cdot CLalphaDot \cdot cw \cdot CYdR \cdot dR \cdot F(1)^4 \cdot m \cdot rhoat^2 \cdot Sw^2 + 16 \cdot CLalphaDot \cdot cw \cdot CYbeta \cdot F(1)^4 \cdot F(2) \cdot m \cdot rhoat^2 \cdot Sw^2 + 8 \cdot bw \cdot CLalphaDot \cdot cw \cdot CYp \cdot F(1)^3 \cdot F(4) \cdot m \cdot rhoat^2 \cdot Sw^2 + 8 \cdot bw \cdot CLalphaDot \cdot cw \cdot CYr \cdot F(1)^3 \cdot F(6) \cdot m \cdot rhoat^2 \cdot Sw^2 - 64 \cdot F(1)^2 \cdot m^2 \cdot Tyw + 16 \cdot F(1)^3 \cdot (2 \cdot CYdA \cdot dA \cdot F(1) + 2 \cdot CYdR \cdot dR \cdot F(1) + 2 \cdot CYbeta \cdot F(1) \cdot F(2) + bw \cdot CYp \cdot F(4) + bw \cdot CYr \cdot F(6)) \cdot m^2 \cdot rhoat \cdot Sw \cdot \cos(F(2)) + 2 \cdot CLalphaDot^2 \cdot cw^2 \cdot CYdA \cdot dA \cdot F(1)^4 \cdot rhoat^3 \cdot Sw^3 \cdot \sec(F(2)) + 2 \cdot CLalphaDot^2 \cdot cw^2 \cdot CYdR \cdot dR \cdot F(1)^4 \cdot rhoat^3 \cdot Sw^3 \cdot \sec(F(2)) + 2 \cdot CLalphaDot^2 \cdot cw^2 \cdot CYbeta \cdot F(1)^4 \cdot F(2) \cdot rhoat^3 \cdot Sw^3 \cdot \sec(F(2)) + bw \cdot CLalphaDot^2 \cdot cw^2 \cdot CYp \cdot F(1)^3 \cdot F(4) \cdot rhoat^3 \cdot Sw^3 \cdot \sec(F(2)) + \dots
\end{aligned}$$

80

$$\begin{aligned}
& bw \cdot CLalphaDot^2 \cdot cw^2 \cdot CYr \cdot F(1)^3 \cdot F(6) \cdot rhoat^3 \cdot Sw^3 \cdot \sec(F(2)) - 32 \cdot CLalphaDot \cdot cw \cdot F(1)^2 \cdot m \cdot rhoat \cdot Sw \cdot Tyw \cdot \sec(F(2)) - 4 \cdot CLalphaDot^2 \cdot cw^2 \cdot F(1)^2 \cdot rhoat^2 \cdot Sw^2 \cdot Tyw \cdot \sec(F(2))^2 + 32 \cdot CD0 \cdot F(1)^4 \cdot m^2 \cdot
\end{aligned}$$

$$\begin{aligned}
& \text{rhoat} * \text{Sw} * \sin(F(2)) + 32 * \text{CL0}^2 * F(1)^4 * K * m^2 * \text{rhoat} \\
& * \text{Sw} * \sin(F(2)) + 64 * \text{CL0} * \text{CLdE} * dE * F(1)^4 * K * m^2 * \\
& \text{rhoat} * \text{Sw} * \sin(F(2)) + 32 * \text{CLdE}^2 * dE^2 * F(1)^4 * K * m \\
& ^2 * \text{rhoat} * \text{Sw} * \sin(F(2)) + 64 * \text{CL0} * \text{CLalpha} * F(1)^4 * F \\
& (3) * K * m^2 * \text{rhoat} * \text{Sw} * \sin(F(2)) + 64 * \text{CLalpha} * \text{CLdE} * \\
& dE * F(1)^4 * F(3) * K * m^2 * \text{rhoat} * \text{Sw} * \sin(F(2)) + 32 * \\
& \text{CLalpha}^2 * F(1)^4 * F(3)^2 * K * m^2 * \text{rhoat} * \text{Sw} * \sin(F(2)) \\
& + 32 * \text{CL0} * \text{CLalphaDot} * cw * F(1)^3 * F(5) * K * m^2 * \text{rhoat} * \\
& \text{Sw} * \sin(F(2)) + 32 * \text{CL0} * \text{CLq} * cw * F(1)^3 * F(5) * K * m^2 * \\
& \text{rhoat} * \text{Sw} * \sin(F(2)) + 32 * \text{CLalphaDot} * \text{CLdE} * cw * dE * F \\
& (1)^3 * F(5) * K * m^2 * \text{rhoat} * \text{Sw} * \sin(F(2)) + 32 * \text{CLdE} * \\
& \text{CLq} * cw * dE * F(1)^3 * F(5) * K * m^2 * \text{rhoat} * \text{Sw} * \sin(F(2)) + \\
& 32 * \text{CLalpha} * \text{CLalphaDot} * cw * F(1)^3 * F(3) * F(5) * K * m \\
& ^2 * \text{rhoat} * \text{Sw} * \sin(F(2)) + 32 * \text{CLalpha} * \text{CLq} * cw * F(1) \\
& ^3 * F(3) * F(5) * K * m^2 * \text{rhoat} * \text{Sw} * \sin(F(2)) + 8 * \\
& \text{CLalphaDot}^2 * cw^2 * F(1)^2 * F(5)^2 * K * m^2 * \text{rhoat} * \text{Sw} * \\
& \sin(F(2)) + 16 * \text{CLalphaDot} * \text{CLq} * cw^2 * F(1)^2 * F(5) \\
& ^2 * K * m^2 * \text{rhoat} * \text{Sw} * \sin(F(2)) + 8 * \text{CLq}^2 * cw^2 * F(1) \\
& ^2 * F(5)^2 * K * m^2 * \text{rhoat} * \text{Sw} * \sin(F(2)) - 64 * F(1)^3 * F \\
& (4) * m^3 * \sin(F(3)) - 32 * \text{CLalphaDot} * cw * F(1)^3 * F(4) \\
& * m^2 * \text{rhoat} * \text{Sw} * \sec(F(2)) * \sin(F(3)) - 4 * \text{CLalphaDot} \\
& ^2 * cw^2 * F(1)^3 * F(4) * m * \text{rhoat}^2 * \text{Sw}^2 * \sec(F(2))^2 * \\
& \sin(F(3)) - 64 * F(1)^2 * g * m^3 * \cos(F(8)) * \sin(F(7)) \\
& - 32 * \text{CLalphaDot} * cw * F(1)^2 * g * m^2 * \text{rhoat} * \text{Sw} * \cos(F \\
& (8)) * \sec(F(2)) * \sin(F(7)) - 4 * \text{CLalphaDot}^2 * cw^2 * F \\
& (1)^2 * g * m * \text{rhoat}^2 * \text{Sw}^2 * \cos(F(8)) * \sec(F(2))^2 * \sin \\
& (F(7)) + 16 * \text{CD0} * \text{CLalphaDot} * cw * F(1)^4 * m * \text{rhoat}^2 * \\
& \text{Sw}^2 * \tan(F(2)) + \dots
\end{aligned}$$

81

$$\begin{aligned}
& 32 * \text{CL0} * \text{CLalphaDot} * cw * F(1)^2 * K * m * \text{rhoat} * \text{Sw} * \text{Tzw} * \tan(F \\
& (2)) + 32 * \text{CLalphaDot} * \text{CLdE} * cw * dE * F(1)^2 * K * m * \text{rhoat} \\
& * \text{Sw} * \text{Tzw} * \tan(F(2)) + 32 * \text{CLalpha} * \text{CLalphaDot} * cw * F \\
& (1)^2 * F(3) * K * m * \text{rhoat} * \text{Sw} * \text{Tzw} * \tan(F(2)) + 16 * \\
& \text{CLalphaDot}^2 * cw^2 * F(1) * F(5) * K * m * \text{rhoat} * \text{Sw} * \text{Tzw} * \tan \\
& (F(2)) + 16 * \text{CLalphaDot} * \text{CLq} * cw^2 * F(1) * F(5) * K * m * \\
& \text{rhoat} * \text{Sw} * \text{Tzw} * \tan(F(2)) + 32 * \text{CL0} * \text{CLalphaDot} * cw * F \\
& (1)^2 * g * K * m^2 * \text{rhoat} * \text{Sw} * \cos(F(7)) * \cos(F(8)) * \tan(F \\
& (2)) + 32 * \text{CLalphaDot} * \text{CLdE} * cw * dE * F(1)^2 * g * K * m^2 * \\
& \text{rhoat} * \text{Sw} * \cos(F(7)) * \cos(F(8)) * \tan(F(2)) + 32 * \\
& \text{CLalpha} * \text{CLalphaDot} * cw * F(1)^2 * F(3) * g * K * m^2 * \text{rhoat} * \\
& \text{Sw} * \cos(F(7)) * \cos(F(8)) * \tan(F(2)) + 16 * \text{CLalphaDot} \\
& ^2 * cw^2 * F(1) * F(5) * g * K * m^2 * \text{rhoat} * \text{Sw} * \cos(F(7)) * \cos \\
& (F(8)) * \tan(F(2)) + 16 * \text{CLalphaDot} * \text{CLq} * cw^2 * F(1) * F \\
& (5) * g * K * m^2 * \text{rhoat} * \text{Sw} * \cos(F(7)) * \cos(F(8)) * \tan(F \\
& (2)) + 2 * \text{CD0} * \text{CLalphaDot}^2 * cw^2 * F(1)^4 * \text{rhoat}^3 * \text{Sw} \\
& ^3 * \sec(F(2)) * \tan(F(2)) + 8 * \text{CLalphaDot}^2 * cw^2 * K * \\
& \text{rhoat} * \text{Sw} * \text{Tzw}^2 * \sec(F(2)) * \tan(F(2)) + 16 * \\
& \text{CLalphaDot}^2 * cw^2 * g * K * m * \text{rhoat} * \text{Sw} * \text{Tzw} * \cos(F(7)) * \\
& \cos(F(8)) * \sec(F(2)) * \tan(F(2)) + 8 * \text{CLalphaDot}^2 *
\end{aligned}$$

```

      cw^2*g^2*K*m^2*rhoat*Sw*cos(F(7))^2*cos(F(8))^2*
      sec(F(2))*tan(F(2)) - 32*CL0*CLalphaDot*cw*F(1)
      ^3*F(6)*K*m^2*rhoat*Sw*sin(F(2))*sin(F(3))*tan(F
      (2)) - 32*CLalphaDot*CLdE*cw*dE*F(1)^3*F(6)*K*m
      ^2*rhoat*Sw*sin(F(2))*sin(F(3))*tan(F(2)) - 32*
      CLalpha*CLalphaDot*cw*F(1)^3*F(3)*F(6)*K*m^2*
      rhoat*Sw*sin(F(2))*sin(F(3))*tan(F(2)) - 16*
      CLalphaDot^2*cw^2*F(1)^2*F(5)*F(6)*K*m^2*rhoat*
      Sw*sin(F(2))*sin(F(3))*tan(F(2)) - 16*CLalphaDot
      *CLq*cw^2*F(1)^2*F(5)*F(6)*K*m^2*rhoat*Sw*sin(F
      (2))*sin(F(3))*tan(F(2)) + 8*CLalphaDot^2*cw^2*F
      (1)^2*F(4)^2*K*m^2*rhoat*Sw*cos(F(3))^2*sin(F(2)
      )*tan(F(2))^2 - 16*CLalphaDot^2*cw^2*F(1)*F(6)*K
      *m*rhoat*Sw*Tzw*sin(F(3))*tan(F(2))^2 - 16*
      CLalphaDot^2*cw^2*F(1)*F(6)*g*K*m^2*rhoat*Sw*cos
      (F(7))*cos(F(8))*sin(F(3))*tan(F(2))^2 + ...
82      8*CLalphaDot^2*cw^2*F(1)^2*F(6)^2*K*m^2*rhoat*Sw*
      sin(F(2))*sin(F(3))^2*tan(F(2))^2 + 8*CLalphaDot
      ^2*cw^2*F(1)^2*F(4)*F(6)*K*m^2*rhoat*Sw*sin(F(2)
      )*sin(2*F(3))*tan(F(2))^2 + 4*F(1)*m*cos(F(3))
      *(16*F(1)^2*F(6)*m^2 + 8*CLalphaDot*cw*F(1)^2*F
      (6)*m*rhoat*Sw*sec(F(2)) + CLalphaDot^2*cw^2*F
      (1)^2*F(6)*rhoat^2*Sw^2*sec(F(2))^2 - 4*
      CLalphaDot*cw*F(1)*F(4)*(2*CL0*F(1) + 2*CLdE*dE*
      F(1) + 2*CLalpha*F(1)*F(3) + CLalphaDot*cw*F(5)
      + CLq*cw*F(5))*K*m*rhoat*Sw*sin(F(2))*tan(F(2))
      - 4*CLalphaDot^2*cw^2*F(4)*K*rhoat*Sw*Tzw*tan(F
      (2))^2 - 4*CLalphaDot^2*cw^2*F(4)*g*K*m*rhoat*Sw
      *cos(F(7))*cos(F(8))*tan(F(2))^2));
83      alphaDot = ((-2*CL0*F(1)^2*rhoat*Sw + 2*CLdE*dE*F(1)^2*
      rhoat*Sw + 2*CLalpha*F(1)^2*F(3)*rhoat*Sw + CLq*cw*F
      (1)*F(5)*rhoat*Sw - 4*Tzw - 4*g*m*cos(F(7))*cos(F(8)
      ))*sec(F(2)) + 4*F(1)*m*(F(5) - F(4)*cos(F(3))*tan(F
      (2)) - F(6)*sin(F(3))*tan(F(2))))/(F(1)*(4*m +
      CLalphaDot*cw*rhoat*Sw*sec(F(2))));
84
85      % Rotation Equations
86      % [4] [5] [6]
87      pDot = Izz/(Ixx*Izz-Ixz^2)*(1/2*rhoat*bw*F(1)^2*Sw*(
      Clbeta*F(2)+CldA*dA+CldR*dR+Clr*bw/(2*F(1))*F(6)+Clp
      *bw/(2*F(1))*F(4))+Ixz/(Ixx*Izz-Ixz^2)*(1/2*rhoat*
      bw*F(1)^2*Sw*(CNbeta*F(2)+CNdA*dA+CNdR*dR+CNr*bw/(2*
      F(1))*F(6)+CNp*bw/(2*F(1))*F(4)))+((Ixz*(Ixx-Iyy+Izz
      ))/(Ixx*Izz-Ixz^2))*F(4)*F(5)+((Izz*(Iyy-Izz)-Ixz^2)
      /(Ixx*Izz-Ixz^2))*F(6)*F(5);
88      qDot = (1/2*rhoat*cw*F(1)^2*Sw*(CM0+CMalpha*F(3)+CMdE*
      dE+CMq*cw/(2*F(1))*F(5)+CMalphaDot*cw/(2*F(1))*
      alphaDot))/Iyy+((Izz-Ixx)/Iyy)*F(4)*F(6)+Ixz/Iyy*(F

```

```

      (6)^2-F(4)^2);
89  rDot = Ixx/(Ixx*Izz-Ixz^2)*(1/2*rhoat*bw*F(1)^2*Sw*(
      CNbeta*F(2)+CNdA*dA+CNdR*dR+CNr*bw/(2*F(1))*F(6)+CNp
      *bw/(2*F(1))*F(4))+Ixz/(Ixx*Izz-Ixz^2)*(1/2*rhoat*
      bw*F(1)^2*Sw*(Clbeta*F(2)+CldA*dA+CldR*dR+Clr*bw/(2*
      F(1))*F(6)+Clp*bw/(2*F(1))*F(4))+((Ixx*(Ixx-Iyy)+
      Ixz^2)/(Ixx*Izz-Ixz^2))*F(4)*F(5)+((Ixz*(Iyy-Ixx-Izz
      ))/(Ixx*Izz-Ixz^2))*F(6)*F(5);
90
91  % Angular velocities in wind axes
92  pw = cos(F(2))*(F(4)*cos(F(3))+F(6)*sin(F(3))) + sin(F
      (2))*(F(5)-alphaDot);
93  qw = -sin(F(2))*(F(4)*cos(F(3))+F(6)*sin(F(3))) + cos(F
      (2))*(F(5)-alphaDot);
94  rw = F(6)*cos(F(3)) - F(4)*sin(F(3)) + betaDot;
95
96  % Euler
97  % [7bis] [8bis] [9bis]
98  muDot = pw+(qw*sin(F(7))+rw*cos(F(7)))*tan(F(8));
99  gammaDot = qw*cos(F(7))-rw*sin(F(7));
100  chiDot = (qw*sin(F(7))+rw*cos(F(7)))/cos(F(8));
101
102  % Kinematic equations
103  % [10] [11] [12]
104  xDot = F(1)*cos(F(8))*cos(F(9));
105  yDot = F(1)*cos(F(8))*sin(F(9));
106  zDot = -(-F(1)*sin(F(8)));
107
108
109  % Fuel mass consumption
110  fuelDot = -Ce*T;
111
112  % Integration vector
113  dFdt = [VDot; betaDot; alphaDot; pDot; qDot; rDot;
      muDot; gammaDot; chiDot; xDot; yDot; zDot; fuelDot];
114
115
116  end

```


C.6 Function for the *Bryan Equations* with quaternions

```

1  function dFdt= BRYANBODYQUATERNIONS(t,F)
2
3  global manoeuvre
4  run('InitialConditionsQuaternions.m')
5  run('AircraftParameters.m')
6
7  % Atmosphere model
8  [Tat,aat,Pat,rhoat] = atmosisa(F(13)); % Function to
    obtain the atmosphere model as a function of
    altitude
9
10 rho0 = 1.225;           % Density at z = 0
11 T0 = 288.16;           % Temperature at z = 0
12 P0 = 101325;           % Pressure at z = 0
13
14 thetaat = Tat/T0;      % Relative temperature
15 sigmaat = rhoat/rho0;  % Relative density
16 deltaat = Pat/P0;      % Relative pressure
17
18 % Value of the controls
19 unitstep = t>=unitsteptime; % Variation of the controls
20 dP = dPinitial+unitstep*(dPfinal-dPinitial);
21 dEO = dEinitial+unitstep*(dEfinal-dEinitial);
22 dAO = dAinitial+unitstep*(dAfinal-dAinitial);
23 dRO = dRinitial+unitstep*(dRfinal-dRinitial);
24
25 % Aerodynamic Angles
26 alpha = atan(F(3)/F(1));
27 beta = asin(F(2)/(sqrt(F(1)^2+F(2)^2+F(3)^2)));
28 alphaDot = 0;
29 betaDot = 0;
30
31 % Thrust
32 % THRUSTMODEL(dP,z,V,mach,alpha,beta)
33 [T,Tx,Ty,Tz,~,~,~] = THRUSTMODEL(dP,F(13),sqrt(F(1)^2+F
    (2)^2+F(3)^2),sqrt(F(1)^2+F(2)^2+F(3)^2)/aat,alpha,
    beta);
34
35
36 % Aerodynamic coefficients
37 % coefficients(V,alpha,alphaDot,p,q,r,beta,betaDot,dE,
    dA,dR)
38 [CL,CD,CY,C1,CM,CN] = coefficients(sqrt(F(1)^2+F(2)^2+F
    (3)^2),alpha,alphaDot,F(4),F(5),F(6),beta,betaDot,

```



```

        dE0 , dA0 , dR0 );
39
40
41 % Euler angles as a function of the quaternions
42 if (F(7)*F(9)-F(8)*F(10)) == 0.5
43     psi = 0;
44     phi = 2*asin(q1/cos(pi/4))+psi;
45     theta = pi/2;
46 elseif (F(7)*F(9)-F(8)*F(10)) == -0.5
47     psi = 0;
48     phi = 2*asin(q1/cos(pi/4))-psi;
49     theta = -pi/2;
50 else
51     phi = atan2((2*(F(7)*F(8)+F(9)*F(10))), (1-2*F(8)
52         ^2-2*F(9)^2));
53     theta = real(asin(2*(F(7)*F(9)-F(8)*F(10))));
54     psi = atan2((2*(F(7)*F(10)+F(8)*F(9))), (1-2*F(9)
55         ^2-2*F(10)^2));
56 end
57 % [1] [2] [3]
58 % uDot=(Tx+1/2*rhoat*Sw*(u^2+v^2+w^2)*(-CD*cos(alpha)*
59     cos(beta)+CL*sin(alpha)+CY*cos(alpha)*sin(beta))-m*g
60     *sin(theta))/m-q*w+r*v;
61 % vDot=(Ty+1/2*rhoat*Sw*(u^2+v^2+w^2)*(-CD*sin(beta)+CY
62     *cos(beta))+m*g*cos(theta)*sin(phi))/m-r*u+p*w;
63 % wDot=(Tz+1/2*rhoat*Sw*(u^2+v^2+w^2)*(-CL*cos(alpha)-
64     CD*cos(beta)*sin(alpha)+CY*sin(alpha)*sin(beta))+m*g
65     *cos(theta)*cos(phi))/m-p*v+q*u;
66
67 % [4] [5] [6]
68 % pDot=Izz/(Ixx*Izz-Ixz^2)*L+Ixz/(Ixx*Izz-Ixz^2)*N+((
69     Ixz*(Ixx-Iyy+Izz))/(Ixx*Izz-Ixz^2))*p*q+((Izz*(Iyy-
70     Izz)-Ixz^2)/(Ixx*Izz-Ixz^2))*r*q;
71 % qDot=MA/Iyy+((Izz-Ixx)/Iyy)*p*r+Ixz/Iyy*(r^2-p^2);
72 % rDot=Ixx/(Ixx*Izz-Ixz^2)*N+Ixz/(Ixx*Izz-Ixz^2)*L+((
73     Ixx*(Ixx-Iyy)+Ixz^2)/(Ixx*Izz-Ixz^2))*p*q+((Ixz*(Iyy
74     -Ixx-Izz))/(Ixx*Izz-Ixz^2))*r*q;
75
76 % [q0] [q1] [q2] [q3]
77 % q0Dot = 1/2*(-q1*p-q2*q-q3*r);
78 % q1Dot = 1/2*(q0*p-q3*q+q2*r);
79 % q2Dot = 1/2*(q3*p+q0*q-q1*r);
80 % q3Dot = 1/2*(-q2*p+q1*q+q0*r);
81
82 % [10] [11] [12]

```

```

74 % xDot=u*cos(psi)*cos(theta)+v*(cos(psi)*sin(theta)*sin
    (phi)-cos(phi)*sin(psi))+w*(sin(theta)*cos(phi)*cos(
75 % yDot=u*cos(theta)*sin(psi)+v*(cos(phi)*cos(psi)+sin(
    theta)*sin(phi)*sin(psi))+w*(-cos(psi)*sin(phi)+cos(
76 % -zDot=-u*sin(theta)+v*cos(theta)*sin(phi)+w*cos(theta)
    )*cos(phi);
77
78 % Variables
79 %u=F(1)          uDot=dFdt(1)
80 %v=F(2)          vDot=dFdt(2)
81 %w=F(3)          wDot=dFdt(3)
82 %p=F(4)          pDot=dFdt(4)
83 %q=F(5)          qDot=dFdt(5)
84 %r=F(6)          rDot=dFdt(6)
85 %q0=(F(7))      q0Dot=dFdt(7)
86 %q1=(F(8))      q1Dot=dFdt(8)
87 %q2=(F(9))      q2Dot=dFdt(9)
88 %q3=(F(10))     q3Dot=dFdt(10)
89 %x=F(11)        xDot=dFdt(11)
90 %y=F(12)        yDot=dFdt(12)
91 %z=F(13)        zDot=dFdt(13)
92
93 % Bryan Equations
94 % Traslation Equations
95 % [1] [2] [3]
96 uDot = (Tx+1/2*rhoat*Sw*(F(1)^2+F(2)^2+F(3)^2)*(-CD*cos
    (alpha)*cos(beta)+CL*sin(alpha)+CY*cos(alpha)*sin(
97 vDot = (Ty+1/2*rhoat*Sw*(F(1)^2+F(2)^2+F(3)^2)*(-CD*sin
    (beta)+CY*cos(beta))+m*g*cos(theta)*sin(phi))/m - F
    (6)*F(1) + F(4)*F(3);
98 wDot = (Tz+1/2*rhoat*Sw*(F(1)^2+F(2)^2+F(3)^2)*(-CL*cos
    (alpha)-CD*cos(beta)*sin(alpha)+CY*sin(alpha)*sin(
    beta))+m*g*cos(theta)*cos(phi))/m - F(4)*F(2) + F(5)
    *F(1);
99
100 % Rotation Equations
101 % [4] [5] [6]
102 pDot = Izz/(Ixx*Izz-Ixz^2)*(1/2*rhoat*bw*(F(1)^2+F(2)
    ^2+F(3)^2)*Sw*Cl) + Ixz/(Ixx*Izz-Ixz^2)*(1/2*rhoat*
    bw*(F(1)^2+F(2)^2+F(3)^2)*Sw*CN) + ((Ixz*(Ixx-Iyy+
    Izz))/(Ixx*Izz-Ixz^2))*F(4)*F(5) + ((Izz*(Iyy-Izz)-
    Ixz^2)/(Ixx*Izz-Ixz^2))*F(6)*F(5);
103 qDot = (1/2*rhoat*cw*(F(1)^2+F(2)^2+F(3)^2)*Sw*CM)/Iyy
    + ((Izz-Ixx)/Iyy)*F(4)*F(6) + Ixz/Iyy*(F(6)^2-F(4)
    ^2);

```

```

104   rDot = Ixx/(Ixx*Izz-Ixz^2)*(1/2*rhoat*bw*(F(1)^2+F(2)
      ^2+F(3)^2)*Sw*CN) + Ixz/(Ixx*Izz-Ixz^2)*(1/2*rhoat*
      bw*(F(1)^2+F(2)^2+F(3)^2)*Sw*C1) + ((Ixx*(Ixx-Iyy)+
      Ixz^2)/(Ixx*Izz-Ixz^2))*F(4)*F(5) + ((Ixz*(Iyy-Ixx-
      Izz))/(Ixx*Izz-Ixz^2))*F(6)*F(5);
105
106   % Quaternions
107   % q0 q1 q2 q3
108   q0Dot = 1/2*(-F(8)*F(4)-F(9)*F(5)-F(10)*F(6));
109   q1Dot = 1/2*(F(7)*F(4)-F(10)*F(5)+F(9)*F(6));
110   q2Dot = 1/2*(F(10)*F(4)+F(7)*F(5)-F(8)*F(6));
111   q3Dot = 1/2*(-F(9)*F(4)+F(8)*F(5)+F(7)*F(6));
112
113   % Kinematic Equations
114   % [10] [11] [12]
115   xDot = F(1)*cos(psi)*cos(theta) + F(2)*(cos(psi)*sin(
      theta)*sin(phi)-cos(phi)*sin(psi)) + F(3)*(sin(theta)
      )*cos(phi)*cos(psi)+sin(phi)*sin(psi));
116   yDot = F(1)*cos(theta)*sin(psi) + F(2)*(cos(phi)*cos(
      psi)+sin(theta)*sin(phi)*sin(psi)) + F(3)*(-cos(psi)
      *sin(phi)+cos(phi)*sin(theta)*sin(psi));
117   zDot = -(-F(1)*sin(theta) + F(2)*cos(theta)*sin(phi) +
      F(3)*cos(theta)*cos(phi));
118
119
120   % Fuel mass consumption
121   fuelDot = -Ce*T;
122
123   % Integration vector
124   dFdt = [uDot; vDot; wDot; pDot; qDot; rDot; q0Dot;
      q1Dot; q2Dot; q3Dot; xDot; yDot; zDot; fuelDot];
125
126   end

```

C.7 Flight simulator

```
1 clear
2 close all
3
4 global manoeuvre
5
6 % WARNING: before running the file, make sure that the
7   files corresponding to the aircraft parameters and the
8   initial conditions are properly filled. Make sure to
9   also select the proper coordinate system
10 % FILL ONLY THE VARIABLES THAT HAVE THE WORD 'COMPLETE'
11   WRITTEN
12
13 run('AircraftParameters.m')
14
15 manoeuvre = ; % COMPLETE
16   % Vertical plane equilibrium -> manoeuvre = 1;
17   % Vertical loop -> manoeuvre = 2; (not available for
18   body-fixed axes)
19   % Gliding flight -> manoeuvre = 3;
20   % Dive recovery -> manoeuvre = 4;
21   % Ascending turn -> manoeuvre = 5;
22   % Horizontal turn -> manoeuvre = 6;
23
24 coordinates = ; % COMPLETE
25   % Body-fixed -> coordinates = 1;
26   % Wind -> coordinates = 2;
27   % Quaternions -> coordinates = 3;
28
29 tf = ; % COMPLETE
30 tspan=(0:tf);
31
32 if coordinates == 1
33
34   run('InitialConditionsBody.m')
35
36   % Vector of initial conditions
37   F0 = [u0; v0; w0; p0; q0; r0; phi0; theta0; psi0; x0;
38         y0; z0; fuelDot0];
39
40   % Solver
41   options = odeset('RelTol', 1e-10, 'AbsTol', 1e-10);
42   [t,F] = ode45(@BRYANBODY, tspan, F0, options);
43
44   % Fuel consumption
45   fuelconsumption = F(end,13)
46
```

```

41 % Plots
42 figure
43 plot(t,F(:,1),t,F(:,2),t,F(:,3))
44 title('Time evolution of linear velocities')
45 xlabel('t [s]')
46 ylabel('Linear velocities [m/s]')
47 legend('u(t)', 'v(t)', 'w(t)')
48
49 figure
50 plot(t,F(:,4),t,F(:,5),t,F(:,6))
51 title('Time evolution of angular velocities')
52 xlabel('t [s]')
53 ylabel('Angular velocities [rad/s]')
54 legend('p(t)', 'q(t)', 'r(t)')
55
56 figure
57 plot(t,F(:,7),t,F(:,8),t,F(:,9))
58 title('Time evolution of the Euler angles')
59 xlabel('t [s]')
60 ylabel('Euler angles [rad]')
61 legend('\phi(t)', '\theta(t)', '\psi(t)')
62
63 figure
64 plot(t,F(:,10))
65 title('Time evolution of position')
66 xlabel('t [s]')
67 ylabel('x(t) [m]')
68
69 figure
70 plot(t,F(:,11))
71 title('Time evolution of lateral position')
72 xlabel('t [s]')
73 ylabel('y(t) [m]')
74
75 figure
76 plot(t,F(:,12))
77 title('Time evolution of altitude')
78 xlabel('t [s]')
79 ylabel('z(t) [m]')
80
81 figure
82 plot(F(:,10),F(:,12))
83 title('Two-dimensional trajectory')
84 xlabel('x(t) [m]')
85 ylabel('z(t) [m]')
86
87 figure
88 plot3(F(:,10),F(:,11),F(:,12)),grid

```

```

89     title('Three-dimensional trajectory')
90     xlabel('x(t) [m]')
91     ylabel('y(t) [m]')
92     zlabel('z(t) [m]')
93
94     figure
95     plot(t,atan(F(:,3)./F(:,1)),t,asin(F(:,2)./(sqrt(F(:,1)
96         .^2+F(:,2).^2+F(:,3).^2))))
97     title('Time evolution of the aerodynamic angles')
98     xlabel('t [s]')
99     ylabel('Aerodynamic angles [rad]')
100    legend('\alpha(t)','\beta(t)')
101
102    figure
103    plot(t,sqrt(F(:,1).^2+F(:,2).^2+F(:,3).^2))
104    title('Time evolution of the airspeed')
105    xlabel('t [s]')
106    ylabel('V(t) [m/s]')
107
108    elseif coordinates == 2
109        run('InitialConditionsWind.m')
110
111        % Vector of initial conditions
112        F0 = [V0; beta0; alpha0; p0; q0; r0; mu0; gamma0; chi0;
113            x0; y0; z0; fuelDot0];
114
115        % Solver
116        options = odeset('RelTol', 1e-10, 'AbsTol', 1e-10);
117        [t,F] = ode45(@BRYANWIND, tspan, F0, options);
118
119        % Fuel consumption
120        fuelconsumption = F(end,13)
121
122        % Plots
123        figure
124        plot(t,F(:,1))
125        title('Time evolution of the airspeed')
126        xlabel('t [s]')
127        ylabel('V(t) [m/s]')
128
129        figure
130        plot(t,F(:,2),t,F(:,3))
131        title('Time evolution of the aerodynamic angles')
132        xlabel('t [s]')
133        ylabel('Aerodynamic angles [rad]')
134        legend('\beta(t)','\alpha(t)')

```

```

135 figure
136 plot(t,F(:,4),t,F(:,5),t,F(:,6))
137 title('Time evolution of angular velocities')
138 xlabel('t [s]')
139 ylabel('Angular velocities [rad/s]')
140 legend('p(t)', 'q(t)', 'r(t)')
141
142 figure
143 plot(t,F(:,7),t,F(:,8),t,F(:,9))
144 title('Time evolution of the Euler angles in wind axes'
145 )
146 xlabel('t(s)')
147 ylabel('Euler angles [rad]')
148 legend('\mu(t)', '\gamma(t)', '\chi(t)')
149
150 figure
151 plot(t,F(:,10))
152 title('Time evolution of position')
153 xlabel('t [s]')
154 ylabel('x(t) [m]')
155
156 figure
157 plot(t,F(:,11))
158 title('Time evolution of lateral position')
159 xlabel('t [s]')
160 ylabel('y(t) [m]')
161
162 figure
163 plot(t,F(:,12))
164 title('Time evolution of altitude')
165 xlabel('t [s]')
166 ylabel('z(t) [m]')
167 legend('z(t)')
168
169 figure
170 plot(F(:,10),F(:,12))
171 title('Two-dimensional trajectory')
172 xlabel('x(t) [m]')
173 ylabel('z(t) [m]')
174
175 figure
176 plot3(F(:,10),F(:,11),F(:,12)),grid
177 title('Three-dimensional trajectory')
178 xlabel('x(t) [m]')
179 ylabel('y(t) [m]')
180 zlabel('z(t) [m]')
181

```

```

182 elseif coordinates == 3
183
184     run('InitialConditionsQuaternions.m')
185
186     % Vector of initial conditions
187     F0 = [u0; v0; w0; p0; q0; r0; q00; q10; q20; q30; x0;
188           y0; z0; fuelDot0];
189
190     % Solver
191     options = odeset('RelTol', 1e-10, 'AbsTol', 1e-10);
192     [t,F] = ode45(@BRYANBODYQUATERNIONS, tspan, F0, options
193                 );
194
195     % Fuel consumption
196     fuelconsumption = F(end,14)
197
198     % Plots
199
200     figure
201     plot(t,F(:,1),t,F(:,2),t,F(:,3))
202     title('Time evolution of the linear velocities')
203     xlabel('t [s]')
204     ylabel('Linear velocities [m/s]')
205     legend('u(t)', 'v(t)', 'w(t)')
206
207     figure
208     plot(t,F(:,4),t,F(:,5),t,F(:,6))
209     title('Time evolution of the angular velocities')
210     xlabel('t [s]')
211     ylabel('Angular velocities [rad/s]')
212     legend('p(t)', 'q(t)', 'r(t)')
213
214     figure
215     plot(t,F(:,7),t,F(:,8),t,F(:,9),t,F(:,10))
216     title('Time evolution of the quaternions')
217     xlabel('t [s]')
218     ylabel('Quaternions')
219     legend('q0(t)', 'q1(t)', 'q2(t)', 'q3(t)')
220
221     figure
222     plot(t,F(:,11))
223     title('Time evolution of position')
224     xlabel('t [s]')
225     ylabel('x(t) [m]')
226
227     figure
228     plot(t,F(:,12))
229     title('Time evolution of lateral position')

```



```

228     xlabel('t [s]')
229     ylabel('y(t) [m]')
230
231     figure
232     plot(t,F(:,13))
233     title('Time evolution of altitude')
234     xlabel('t [s]')
235     ylabel('z(t) [m]')
236
237     figure
238     plot(F(:,11),F(:,13))
239     title('Two-dimensional trajectory')
240     xlabel('x(t) [m]')
241     ylabel('z(t) [m]')
242
243     figure
244     plot3(F(:,11),(F(:,12)),F(:,13)),grid
245     title('Three-dimensional trajectory')
246     xlabel('x(t) [m]')
247     ylabel('y(t) [m]')
248     zlabel('z(t) [m]')
249
250     figure
251     plot(t,atan(F(:,3)./F(:,1)),t,asin(F(:,2)./(sqrt(F(:,1)
        .^2+F(:,2).^2+F(:,3).^2))))
252     title('Time evolution of the aerodynamic angles')
253     xlabel('t [s]')
254     ylabel('Aerodynamic angles [rad]')
255     legend('\alpha(t)', '\beta(t)')
256
257     figure
258     plot(t,atan2((2*(F(:,7).*F(:,8)+F(:,9).*F(:,10))),
        (1-2*
        F(:,8).^2-2*F(:,9).^2)),t,asin(2*(F(:,7).*F(:,9)-F
        (:,8).*F(:,10))),t,atan2((2.*(F(:,7).*F(:,10)+F(:,8)
        .*F(:,9))),
        (1-2.*F(:,9).^2-2.*F(:,10).^2)))
259     title('Time evolution of the Euler angles')
260     xlabel('t [s]')
261     ylabel('Euler angles [rad]')
262     legend('\phi(t)', '\theta(t)', '\psi(t)')
263
264     figure
265     plot(t,sqrt(F(:,1).^2+F(:,2).^2+F(:,3).^2))
266     title('Time evolution of the airspeed')
267     xlabel('t [s]')
268     ylabel('V(t) [m/s]')
269
270 end

```